Investigating sediment transport on the Waipaoa margin: linking *in situ* observations with preserved deposits

Richard Prescott Hale

A dissertation
submitted in partial fulfillment of the
requirements for the degree of

Doctor of Philosophy

University of Washington

2014

Program Authorized to Offer Degree:
School of Oceanography

University of Washington

Abstract

Investigating sediment transport on the Waipaoa margin:
linking *in situ* observations with preserved deposits

Richard Prescott Hale

Co-chairs of the Supervisory Committee:

Professor Andrea Ogston
School of Oceanography

Professor Charles Nittrouer
School of Oceanography

Connecting the processes that control sediment transport to the deposits they leave behind is critical for understanding sedimentary system dynamics on modern timescales. Small mountainous river systems (SMRs) have been the focus of intense investigation for several decades, as they provide an ideal setting in which to study the conditions responsible for generating and preserving individual event deposits. In this study, bottom-boundary-layer tripods were deployed in three locations on the continental shelf seaward of the Waipaoa River (New Zealand), to monitor sediment and water movement from January 2010 to February 2011. Four research cruises were conducted at approximately four-month intervals during this time period to service and repair instrumentation, as well as to collect short (<50 cm) sediment cores at repeat locations across the shelf. Cores were examined for their textural and radiochemical properties as evidence of recent sediment deposition.

Typical of SMRs, water and sediment discharge from the Waipaoa River is episodic, with the potential for relatively major (>2000 $m^3 s^{-1}$) events to occur in any season. Sediment

transport on the Waipaoa margin is similarly event driven, with the majority of near-bed sediment transport occurring in 36 discreet events (defined in this study by U_{*wc} >0.03 m s^{-1}) of <60 h duration. Events which result in a net aggradation of the seabed tend to have longer duration than erosive events (~100 h), though on an annual timescale this is still rapid. In general, short-duration events with relatively low-height, long-period waves result in seabed erosion on the mid-shelf. Longer-duration events with tall-height, short-period (i.e., steep) waves typically result in sediment deposition. Event duration is particularly important in the case of large floods of the river, as the associated sediment requires a minimum of ~120 hours of event-level shear velocity before being deposited on the mid-shelf.

When events (both discharge and U_{*wc}) occur coincidentally, and are of sufficiently long duration, wave-supported fluid mud (WSFM) can form at the mid-shelf. Near-bed suspended-sediment concentrations (SSC) >50 g l^{-1} are observed in the near-bed layers (<26 cm above bed), which is well above the theoretical threshold for downslope travel under the influence of gravity. Gravity-driven velocity is slow at the mid-shelf due to the shallow slope, however material travelling from the mid-shelf under the influence of gravity alone can reach the shelf break in ~50 h during periods of highest SSC.

The deposit from a WSFM that occurred in early July, 2010, was plainly visible in X-radiographs of sediment cores collected at 17 locations in September 2010, and again at the same locations in February 2011. The deposit is identified as relatively low-bulk-density material, 1-12 cm thick, which tends to be physically stratified, especially at greater thicknesses. Using a newly developed method for estimating the degree of physical lamination, 10 locations show more surface variability in September than in February, while the opposite is true in 5 locations. Visual inspection of the cores agrees with these results, which demonstrate how biological

mixing of event layers destroys strata, and prevents long-term event-bed preservation. This new method for using down-core bulk-density to analyze quantitatively sediment x-radiographs over a decadal-to-century scale faithfully reproduces the results of qualitative analyses performed in this location by previous studies.

TABLE OF CONTENTS

Page

LIST OF FIGURES

LIST OF TABLES

ACKNOWLEDGEMENTS

First and foremost, I thank my advisors Andrea Ogston and Chuck Nittrouer, for their support, their guidance, and most of all, their tireless patience. With constant encouragement they have fostered my interests as both an instructor and a researcher throughout my time at the University of Washington. Many thanks also to my committee members J.P. Walsh, Rick Keil, Alex Horner-Devine, and Jim Thomson, whose insight and assistance have proven invaluable. I cannot thank enough, my officemate Katie Boldt, whose friendship has through six years of office cohabitation buoyed me through both all manner of tumult. I also could not have survived this experience without the help of my labmates, Dan Nowacki, Aaron Fricke, Emily Eidam, Kristen Lee, Emilie Flemer, and Tina Drexler, whose humor and wisdom have made this process so wonderful.

I would like to thank the captains and crews of the *R/V Revelle*, and the *R/V Kaharoa*, without whom sample collection could never have happened. Thanks also to the volunteers, graduate students, and collaborating scientists, whose help on this project was both a gift and an inspiration. Thank you to the National Science Foundation and the National Institute of Water and Atmospheric Research (NZ) for funding this research. I would also like to thank the administrative staff of the School of Oceanography who make everything run smoothly, and the Ocean Engineering group who provide the tools and knowledge necessary to keep us moving forward.

Finally, a huge thank you to my family and friends, without whose love and support none of this could have happened. You instilled in me the curiosity to ask questions, and the confidence to seek answers.

Chapter 1:
Introduction and organization of the text

1.1 Introduction

The delivery of sediment from rivers to oceans involves a complex system of tectonic and climatic forces, which act to generate, transport, and deposit terrigenous material in a variety of settings. During sea-level highstands like the present day, the link between river mouth and deep-ocean sediment sinks is disjointed in many systems due to unfilled estuaries and wide continental shelves (e.g., Walsh and Nittrouer, 2009). However during periods of lowstanding sea level, which have occurred throughout earth history, sediment can be exported relatively quickly and easily off of the continental shelf. As much as 90% of the sedimentary rock record currently visible on continents was originally deposited in a marine environment, and the processes by which this material was transported can best be understood by examining similar systems in the modern epoch. Small mountainous river systems (SMRs) typically occur on active continental margins which are characterized by narrow shelves that maintain a direct link between sediment source and sink typical of sea-level lowstands (Milliman and Syvitski, 1992). The specific processes by which sediment is actively being transported and deposited in SMRs provide insight to past geologic eras.

SMRs provide an opportunity to study sediment transport and depositional processes across a wide range of environments, as the entire sedimentary pathway is included in a relatively short-reach, source-to-sink system (e.g., Nittrouer, 1999; Carter et al., 2010). SMRs are also known for their high sediment yield (Milliman and Meade, 1983), which provides a strong signal to follow through the entire system. Understanding the fate of the material is important for a variety of reasons. For example, the fine-grained particles debouched by rivers into the ocean carry with them ~ 90% of the particulate organic matter entering the marine

environment (Keil et al., 1995). As such, research investigating the fate of organic carbon, heavy-metal, and other particle-associated pollutants depends on an understanding of the sediment-transport processes responsible for moving this material from the river mouth to its site of final deposition. While substantial research has been conducted investigating sediment transport across continental shelves in a variety of environments, there exists sufficient complexity in the natural setting to prevent, as yet, a complete global understanding. The joint US-New Zealand *Source-to-Sink* initiative, part of the MARGINS Program of the U.S. National Science Foundation (http://www.nsf.margins.org/), was designed to investigate the processes responsible for shaping and transforming landscapes across a variety of spatial and temporal scales. The Waipaoa Sedimentary System (WSS), located on the east coast of the North Island of New Zealand (Fig. 1.1), was selected to address these questions.

The WSS features a geographic setting typical of SMRs, with an ideal combination of a wet, maritime climate and highly fractured, easily erodible rock that combine to generate and deliver approximately 15 MT of sediment to the coastal system per year (Hicks et al., 2000). This sediment-supply rate, combined with the relatively small watershed, makes the Waipaoa one of the highest-yield rivers globally (Walling and Webb, 1996), and an excellent place to investigate sediment-transport and depositional processes, as such events tend to occur dramatically and frequently (e.g., Reid, 1999; Bever et al., 2011; Kniskern et all., 2014).

In addition to a high sediment yield, the WSS boasts an energetic shelf environment, with powerful oceanic storms capable of occurring throughout the year (Healy et al., 2002; Kniskern et al., 2014). Previous research has identified that sediment from river floods may be temporarily stored within Poverty Bay (Fig. 1.1; Bever et al., 2011). Subsequent offshore advection delivers the sediment to loci of enhanced accumulation in depocenters both on and off

the continental shelf (Miller and Kuehl, 2010). Textural analysis has identified the types of sedimentary facies observed in both the modern setting, and throughout the Holocene (Rose and Kuehl, 2010), however the processes directly linked to strata formation and preservation have not been observed *in situ*, and are the focus of this research.

Gravity-driven flow on continental margins has been recognized as an efficient mechanism by which vast quantities of sediment are rapidly moved across long distances (e.g., Wright et al., 1990). In recent years, wave-supported fluid muds have been identified as important mechanisms for across-shelf sediment transport, on both passive and active continental margins (e.g., Wright et al., 1990; Traykovski et al., 2000; Jaramillo et al., 2009). Deposits from wave-supported fluid muds have been identified elsewhere in the rock record (Macquaker et al., 2010), and while their occurrence has been suspected on the Waipaoa margin, they have not been observed directly.

These near-bed processes can occasionally be observed in the generation and destruction of seabed strata, as observed in x-radiographs of repeat sediment cores. To understand the geologic importance of the events occurring during this single year relative to the longer-term (decadal-to-century scale) sediment deposition history, a new method for quantitatively analyzing x-radiograph images is envisioned. The scientific merit of such a method is highlighted by its successful application to recent research in a variety of depositional environments, including the Waipaoa margin and near the mouth of the Rhône River, each of which has been the site of significant previous analyses using a variety of textural and radiochemical tools (e.g., Miller and Kuehl, 2010; Rose and Kuehl, 2010; Walsh et al., 2014; Drexler and Nittrouer, 2008). By observing how processes modify the seabed, and determining how frequently these types of events occur and are preserved across the shelf, it becomes

possible to understand the geologic evolution of a modern continental margin, which can subsequently be placed in a broader geologic context.

1.2 Organization of the text

The goal of this study is to examine the processes responsible for sediment transport and deposition on the Waipaoa margin using time-series data from *in situ* instrumentation, combined with repeat sediment cores. This research will contrast conditions associated with strata formation and destruction over approximately one year of field study, and connect individual events observed in the instrumental data with their associated seabed deposits. By combining observational data with physical seabed samples, this research addresses questions raised by previous studies involving sediment accumulation across a variety of time scales.

The research associated with this dissertation is divided into three research sections. In Chapter 2, one year of near-bed hydrodynamic data are examined and used to identify the processes responsible for strata development and change. During this year of study, a wave-supported fluid mud was observed in the instrumental data, the formation and significance of which are examined in greater detail in Chapter 3. The deposit formed by this event was identified in seabed x-radiograph images and, if preserved, can be used as evidence of previous event-based sedimentation. Chapter 4 uses results from this and other research to develop a method for quantitatively extracting data from x-radiograph images, which is used to examine seabed change on time scales ranging from seasonal to decadal, and longer. Chapter 5 summarizes the contributions of this work, and considers how these results impact the broader field of sedimentological research.

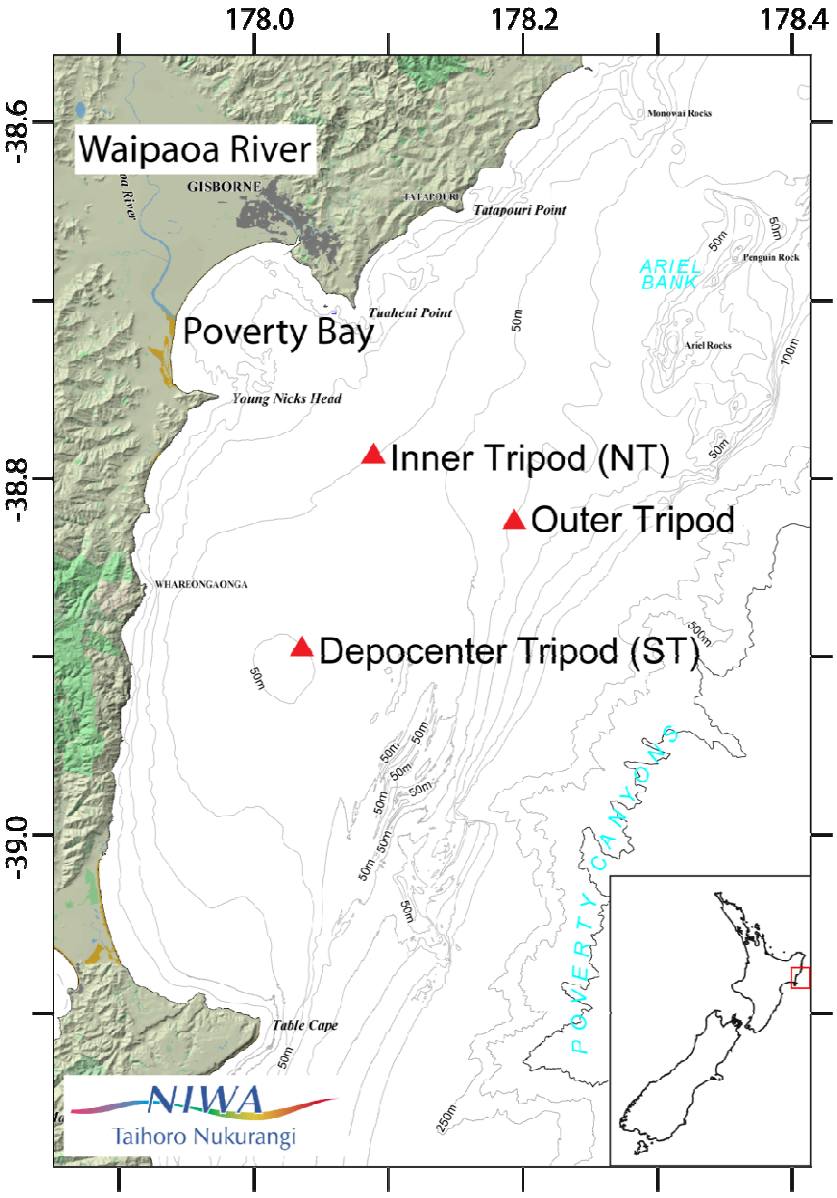

Figure 1.1 – Map of the study area, including the Waipaoa River, Poverty Bay, and the locations of three bottom-boundary-layer tripods.

Chapter 2:

Sediment transport and event deposition on the Waipaoa River shelf, New Zealand

2.1 Introduction

Recent initiatives have sought to understand the dynamics of sediment transport and accumulation on continental shelves nourished by small mountainous river systems. A fundamental question has been the role of river-ocean coherence in moving sediment quickly from river mouths and coasts, across, and off the continental shelf to the site of ultimate deposition (e.g., Farnsworth and Warrick, 2007; Warrick et al., 2008; Wheatcroft et al., 2010; Kniskern et al., 2011). Marine deposits that are the direct result of river floods can be formed either in a single event from river plume settling, or in sequential steps between the river mouth and the final site of deposition. Which route, or combination of pathways, can determine the behavior of material fluxes and the architecture of the stratigraphic record (e.g., Sommerfield and Nittrouer, 1999; Palinkas and Nittrouer, 1999). Sediment fluxes in small mountainous river systems tend to be episodic and controlled by individual storm events (e.g., Ogston and Sternberg, 1999; Guillén et al., 2006; Fain et al., 2007; Traykovski et al., 2007). Energetic oceanographic and fluvial conditions can create situations that encourage the formation of sediment gravity flows, identified as important mechanisms for off-shelf sediment transport in many sedimentary systems (e.g., Eel River, CA – Ogston et al., 2000; Waiapu River, NZ – Ma et al., 2008; Atchafalaya River, LA – Jaramillo et al., 2009). However, due to their ephemeral spatial and temporal nature, as well as the specific combination of conditions required for their formation, documenting such flows *in situ* is problematic. As such, quantifying and understanding episodic system behavior using field measurements presents a unique challenge. Typically, these issues are addressed in one of two ways: via time-series data collected with

acoustic and optical instrumentation, or high-resolution stratigraphic analysis of sediment cores that capture a composite of processes over decadal timescales. Integrating these datasets to correlate observed environmental conditions and associated seabed deposits, as well as the preservation potential of these deposits, has been the focus of several recent studies (e.g., Traykovski et al., 2000; Martin et al., 2008; Palinkas et al., 2010). Time-series data underpin a hydrodynamic interpretation of the bed morphology, capturing oceanic drivers operating across a range of timescales. Sequential cores collected over consecutive seasons can provide a physical record of the seabed response to the environmental conditions.

Event-scale processes have important implications for both long-term and seasonal sediment accumulation patterns. The Waipaoa River drains the steep hinterland of the Raukumara ranges of northeastern New Zealand. Using a mass balance approach from ^{210}Pb (century-scale) accumulation, previous work has shown that as little as 18% of the sediment debouched is actively accumulating on the continental shelf, suggesting efficient off-shelf transport (Alexander et al., 2010). Seasonal resolution can be achieved from ^{7}Be inventories (Rose and Kuehl, 2010; Alexander et al., 2010), and these data indicate strong temporal coherence and rapid delivery of terrestrial material from the landscape source to the shelf. Here, a quantitative understanding of the mechanisms that control sediment transport and deposition is especially important, as wholesale deforestation and conversion to pasture in the Waipaoa catchment since the mid-19th century led to a nearly order-of-magnitude increase in erosion and fluvial sediment yield (e.g., Kettner et al., 2007, Page et al., 2010), modifying shelf dispersal and the loci of accumulation (e.g., Orpin et al., 2006; Miller and Kuehl, 2010). Today, as much as 90% of the terrestrial organic matter entering the world's oceans moves with fine-grained sediment fluxes, making a quantitative understanding of mud dispersal on the shelf critical for

models of carbon sequestration and global carbon budgets (Keil et al., 1997). Furthermore, the episodic delivery of carbon during extreme events is poorly constrained. As an example, on the Waipaoa margin, Brackley et al. (2010) identified an event layer in surface sediment cores, which contained high concentrations of organic carbon that was possibly from Cyclone Bola in 1988. However, the hydrodynamic conditions that generated this deposit are unknown.

This study, which was part of the NSF MARGINS Source-to-Sink program, examines one year of water-column and near-bed observations from benthic-boundary-layer tripods located on the continental shelf offshore of the Waipaoa River. The overarching goal of the current study was to quantify the link between known shelf accumulation patterns and observed physical forcing using sediment-transport time-series data and seabed signatures. Data from acoustic and optical instrumentation, including hourly seabed elevation changes, are interpreted alongside physical structures from short sediment cores collected in four-month intervals throughout the study year to explore the development of bed strata.

The three specific objectives of this investigation on the Waipaoa margin were:

1) to examine the physical processes responsible for erosion and deposition on the continental shelf;

2) to understand the pathways and timeframe for flood-derived sediment to reach the shelf; and,

3) to evaluate the stratigraphic manifestation of recorded events on the shelf.

2.1.1 Regional setting

The Waipaoa Sedimentary System (WSS, Fig. 2.1) provides an excellent opportunity to study source-to-sink sedimentation over a relatively small spatial scale. The vigorous marine climate generates significant rainfall (100 cm yr^{-1} at the coast and 250 cm y^{-1} at the headwaters; Hicks et al., 2000; Page et al., 2001). The Waipaoa catchment drains the Raukumara Ranges,

which is located on the tectonically active northern Hikurangi Margin, and is dominantly comprised of highly erodible and fractured sedimentary rock, including sandstones, argillites, and mudstones. The combination of the small catchment (2205 km^2) and significant sediment delivery (15 Mt y^{-1} of suspended sediment, 0.15 Mt y^{-1} of bedload), result in very high landscape sediment yields (Hicks et al., 2000; Walling and Webb, 1996). Over the 20th century the largest floods were >1900 $m^3 s^{-1}$ and can occur throughout the year, although they are most frequent in the austral fall and early winter months (April-June; Reid, 1999). While some uncertainty exists regarding the sediment rating curve during very high discharge events, Hicks et al. (2004) suggest that suspended-sediment concentrations during floods can exceed the threshold for hyperpycnal plume generation (40 g l^{-1}) with an estimated forty-year return frequency.

The Waipaoa River drains southeastward to empty into Poverty Bay, which is exposed to frequent, powerful storms generated in the tropics and mid-latitude Southern Pacific to the northeast, and Southern Ocean to the south, with high waves (>5 m) occurring several times each year (Healy et al., 2002). Poverty Bay is confined by headlands to the north and south, is relatively small (62 km^2) and shallow (<30 m). The bay and inner shelf serve as temporary storage for the majority of sediment entering from the Waipaoa River (Bever et al., 2011). The processes necessary for exporting sediment from the bay to the middle shelf, and responsible for the sediment accumulation patterns observed on the shelf from previous studies (Bever et al., 2011; Rose and Kuehl, 2010; Miller and Kuehl, 2010) are not well understood and are the focus of this study.

The Waipaoa shelf (Fig. 2.1) is relatively narrow (~20 km wide), bounded on its seaward edge by emergent anticlines. Three loci of modern, steady-state sediment accumulation have been identified: the northern mid-shelf, the southern mid-shelf, and an outer shelf lobe (Miller

and Kuehl, 2010). High sediment accumulation rates (~2 cm yr^{-1}) were measured landward of the anticlinal ridges, as well as on the outer shelf and upper slope (Walsh et al., 2007; Alexander et al., 2010; Miller and Kuehl, 2010). Previous sediment budgets estimate that 18-30% of the annual sediment load accumulates on the shelf (Miller and Kuehl, 2010), while another 13-18% accumulates on the slope, leaving perhaps 55-71% being dispersed beyond the proximal vicinity of the WSS (Alexander et al., 2010).

In this study, instrumented tripods were strategically placed to measure sediment dispersal and to record ocean conditions. The two shelf sites are located in the area immediately outside Poverty Bay (Northern Tripod, "NT", 37 m water depth), and at the southern depocenter (Southern Tripod, "ST", 50 m water depth; Fig. 2.1, Table 2.1).

2.1.2 Shelf sediment transport and sediment gravity flows

Research at many river dispersal systems has focused on the problem of diffuse transport in the bottom-boundary layer (e.g., Sternberg and Larsen, 1976). Current, wave, and river discharge events can resuspend sediment in low to moderate concentrations, which is then subject to along- and across-shelf advection (e.g. Ogston and Sternberg, 1999). In many regions, continental shelves develop a mid-shelf mud deposit, constrained at their shoreward edge by shoaling waves, and their seaward edge by strong parabathic currents (e.g. Washington Shelf – Nittrouer, 1979; Eel Shelf – Wheatfield and Borgeld, 2000; Gulf of Lions – Drexler and Nittrouer, 2008).

Studies on the Amazon and Eel margins, highlighted the significant contribution of sediment gravity flows to mass transport on continental margins with much fluvial sediment impact (e.g., Kineke et al., 1996; Traykovski et al., 2000). Sediment gravity flows can occur when the suspended-sediment-enhanced density of a fluid parcel exceeds the density of the

surrounding seawater, causing the parcel to gravitationally flow down the bathymetric gradient. This process was initially identified in association with estuarine mixing processes (e.g., Allen, 1980; Wells and Coleman, 1981; Cacchione et al., 1995; Kineke et al., 1996). Subsequent investigation revealed that muddy, high river discharge and energetic ocean conditions are also capable of generating sediment gravity flows, such as wave-supported fluid muds, which are generated by sediment resuspended and/or maintained in suspension by wave energy (e.g., Traykovski et al., 2000; Wiberg, 2000, Puig et al., 2004). When seawater is the dominant entraining fluid, suspended-sediment concentrations (SSC) of >10 g l^{-1} are required before flows can travel down gradient under the influence of gravity (e.g., Wright et al., 1990). Wave-current gravity flows are similar in concept to wave-supported fluid muds, with energy for suspenision provided by a combination of wave and current conditions (e.g. Wright and Friedrichs, 2006). In either case, in order for resuspension to occur, near-bed shear velocity must exceed the resuspension velocity.

To date, wave-supported fluid muds have been observed as an important means of cross- and off-shelf sediment transport in many regions. On the Eel shelf, wave-supported fluid muds occur when waves are sufficiently high to generate a wave boundary layer of approximately 5 cm (Traykovski et al., 2000), and have been identified as the dominant means of cross-shelf sediment transport (Ogston et al., 2000). Wave-supported fluid muds form on the Po delta, even when the river is not flooding, by resuspending previously deposited seabed material (Traykovski et al., 2007). Similarly, the fluid muds formed on the Atchafalaya shelf formed in the absence of a flood, and were generated by wave-induced sediment resuspension (Jaramillo et al., 2009). Research on the Atchafalaya shelf also demonstrated the role of seabed liquefaction due to differential pressure from passing wave trains, which fluidized the bed and resulted in the

tripod settling several cm (Jaramillo et al., 2009). In other systems, such as the Huanghe delta, fluid muds form when strong tidal currents resuspend seabed sediment, advecting these high-concentration flows along and across the delta (Wright et al., 1990). Offshore of the very muddy Waiapu River (annual suspended sediment load of 35 Mt yr^{-1}), located ~115 km north of the Waipaoa in New Zealand, both wave and current resuspension are required to generate and maintain fluid muds (Ma et al., 2008).

2.2 Methods

2.2.1 Instrumentation

In this study, data are examined from two instrumented tripods deployed for 11.5 months on the Waipaoa River continental shelf (Fig. 2.1), beginning January 15, 2010. Tripods were initially deployed from the R/V *Roger Revelle*, and were serviced at ~4 month intervals by the R/V *Kaharoa*. At the ST site, an impact from a fishing trawler in Sept 2010 severely damaged the instrumentation, which made for a shorter and less definitive record, as much of the spring and summer seasons were absent. A complete list of instrumentation deployed and their configuration can be found in Table 2.1. Measurements for all instruments were collected hourly, in six-minute bursts, with individual bursts averaged into a single data point (or profile) for each hour. In general, near-bed velocities (mean and root mean squared-orbital) were measured using an acoustic doppler velocimeter (ADV, Nortek Vector and Sontek Ocean-Hydra), and suspended-sediment concentrations were measured using calibrated optical backscatter sensors (OBS, D&A Instruments). The NT site benefited from the use of a three-channel (1, 2, 4 MHz) acoustic backscatter sensor (ABS, Aquatec), which provided a proxy for SSC in the bottom ~1 m of the water column. Data were corrected for range and spherical spreading as described by Thorne et al., 1993. The 1 MHz channel of the ABS also provided

bed-elevation data, allowing for characterization of events resulting in change >1 cm (e.g. Traykovski et al., 2007). Bed-elevation was defined as the strongest gradient in the response of the 1 MHz sensor, as this is indicative of a distinct change in the acoustic media. The multiple 1-cm fluctuations with no associated increase in SSC are likely a product of the coarse bin spacing of the sensor (1 cm) and subtle changes in ABS response at the bin boundaries. In contrast, bed elevation at the ST site was measured using an acoustic altimeter on the ADV (Nortek Vector) with 1-mm resolution, allowing for a more detailed understanding of the timing and vertical resolution during and after bed-shaping events. Acoustic signals were used to measure seabed elevation. This approach change requires a degree of caution, however, as several studies have shown that seabed liquefaction and/or scour under the tripod feet can cause the tripod to sink into the sediment, resulting in apparent accumulation (e.g., Jaramillo et al., 2007, Palinkas et al., 2010). To verify that apparent deposition was due to accumulation of new material rather than tripod setline, pressure data were low-pass filtered to remove tidal signals. To determine the specific processes responsible for the observed trends in the bed-elevation data, the first-order controls on bed stress were examined, namely wave height and period, and near-bed current speed and direction. Their influence was evaluated relative to location and concurrent bed-change type

SSC from OBSs was calculated based on the linear relationship between the instrument voltage response to known concentrations of local sediment in a laboratory setting following field deployment (Ogston et al., 2000). Biofouling of optical instrumentation was an issue, particularly at the ST site, where sensors became obscured within weeks after deployment. As a result, SSC data presented from the ST site are estimated from the acoustic response of the ADV correlated with the calibrated OBS response at 1 meter above bed (mab) during the period at the

start of each deployment before biofouling. Sediment flux was calculating by summing the product of suspended-sediment concentration and ADV-measured water velocity over the periods indicated.

Wave heights were calculated by extrapolating near-bed velocity and pressure fluctuations, using linear wave theory. Shear velocities were estimated based on the Grant-Madsen model (Madsen, 1994), which incorporates current velocity, wave-orbital velocity, wave period, and bed roughness. An estimate of the resuspension velocity was determined by comparing combined wave-current shear velocity (U_{*wc}) with OBS-obtained SSC. The average of the minimum bed stresses at which the lowermost OBS (26 cmab) showed an increase in backscatter was selected as representative of the resuspension threshold.

Tripods had simple sediment traps for collecting sediment used to perform OBS calibrations. Bulk trap material was also analyzed for the presence of ^{7}Be via gamma spectroscopy (Ortec and Canberra planar detectors) using a method modified from Sommerfield et al. (1999). ^{7}Be is a naturally occurring radioisotope with a relatively short (~53 days) half-life, produced from cosmic-ray spallation in the atmosphere (Olsen et al., 1986). ^{7}Be is typically detectable for 4-5 half lives, and as such, the presence of ^{7}Be in sediment suggests recent (<6 month) input of terrigenous material to the ocean environment (Sommerfield et al., 1999).

In addition to the instrumented tripods, gauged water-discharge data, and selected suspended-sediment measurements for the Waipaoa River were obtained from the Gisborne District Council (G. Hall and D. Peacock, pers. comm.).

2.2.2 Seabed Coring

Cores were collected during surveys undertaken in January 2010, May 2010, September 2010, and February 2011 to monitor seasonal changes in the seabed. An Ocean Instruments

MC800 multi-corer was used to collect all cores, which were ~10 cm in diameter and <60 cm in length. For more textual and geochemical analysis see Walsh et al. (2014). In this study, we focus on x-radiographs of cores collected at the tripod sites. Rectangular slabs from the multicores (8W x 2.5D x 60L cm), were x-rayed using a Varian PaxScan 4030E flat panel digital imaging system and an Ecotron EPX-F2800 portable veterinary x-ray generator. Exposure type, grey-level mapping, and exposure window/level were controlled via proprietary Varian software (ViVA 2.0, Revision L.04), and typical generator settings were 50 kV and 25 mA. X-radiography reveals changes in bulk density invisible to the naked eye; lighter colors represent higher bulk densities, typically from coarser-grained sediment. Images were further adjusted to maximize contrast between individual strata. As a result, while relative density changes might be visible within an individual core, comparison of absolute density between separate cores is not possible.

2.3 Results

The 2010 study year was a typical discharge year, with total-annual water discharge representing the median for the preceding five years (data not shown). The austral winter months (June-Sept) exhibit the greatest amount of total river discharge, although the three largest floods during our study year were evenly spaced in January (2451 $m^3 s^{-1}$), July (1737 $m^3 s^{-1}$), and October (2161 $m^3 s^{-1}$) (Fig. 2.2), with measured SSC's at peak discharges >10 g l^{-1}. The austral winter provided the most energetic wave and current conditions, though large waves were observed throughout the year (Fig. 2.2). Reflective of the dynamics on the shelf, ^{7}Be was detected in the sediment traps from both tripods in May and September 2010, but not in February 2011.

2.3.1 Near-bed conditions

At the NT site, near-bed currents were typically oriented along-shore (NE-SW), with maximum speeds at 1 meter above bed (mab) approaching 0.50 m s^{-1}, and a mean of 0.09 m s^{-1} (Fig. 2.2). The mean of the measured significant wave heights was 1.4 m, with a maximum height of 5.6 m. The mean wave period was 11.5 s, with a maximum of 14.9 s. Wave-orbital velocities were 0.01 m s^{-1} - 0.61 m s^{-1}, with a mean of 0.13 m s^{-1}. Suspended-sediment concentration (SSC) at 26 centimeters above bed (cmab) varied considerably from 0.01-4.30 g l^{-1}, with a mean of 0.14 g l^{-1}. In general, SSC increased proportionally with wave-orbital velocity.

At the ST site, near-bed currents measured at 0.3 mab were also generally oriented shore parallel (NE-SW) though slightly weaker and more directionally variable than those measured at 1 mab at the NT site, with a peak speed of 0.35 m s^{-1} (Fig. 2.3). When data were available, peak currents measured at 1 mab were, on average, 0.01 m s^{-1} faster than at 0.3 mab at this location. Mean significant wave height was 1.5 m and peaked at 6.0 m. Mean wave period here was 11.9 s and peaked at 15.5 s. SSC ranged from 0.01-0.32 g l^{-1}, with a mean of 0.02 g l^{-1}. SSC was generally lower in magnitude at the ST site than the NT site, though direct comparison is complicated by differences in instrument elevations at each site.

2.3.2 Event characterization and seasonal distribution

For this study, we define a bed-resuspension event in this system as any oceanographic period during which peak U_{*wc} exceeded 0.03 m s^{-1} at the NT site (Fig. 2.4). This peak is three-times greater than the estimated threshold for sediment resuspension (0.01 m s^{-1}) and encompasses 33 instances of elevated near-bed SSC evident in the ABS record at the NT site. Over the complete time series, the minimum resuspension threshold is exceeded much of the time (85%), but only 22% of the time (1914 hours) do conditions meet the “event” criteria described above.

The NT site record was selected as the most appropriate for event definition due to its more comprehensive instrumentation package, and the complete year-long record. At the ST site, SSCs were typically elevated during events defined at the NT site (Fig. 2.5). Each location only had one instance of apparent deposition (i.e., an increase in bed elevation) despite water-column conditions remaining below the defined event threshold. These apparent depositional events (NT site April 5; ST site May 10) are included in the event examination.

Tidally filtered pressure data (not presented) indicates that tripod settling occurred during the events in early March and early July. In the case of the March event, settling was commensurate with apparent deposition (~3 cm), to the best of our resolution capabilities. Because seabed and geochemical evidence suggest that fresh terrestrial material was deposited during this event (section 3.6; Walsh et al., 2014), we also consider this event to be depositional. During the July event, the NT settled ~7 cm, resulting in net deposition of ~5 cm. The 5 April event with apparent deposition, on the other hand, was most likely a product of the tripod experiencing a direct impact from an external force, such as a trawl net or anchor. At this time the wave climate remained relatively small (2.5 m max), currents were weak (~0.13 m s^{-1}), as were the resultant bed shear velocities (0.02 m s^{-1} max; Fig. 2.3). SSC peaked at 0.07 g l^{-1}, which, while above the minimum observed concentration from the first deployment (0.01 g l^{-1}), still falls below the mean (0.09 g l^{-1}; Fig. 2.2). These changes were coincident with a near-instantaneous change of 2^{o} in the tripod's roll, as well as a 2 cm increase in mean water pressure.

In general, the Austral winter months (June-August) were the most energetic with 11 total events, compared to 9 in spring (Sept-Nov), 9 in autumn (Mar-May), and 4 events over summer (Dec-Feb, Fig. 2.4). At the NT site, erosional and depositional events were most common during fall-spring, while events with no discernible seabed gain or loss (i.e., "no-change" events) were

distributed evenly throughout the year. At the ST site, erosional events are more common than no-change events, and the only example of deposition at the ST site occurred during a period of weak ocean forcings in early May 2010 (Fig. 2.5). No-change events typically had weaker currents than erosional events and smaller waves than depositional events, and will subsequently not be discussed at length.

2.3.3 NT bed-modifying events

Depositional events are responsible for the majority of seabed change which can be preserved in the stratigraphic record. At the NT site, there were 9 depositional events of >1 cm bed thickness over the course of the study year (Fig. 2.4). Apparent deposition was 1–12 cm in thickness for individual events, and the net change was 1–10 cm over the span of a four-month deployment. Deposition occurred in events that were, with one exception, coincident with increased near-bed SSC. Because U_{*wc} at both locations was largely controlled by wave shear stress (U_{*w}), the frequency distribution of shear-stress during events is very similar to that of the wave height. For this reason, distributions of wave characteristics during each event type are summarized in Fig. 2.6. In general, waves were lower and currents were weaker during depositional events, when compared to erosional events.

Depositional events were characterized by peak wave heights of 3–6 m (2.5–5 times the annual mean), with the bulk of the distribution (55%) occurring when wave heights peaked between 3-4 m (Fig. 2.6). Wave periods during depositional events were typically <11.5 s, and approximately 90% of depositional events occurred when mean current speeds were <0.15 m s^{-1} (1.6 times annual mean, Fig. 2.6).

Seabed deposition predominantly occurred during longer-duration events. Over 75% of depositional events coincided with storms lasting >60 hours, and every event that lasted >100

hours resulted in apparent bed-elevation increase. River discharge at the time of the event is poorly correlated with deposition (Fig. 2.2). With the exception of the major event in July, most deposition occurred when riverine discharge was approximately at its base level, <100 $m^3 s^{-1}$, which is <5% of the peak flows that occurred over the course of the study period (Fig. 2.4).

Ten bed-eroding events were captured, typically of lower magnitude than their depositional counterparts (Fig. 2.4). Erosion occurred exclusively during intense storms of short-duration lasting <54 hours, and 50% of these events lasting <40 hours. Furthermore, as was the case with depositional events, erosional events were coincident with near base-level flow (<100 $m^3 s^{-1}$) (Fig. 2.2). Although waves were elevated during erosion events, peak waves were typically <4 m (3.3 times annual mean) and wave periods were >11 s (Fig. 2.6). Around 70% of erosion occurred when mean current speeds were >0.10 m s^{-1}, and 40% occurred with mean speeds >0.15 m s^{-1} (Fig. 2.6).

2.3.4 ST bed-modifying events

Only a single instance of apparent deposition of 1.1 cm was recorded (Fig. 2.3) at the ST site, but it occurred when U_{*wc} <0.03 m s^{-1} (the threshold for events). The peak current speed during the period of apparent deposition was 0.05 m s^{-1}, and waves were <2 m in height (Fig. 2.3). Corresponding wave-orbital velocities were <0.15 m s^{-1}, and while there was a slight increase in SSC (peak of 0.06 g l^{-1}) immediately prior to the bed elevation increase, SSC during the event was less than 0.02 g l^{-1}. Immediately following the apparent deposition, there was a sharp peak (<1 hr duration) in U_{*wc}. Furthermore, there was no change in the instrument heading, pitch, or roll data (not presented), ruling out the possibility of a physical strike or shift of the instrument. Collectively, we interpret this information to suggest an electronic transient or animal burrowing beneath the sensor was responsible.

In the absence of depositional events, the ST site experienced 13 net-erosional events, and 11 no-change events. There was no obvious difference in current speeds between erosional and no-change events, though waves during erosional events were often taller in height (Fig. 2.6). Here, maximum wave heights were 2–6 m during periods of erosion (1.4–4 times annual mean), with the majority of events occurring with peak waves of 1.5–2.0 m (Fig. 2.6). Peak currents during erosive events ranged from 0.05–0.30 m s^{-1} (Fig. 2.6). Only the largest six erosion events resulted in the removal of >0.4 cm, which was considered to be relatively similar in magnitude to the >1.0 cm events recorded at the NT site due to the difference in sensor resolution.

2.3.5 Sediment flux

Sediment flux is stochastic at both tripod locations (Figs. 2.7-2.8). A single event in early July accounts for 40% of the net-annual, across-shelf flux at the NT site (~3000 g cm^{-2}) and the majority of along-shelf flux (to the north east) for both mid-shelf locations. No across-shelf event resulted in flux of >300 g cm^{-2} for the ST site (Fig. 2.8).

The NT site is estimated to experience approximately seven times greater flux than the ST site in the along-shelf-positive (i.e. to the northeast) direction (~7000 g cm^{-2} vs. ~1000 g cm^{-2}; Figs. 2.7-2.8). While the net-annual offshore flux in the north was approximately the same as the net across-shelf direction (~7000 g cm^{-2}), there was a negligible amount of net flux across the southern shelf, relative to the along-shelf component.

2.3.6 X-radiography

X-radiographs of cores show a wide array of structures and stratigraphic variability at the NT site (Fig. 2.9; Walsh et al., 2014). A comparison of replicate cores collected from the tripod sites over 13 months shows distinct changes to the surficial strata. In January 2010, there were

alternating layers of higher and lower bulk density (~2-3 cm thick), with bioturbation features visible in the upper ~5 cm. In contrast, the core collected at the same location in May 2010 showed lower-bulk-density material in the surface 2-3 cm, overlying a mottled and more x-ray-opaque layer. This mottled layer resembles the surface of the January 2010 core in both thickness and relative bulk density. The core from September 2010 had a surface layer with 3 cm of lower-bulk-density sediment overlying 2 cm of wavy bedding, overlying a bioturbated layer. The core from February 2011 resembled the September 2010 core, but with a higher degree of bioturbation at the surface (Fig. 2.9).

Most cores collected at the ST site had mottled sediment with little or no evidence of physical lamination, suggesting a relatively high degree of bioturbation. The ST core from February 2011 showed subtle wavy laminae at the uppermost surface; however, instrument loss precluded our ability to observe bed-elevation change (Fig. 2.9).

2.4 Discussion

Bed-elevation changes (i.e., erosion or deposition) at broad scales are controlled by the divergence or convergence of flux, respectively. Point measurements of water-column and near-bed processes reflect divergence or convergence in a region of the shelf seabed potentially undergoing deposition or erosion. Evidence suggests that sediment flux is largely controlled by discrete events (Figs. 2.7-2.8), and over the course of this one-year study, 33 events were identified during which near-bed processes generated elevated SSC on the shelf. The July event, which will be addressed specifically, was responsible for ~40% of the f flux at this location and resulted in deposition of up to 5 cm of new seabed material in the region of Poverty Gap. Despite similar wave and current conditions, the ST site showed ~1.5 cm of erosion during the same event, suggesting flux divergence across the two shelf regions.

Small mountainous rivers in temperate regions are typically characterized as having strongly seasonal river discharge and oceanic energy (Kniskern et al., 2011; Milliman and Syvitski, 1992), with these two factors being well correlated in time. Although our time-series data from the Waipaoa sedimentary system shows that the majority of events (of all types) occurred during the Austral winter months (June-August - 16 events), we do observe examples of major sediment discharge and depositional events in all seasons. Such a wide temporal distribution in forcing processes has been documented elsewhere, and contrasts with the more seasonal pattern observed at other temperate small mountainous rivers, such as the Eel (Ogston et al., 2000), Pescara (Fain et al., 2007), and southern California rivers (Warrick and Milliman, 2003).

2.4.1 Conditions promoting deposition and erosion

While the two locations on the Waipaoa shelf experienced similar physical forcings such as wave heights and current speeds, sediment transport and sedimentation between the two sites varied greatly. A comparison of bed stressors to seabed-elevation change suggests that long-duration storms with high waves and weak currents are most likely to result in deposition at the NT site (Table 2.2). While deposition can occur over a range of conditions, it appears that deposition is more likely (than erosion or no-change) when waves are >3 m with periods <11.5 s, and current speeds are <0.1 m s^{-1} (Fig. 2.6). This implies that, in the absence of a strong circulation pattern, resuspended material on the mid-shelf was not typically removed by energetic wave conditions, and that new material was supplied via advective fluxes from shallower and more strongly wave-resuspended areas. While sediment was ultimately sourced from the Waipaoa River, as suggested by the ^{7}Be signature, the distance (10-20 km) and weak across-shelf currents indicate that flood discharge did not directly replenish the seabed during

these resuspension events (Fig. 2.2). Only the largest July 2010 event resulted in river-fed accumulation at any tripod site, during a period of elevated discharge.

In contrast, erosional events at the NT site tend to coincide with relatively smaller wave heights (<2.5 m) but longer periods (>11 s) than depositional events (Fig. 2.6, Table 2.2). Currents were typically stronger during erosional events than depositional events, so it appears that material resuspended by waves and currents is removed from the vicinity, rather than redeposited after the seabed energy subsides. Stronger circulation on the shelf is evident from modeling studies, which likely induces along-shelf transport that disperses sediment from the local area (Moriarty, 2012). Erosion occurs during shorter-duration storms that typically last <48 hours. These shorter-duration events with lower-height and longer-period waves appear to move sediment along-shelf and away from local sites of deposition while shorter-period and higher waves result in deposition. These steeper waves (larger height, shorter period; Fig. 2.6) produce greater orbital acceleration, in addition to orbital velocity, and may be an important control of sediment resuspension on wave-dominated shelves, expanding on the findings of Woeffel and Elgar (2003). The implication is that if steep waves are effective at resuspending sediment near the mid-shelf, resuspension will be more intense in shallower waters including sediment-laden Poverty Bay, which can act as a short-term sediment repository (Bever et al., 2011). This newly available material can then be delivered to the mid-shelf via diffusive, advective and/or gravity-driven flow.

Although the ST site experienced similar environmental conditions to the NT site, it was net erosional over the study period, losing ~4 cm of bed elevation (Fig. 2.5). Here, waves tended to be slightly taller and steeper during erosional events than during no-change events, while current speeds were almost indistinguishable (Fig. 2.6). This observation further stresses the

importance of readily available sediment for resuspension and deposition. The ST site is located >20 km from the mouth of the Waipaoa River, and is not directly down bathymetric slope from the mouth of Poverty Bay, so it lacks a direct pathway between sediment source and the deposit. Net erosion during the study was an unexpected result, given that previous work has shown that this region of the shelf is the locus of rapid accumulation on multi-decadal (Miller and Kuehl, 2010) and millennial time scales (Gerber et al., 2010). Though the seabed was net erosional during this study, ^{7}Be was detected in the sediment traps mounted at several elevations on this tripod during all but the final deployment (when the tripod was damaged and moved by fishing activities, and no traps were retrieved), suggesting that new terrestrial sediment was nourishing this region, but not building the bed. A possible explanation for this difference across accumulation timescales is annual to decadal-scale fluctuations in the circulation and resulting accumulation pattern on the shelf. Currents were predominantly to the north and east at both tripod locations (Figs. 2.2 and 2.3). Data in Walsh et al. (2014) and Kniskern et al. (2014) show widespread ^{7}Be deposition on the shelf, particularly on the northern shelf. Although event deposition sites off small mountainous rivers can be co-located with century-scale accumulation sites (e.g. Eel River – Sommerfield and Nittrouer, 1999), the Waipaoa shelf may be more similar to larger systems such as the Fly River, where temporal changes in the locus of deposition on the shelf can be controlled by subtle changes in shelf bathymetry or inter-annual climatic forcing, as discussed in Slingerland et al. (2008).

Conditions at both sites during the events that resulted in no bed elevation change tended to be less energetic than during erosional periods. This suggests that limited amounts of bed material is locally resuspended, but not removed from the area. Importantly, we provide

evidence that typical energetic oceanic events alone resulted in negligible seabed change and thus have little chance of being recorded in the stratigraphic record.

2.4.2 Role of river discharge and event duration

On three occasions in the 2010 study year, river water discharge exceeded 2000 $m^3 s^{-1}$, with river SSC likely >10 g l^{-1}. Surprisingly, in two of these cases (January and October) there was no corresponding increase in SSC recorded at the shelf tripods or in seabed elevation on the mid shelf. Bever et al. (2011) used data from an ADCP at the 15-m isobath within Poverty Bay to demonstrate that sediment was temporarily stored following a major discharge event, until subsequent high waves acted to move this material offshore. In their study, an ephemeral sediment deposit of ~7 cm remained in Poverty Bay for one week following peak discharge, until a wave event with peak U_{*wc} >0.03 m s^{-1} evacuated this newly delivered sediment. During our study, a core collected within inner Poverty Bay in May 2010 (Waipaoa River discharge ~500 $m^3 s^{-1}$, Fig. 2.2) had a surface layer of ~10 cm of fluidized mud (Walsh et al., 2014). A weak wave climate and hindered settling prevented consolidation of this layer, which would have been readily available for removal offshore in a subsequent wave event. This is not to say that no sediment leaves Poverty Bay during a major flood. Kniskern et al. (2014), using ^{7}Be and geochemical tracers, observe shelf accumulation accounting for >49% of the total flood discharge in relatively well-constrained deposits between the tripods and on the northern shelf, following the January flood. This layer of terrestrial material appears both thicker and more broadly dispersed in cores collected in May 2010, following periods of intense bed stress with minimal additional discharge from the Waipaoa River.

Our observations on the shelf are consistent with the insights of Bever et al. (2011) and Kniskern et al. (this study) which suggest that while river flooding is important, post-flood

conditions determine how and when material moves offshore. With each of the three examples of major flooding, considerable deposition of fine-grained sediment occurred at the NT site after a total of ~120 hours of event conditions (peak U_{*wc} >0.03 m s^{-1}, see section 2.2). Between the January flood and the next event with apparent deposition in March, a total of ~110 hours of event-level bed stress elapsed (Fig. 2.10). After accounting for tripod settling, this event resulted in no net change in bed elevation. It seems that during the early phase of event, strong wave activity eroded several centimeters of bed material, which was advected offshore. This material was replaced by the low-bulk-density material observed in x-radiograph, which is assumed to have been sourced from reworked material originally deposited in Poverty Bay during the flood in January 2010 and advected seaward under the influence of elevated near-bed oscillatory wave motions from the passing storm. Similarly, during the major discharge event in October 2010, the seabed does not show deposition until early November, after ~130 hours of event-level bed stress. In both of these cases, sediment has travelled ~15 km over a ~120 hour period, which suggests an average cross-shelf velocity of ~0.03 m s^{-1}. Cross-shelf velocities of this magnitude could be driven by downwelling currents (e.g., Puig, et al., 2001), shelf circulation (e.g., Pullen and Allen, 2000) or density-driven flow (e.g., Traykovski et al., 2007).

The single example of concurrent deposition with major river discharge (July 2010) resulted in enhanced bed building. After several weeks of minor river-discharge events, the July event was driven by an intense low-pressure meteorological system which stalled offshore for nearly a week (140 hours) with intense precipitation and high waves from the southeast. Approximately 40 hours after the start of the major flood on July 1, a significant 5-cm increase in bottom elevation was recorded at the NT site, after accounting for tripod settling. Prior to July 1, a series of smaller floods had occurred, and ~110 hours of “event-level” bed stress occurred

between these smaller floods and the observed deposition. A detailed examination of the ABS data during the depositional event reveals two strong reflectors; one at the top of the lutocline, and one coincident with the seabed prior to, and following, the wave event, interpreted as the seabed (Fig. 2.4, inset). Typically, the ABS response shows increasing backscatter from the lutocline to the seabed. That the acoustic signal was almost entirely attenuated by the high SSC suggests that a combination of prolonged wave energy and elevated discharge resulted in the formation of a gravity flow on the inner shelf, which flowed to the mid-shelf and caused a rapid bed accumulation at the NT site. Assuming a standard Rouse SSC profile, and using settling velocities typical of the sediment at this location (.03-.5 cm s^{-1}), concentrations at the top of the wave-boundary layer approach 10 g l^{-1} during this event. Furthermore, benthic-boundary-layer current directions indicate that this flow may have carried material offshore through Poverty Gap. This gravity-flow pathway is consistent with radiochemical evidence of ^{7}Be measured from a core collected in Poverty Gap in September 2010 (Walsh et al., 2014). Despite the fact that oceanographic forcings were not the most energetic recorded (i.e., U_{*wc} was not superlative, Fig. 2.2), it seems that the longevity of near-bed motions generated by this storm were sufficient to support the delivery of the river discharge pulse to the study area.

These results provide a timeframe for a previously under-explored factor in seabed morphology for small mountainous river systems. While the Waipaoa system was initially selected to compare and contrast with other focus sites that have undergone similar styles of investigation such as the Eel River (e.g., Ogston and Sternberg, 1999; Traykovski et al., 2000), it appears that despite similar dimensions and physical conditions to the Eel, storm duration takes precedence over intensity in controlling shelf sediment supply. Similarly, while the Waipaoa and Waiapu systems are geographically close, both drain the Raukumara ranges and are subject

to the comparable climates and storm impacts, differences in river flow characteristics and shelf dynamics result in different responses to storm events and river floods. On the muddier Waiapu (average annual sediment discharge of 35 Mt yr^{-1}, Hicks et al., 2011), the river frequently achieves hyperpycnal sediment concentrations (Hicks et al., 2004), and the inner shelf lacks a sheltered receiving embayment like Poverty Bay, resulting in strong coherence between river flood and shelf response (Ma et al., 2008). Although storms and floods are often coherent in the WSS, evidence presented herein implies that flood-event layer deposition is a function of marine conditions; fresh riverine material is seldom immediately delivered to or beyond the inner shelf.

2.4.3 Seabed manifestation

While every event contributes to the sediment flux on the shelf, the data herein highlight that not every event is recorded in the seabed strata everywhere, nor do all event deposits get preserved. On the Waipaoa mid-shelf, it appears that only two events (March 2010, July 2010; Fig. 2.4) during our study year were translated into the initial marine sedimentary record at the tripod sites (Fig. 2.9). These events each led to several centimeters of apparent deposition around the NT site according to x-radiographs and radiochemistry (see Walsh et al., 2014), and in the case of the July event, the seabed elevation data. While the sediment cores provide snapshots for bed modification on months-long timescales, the seabed is in a state of nearly constant change.

The lack of significant seasonal change in the strata of the southern shelf is consistent with the observations of Rose and Kuehl (2010), who report minimal evidence of physically laminated sediment and accumulation rates of 0.25-1.4 cm yr^{-1}. This is below the accumulation rate threshold at which benthic fauna typically cannot survive (2 cm yr^{-1}, Kuehl et al., 1985), suggesting that even when riverine or recently mobilized inner-shelf sediments are delivered to

this region, biological activity will destroy evidence of physical strata. Based on the tripod records suggesting consistent erosion, we did not expect to see the creation of any new depositional strata. Only one of four cores collected simultaneously at the ST site in February 2011 (at the conclusion of our field experiment) shows wavy laminations consistent with wave reworking of the seabed. The lack of ^{7}Be in this layer suggests that this resulted from wave resuspension and bed reworking, rather than the arrival of fresh terrestrial material.

At the NT site, all cores collected were physically laminated with moderate bioturbation, similar to the observations made by Rose and Kuehl (2010), which confirms that physical processes dominate the stratigraphic record in this region of the shelf. The 2-3 cm of low-density sediment observed in the core collected during May 2010 (Fig. 2.9) is most likely sourced from the January flood-derived sediment initially deposited within the shallow confines of Poverty Bay. This sediment was transported seaward onto the shelf after an extended period (~110 hours) of strong bed stress over the succeeding 3 months. The wavy laminated units overlain by low-density material in the September 2010 core (Fig. 2.9) imply wave resuspension, followed by the settling of fine-grained sediment.

Combined, the sedimentary structures and times-series data are consistent with deposits and depositional mechanisms attributed to the wave-supported-gravity flows (Macquaker et al. 2010), where a typical deposit should contain evidence of wave-resuspension, silt and clay laminae, and evidence of fine-grained particle settling. Absence of ^{7}Be in the tripod sediment trap during the third deployment, the lack of obvious newly deposited material in the February 2011 core, and the increased degree of bioturbation in the surface layers (Fig. 2.9), are compatible with the relatively quiescent ocean conditions recorded during the third tripod deployment observed during the summer months (Fig. 2.3). This time-series of seabed structures

shows that, as expected, centimeters-thick event layers are created on the Waipaoa mid-shelf area, but, in the absence of new deposition, bioturbation destroys laminations within several months of emplacement, consistent with the hypothesis proposed by Wheatcroft et al. (2007) for other continental shelves.

2.5 Conclusions

In 2010, we observed 33 instances of bed stress sufficiently higher than the threshold for seabed resuspension that generated increased near-bed suspended sediment concentrations at the NT site, located on the mid-shelf immediately seaward of Poverty Bay. In 19 of these examples, seabed elevations changed by >+/- 1 cm, due to strong physical forcing. During the 8 months of simultaneous recordings at the ST site, 13 erosional events and 11 no-change events occurred. In general, high and short-period (steeper) waves tend to cause a flux convergence and result in deposition at the NT site, while strong currents and smaller height, longer-period waves lead to erosion. In addition, longer-duration events are responsible for the majority of bed-level increase. A lag of ~120 hours of event-level bed stress was observed prior to Waipaoa flood-derived sediment arriving at the NT site, with dispersal typically occurring in a series of short, episodic periods, or one continuous, longer-duration event. In the two examples of apparent seabed accumulation, >3 cm corresponding strata are also visible in x-radiographs of cores collected several months later. These results demonstrate that event duration is an important control on shelf strata formation and preservation.

We also begin to address the four-dimensional nature of shelf systems, where time and space are both important factors for consideration in the development of the shelf sedimentary structure. On decadal scales, both tripod locations are depositional. Despite similar bed stresses, and a similar distance from the coastline as the NT location, the ST site experienced net erosion

during this year-long study. This is due, at least partially, to the distance of downslope sediment travel from its source in Poverty Bay to an off-shelf sink.

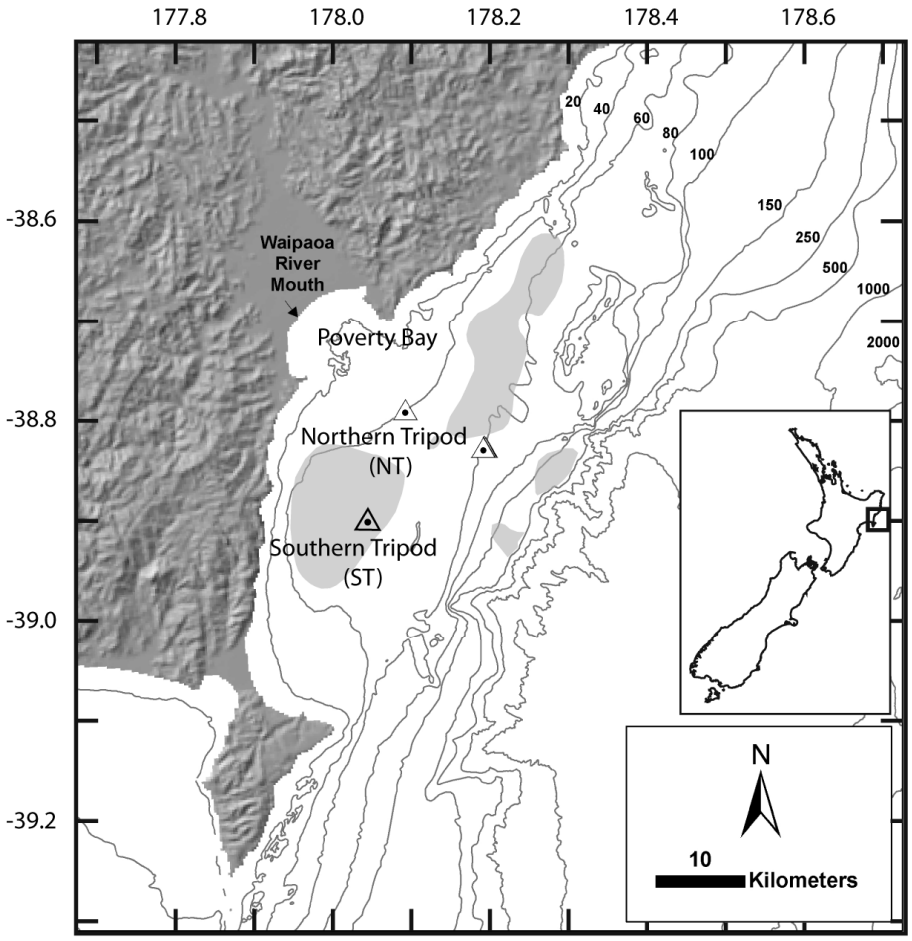

Figure 2.1 – Map of the study area, the Waipaoa Sedimentary System, NZ. Approximate regions of enhanced steady-state accumulation (from Miller and Kuehl, 2010) are shaded in gray.

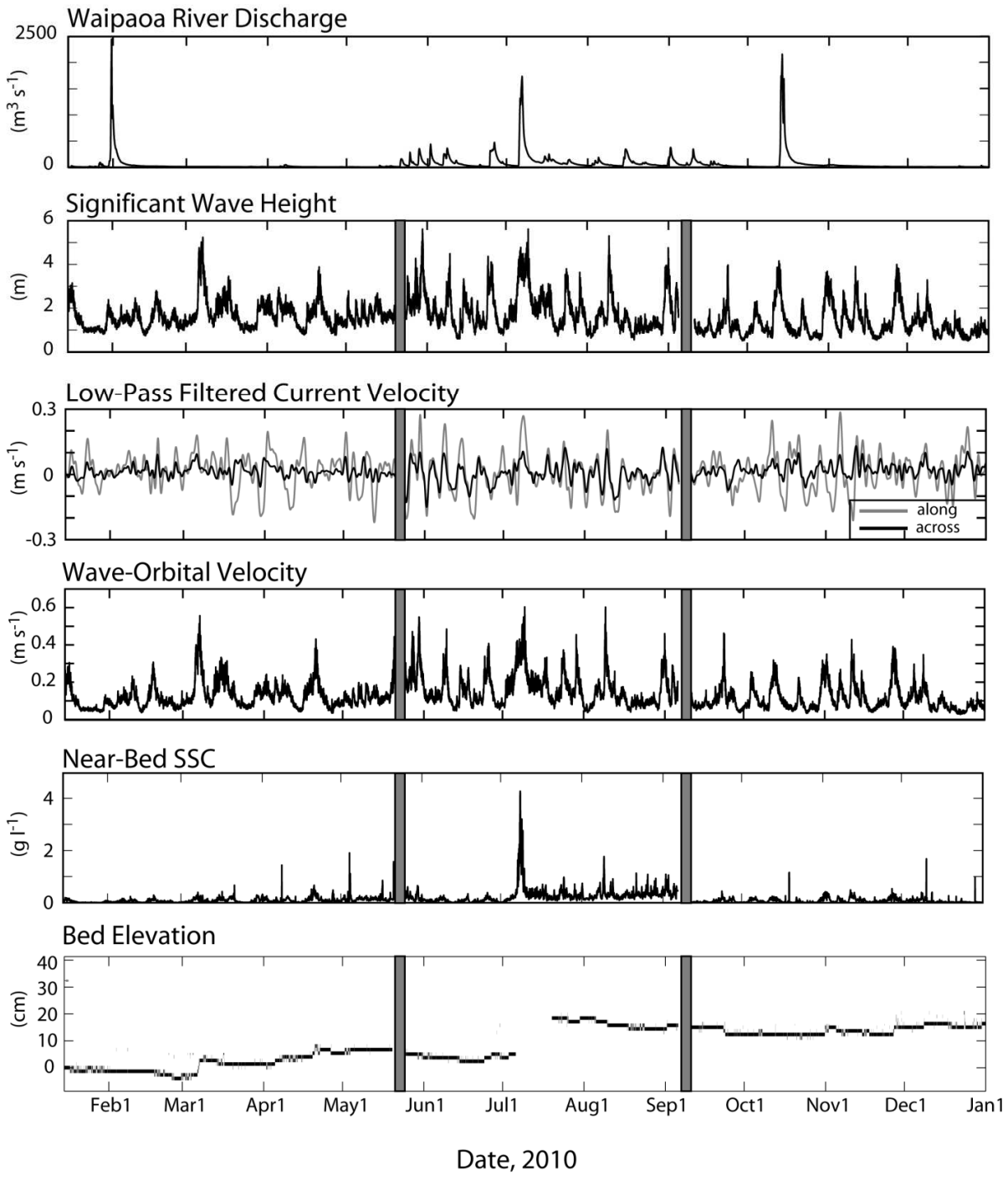

Figure 2.2 – Time series of water discharge from the Waipaoa River, and significant wave height, low-pass filtered current velocity, wave-orbital velocity, SSC at 26 cmab, and seabed elevation change from the Northern Tripod. Gray bars indicate periods of tripod refurbishment. Major water discharge events (>2000 $m^3 s^{-1}$) occur in winter, spring, and summer. Wave events occur year round, with the highest concentration in winter. Note also, that the seabed is net depositional. Gap in seabed data in July is due to attenuation of the acoustic signal by suspended sediment.

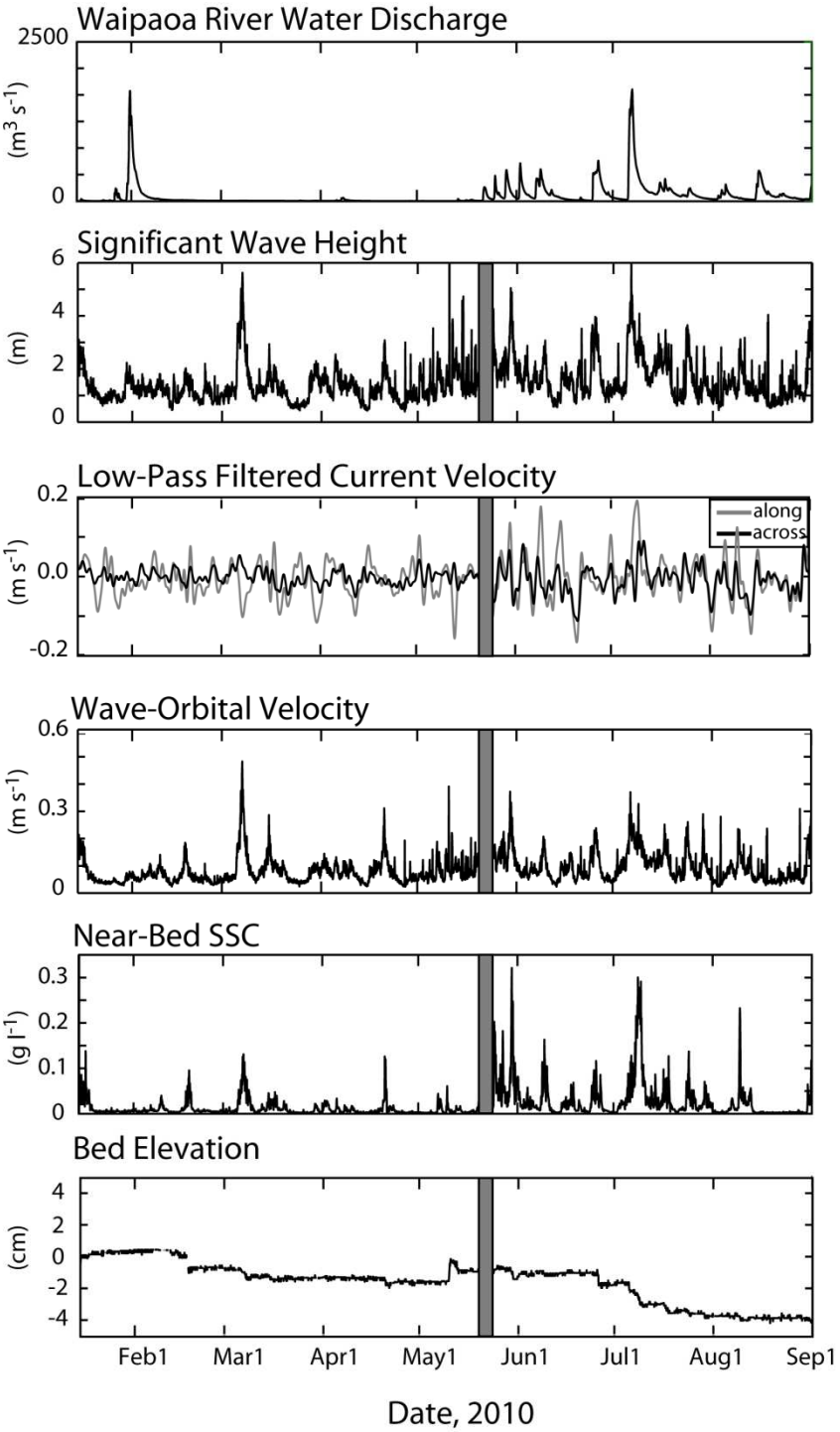

Figure 2.3 – Time series of river water discharge, significant wave height, low-pass filtered current velocity, wave-orbital velocity, SSC at 26 cmab, and seabed elevation change from the Southern Tripod. Gray bars indicate periods of tripod refurbishment. Note that SSC values remain below 0.3 g l^{-1}, and that seabed elevation is net erosional.

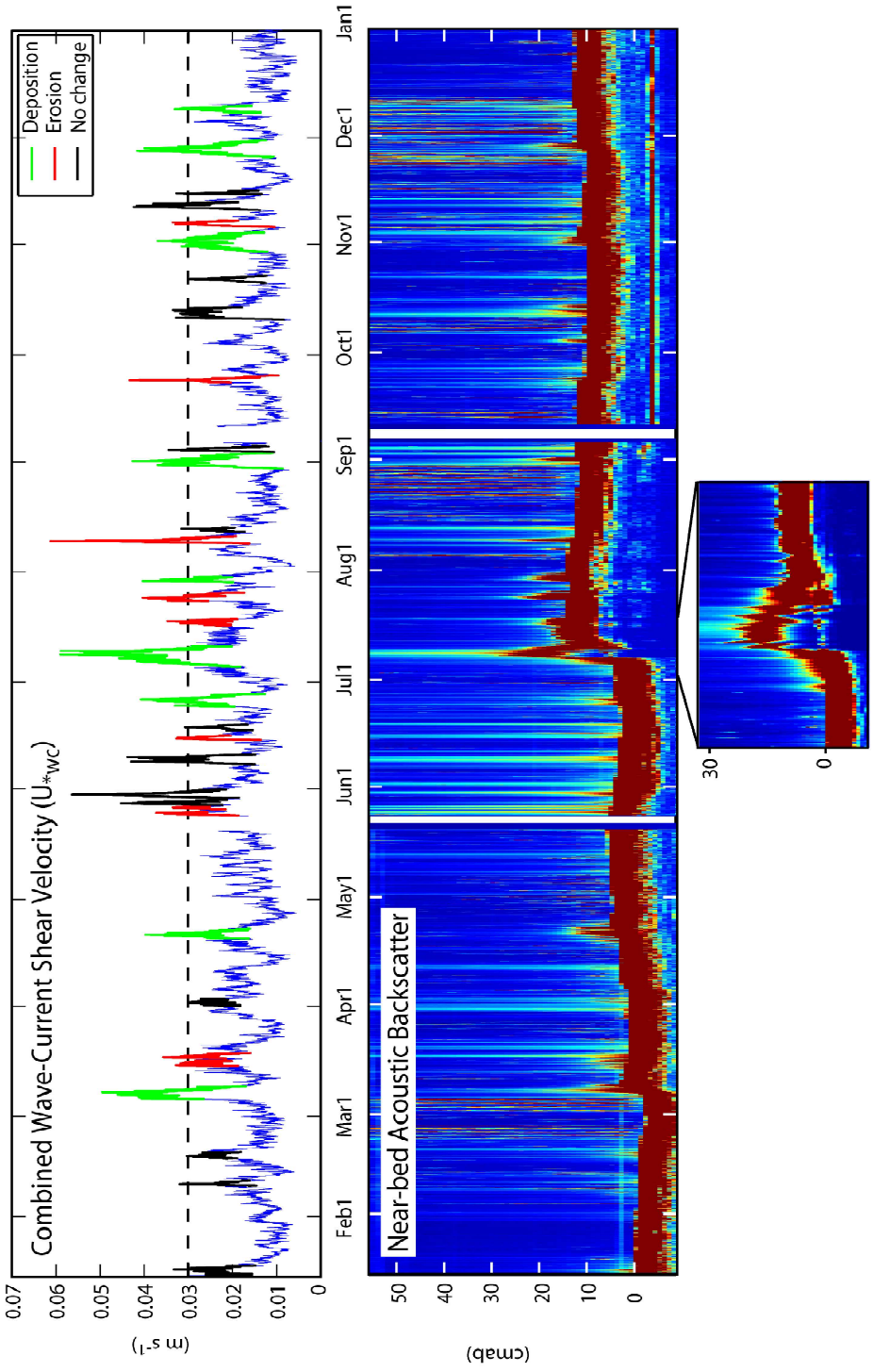

Figure 2.4 – Time series of wave-current shear velocity (U_{*wc}) and near-bed acoustic backscatter from the Northern Tripod. Events are defined as periods surrounding peak U_{*wc} >0.03 m s^{-1}, with depositional events highlighted in green, erosional events in red, and no-bed-change events in black. With few exceptions, elevated near-bed acoustic backscatter occurs during event periods.

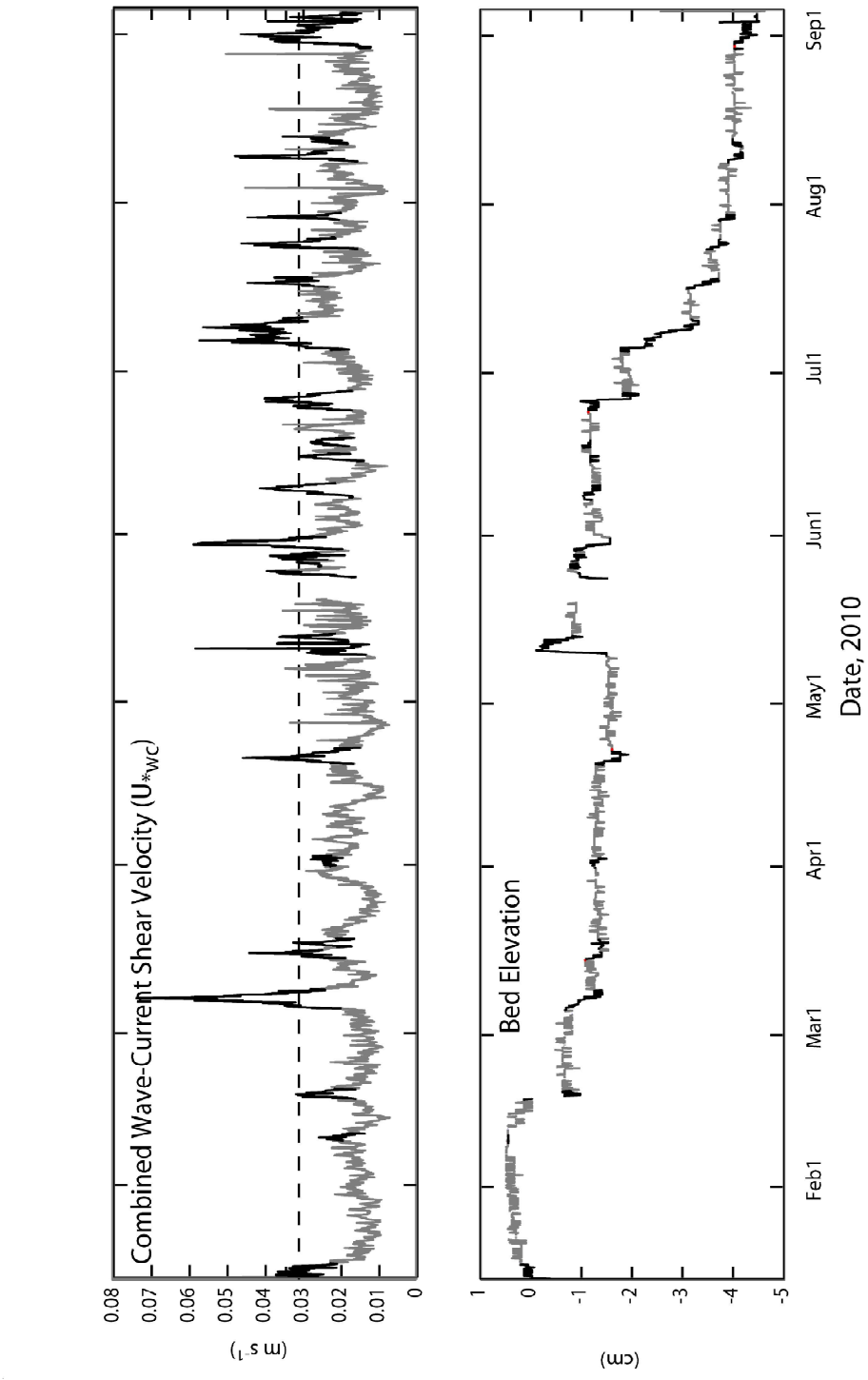

Figure 2.5 – Time series of wave-current shear velocity (U_{*wc}) and bed-elevation change from the Southern Tripod. Events periods (bold) were defined by conditions at the Northern Tripod site, although in general, the timing of peaks in U_{*wc} was similar between sites.

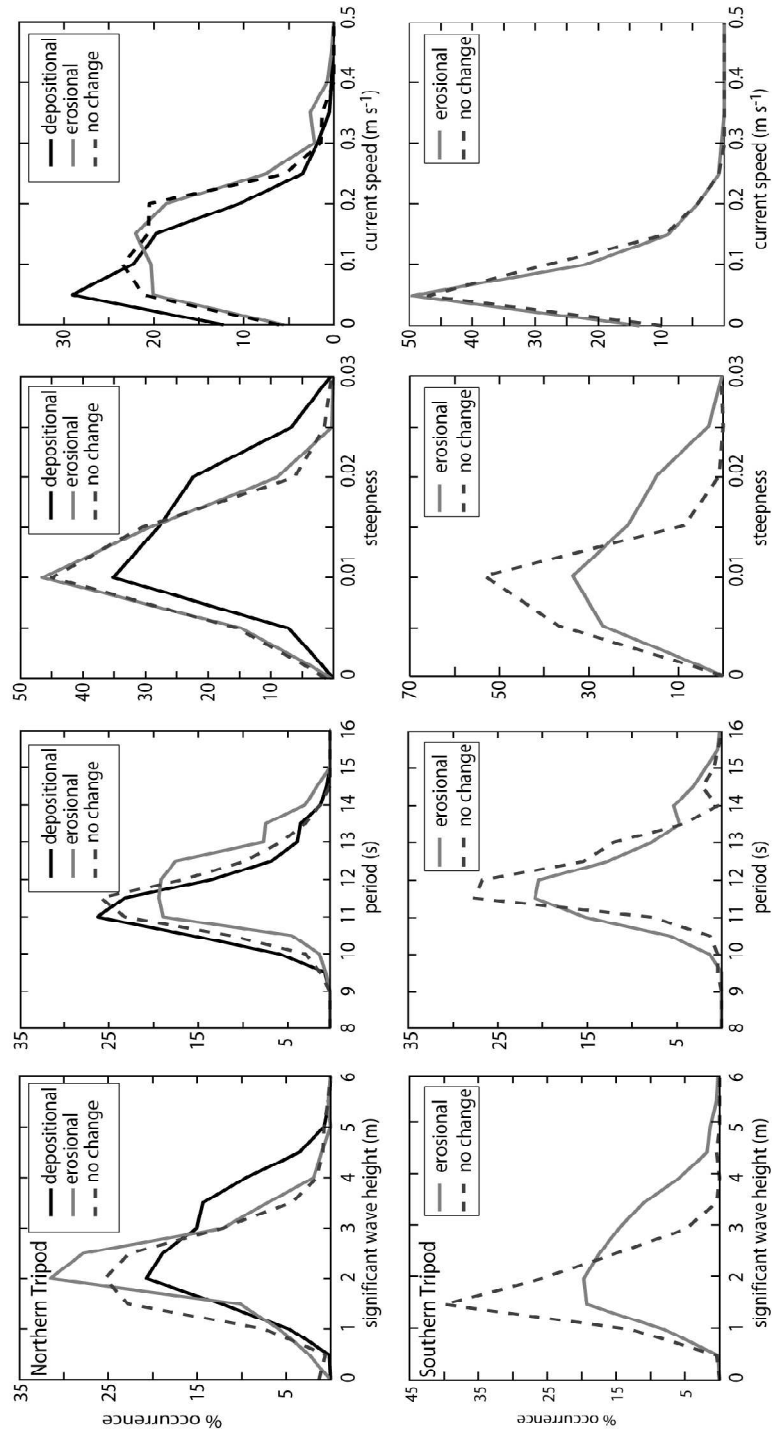

Figure 2.6 – Frequency distributions of wave height, wave period, wave steepness, and near-bed current speed, for the Northern (top) and Southern (bottom) Tripod sites. Deposition at the Northern Tripod site occurs during relatively high waves of short period (i.e. steeper), and relatively slower current speeds, while erosion tends to result from events with shorter-height, longer-period (i.e. less steep) waves and stronger currents. At the Southern Tripod, steeper waves tend to correlate with the observed erosional events.

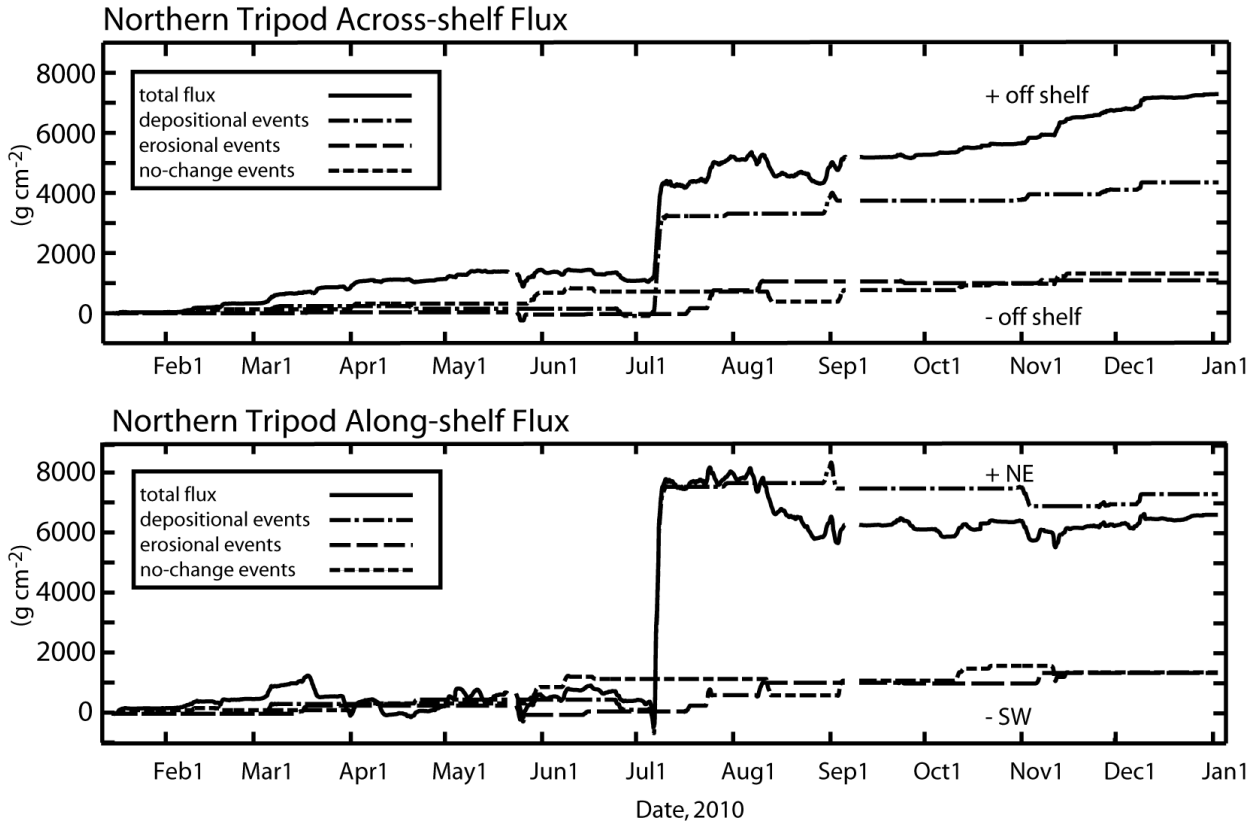

Figure 2.7 – Northern Tripod cumulative sediment flux in the across (top) and along-shore (bottom) directions. Positive flux is offshore (top) or to the north (bottom). In addition to total flux (solid line), flux during each type of event is depicted with a dashed line (see legend). Note that the July event contributes the greatest amount of any individual event to the total flux in both the across and along-shelf directions.

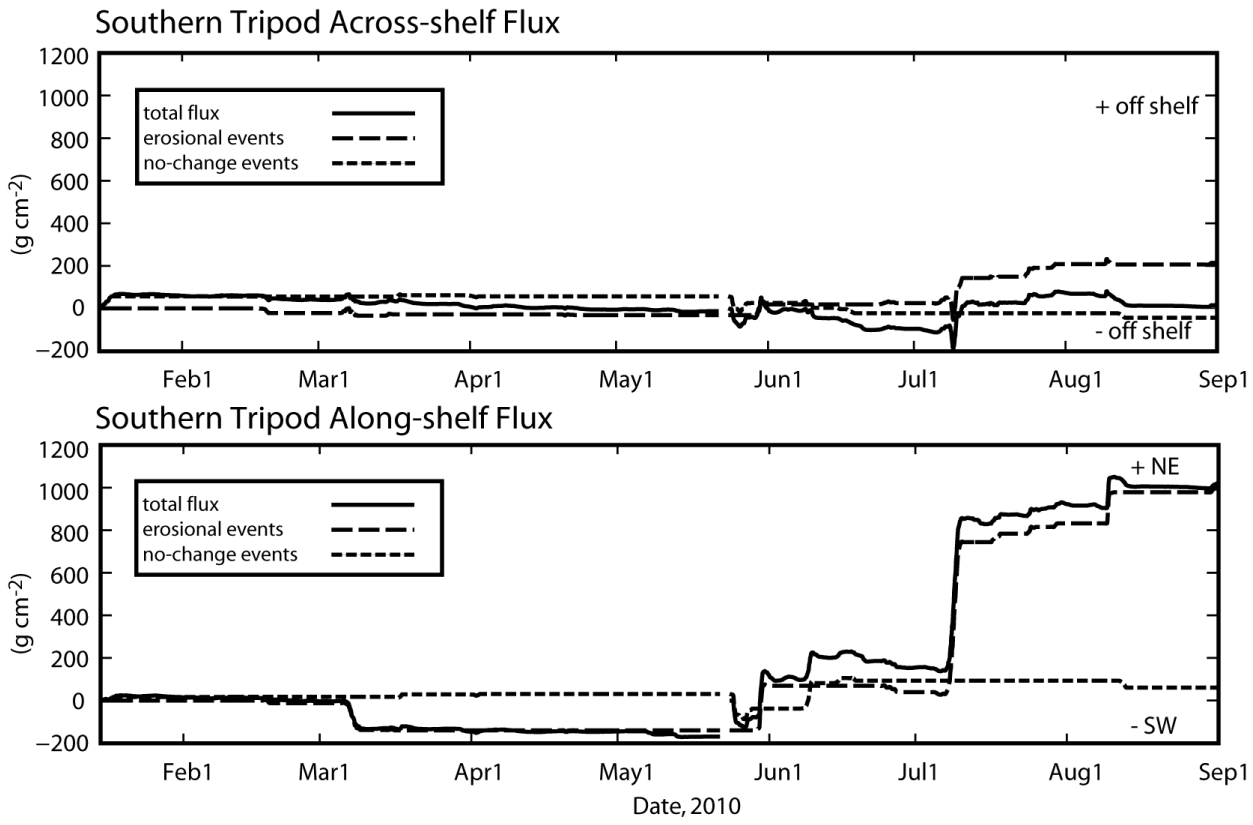

Figure 2.8 – Southern Tripod cumulative sediment flux in the across (top) and along-shore (bottom) directions. Positive flux is offshore (top) or to the north (bottom). Note that cumulative flux is an order of magnitude lower in the along-shelf direction than at the Northern Tripod site, and that across-shelf flux is negligible (~0 g cm^{-2}) at this site.

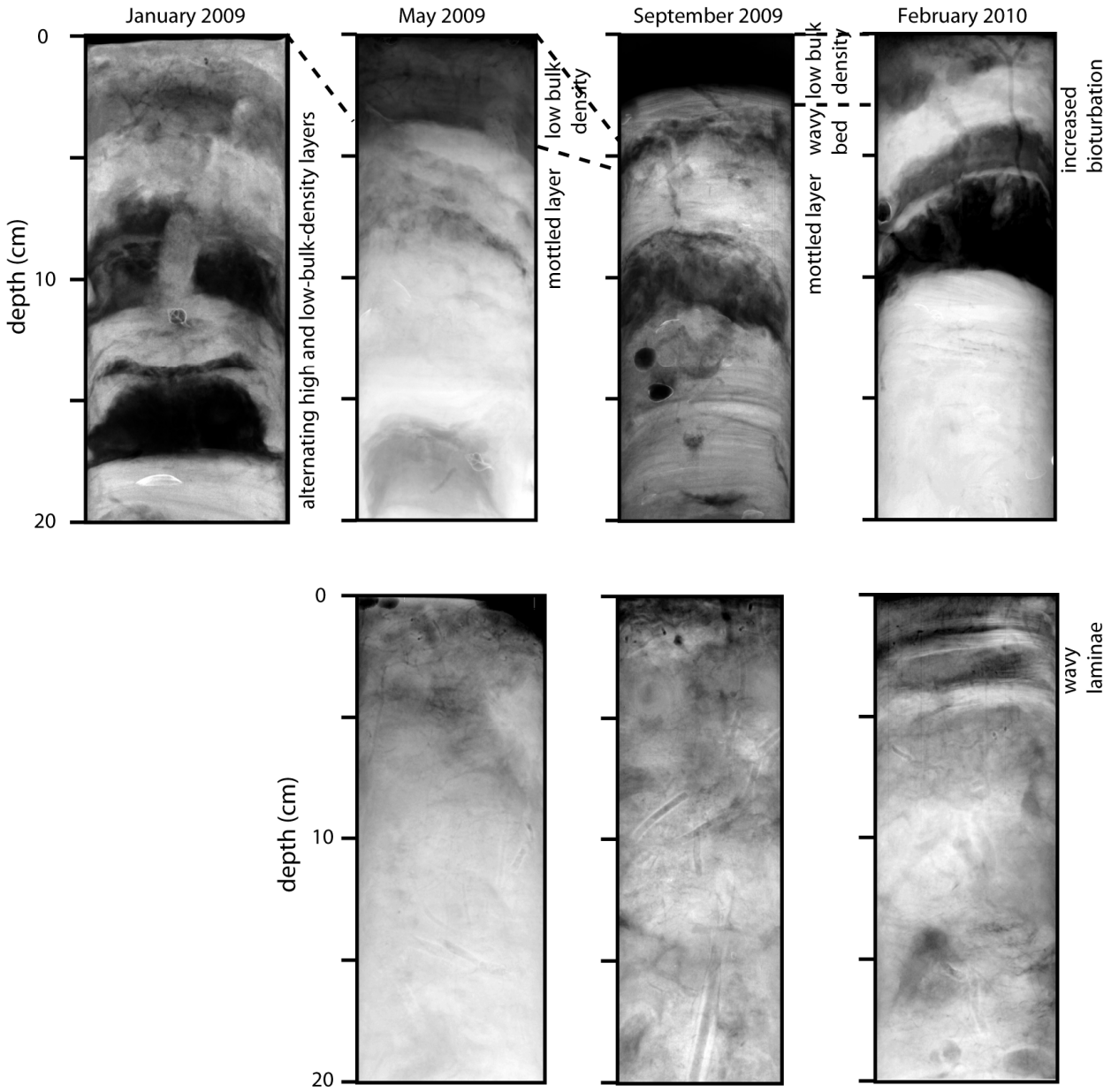

Figure 2.9 – X-radiograph negatives from the Northern Tripod (top) and Southern Tripod (bottom). Darker material corresponds to material of lower bulk density. Significant physical lamination in the Northern Tripod x-radiographs preserves evidence of wave reworking of existing seabed material, as well as the emplacement of fine-grained (presumably) river sediment. Southern Tripod cores show increased bioturbation and minimal physical lamination, consistent with the observed, less energetic near-bed conditions.

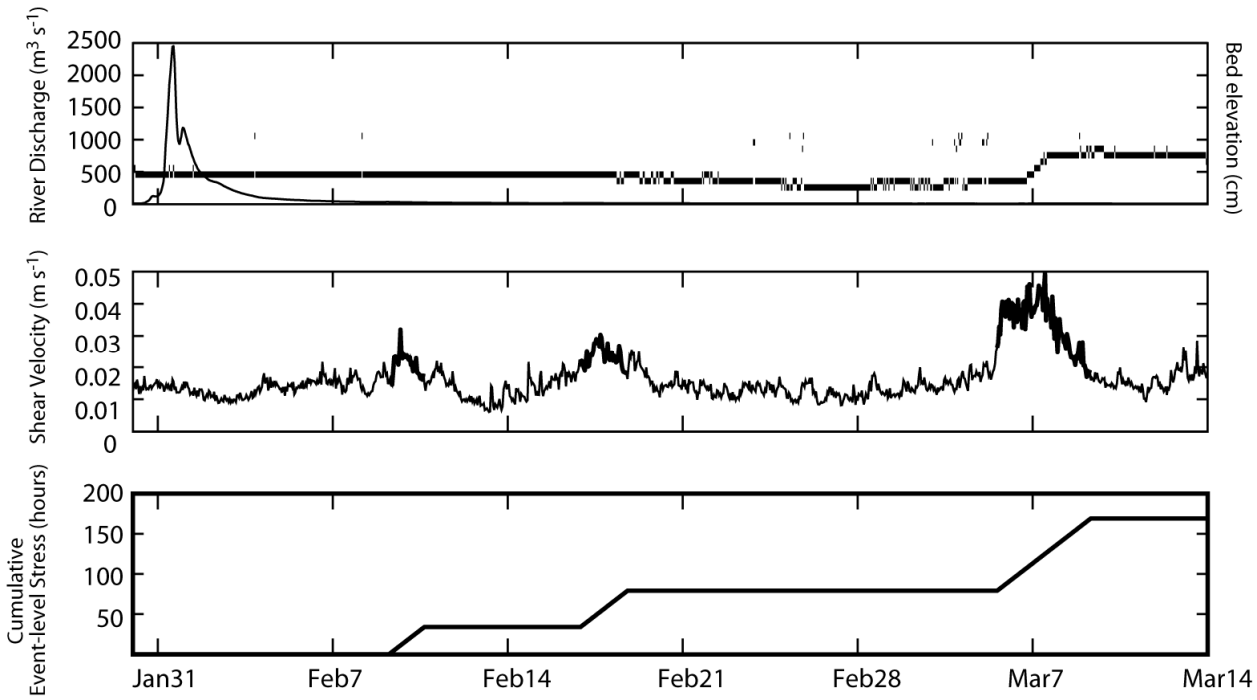

Figure 2.10 – Example of time lag between river discharge, event-level bed stress, and deposition at the Northern Tripod site. Approximately 120 hours of event-level bed stress are required between the peak in flood discharge and bed-elevation change. A similar relationship was observed following each of the three major discharge events.

Instrument	Instrument Elevation – NT (cmab)	Instrument Elevation – ST (cmab)	Purpose
Pressure sensor	140	--	Water surface elevation
Acoustic Altimeter	--	30	Seabed elevation
Electromagnetic Current Meter	30	--	Point velocity measurement
Acoustic Doppler Velocimeter	100	30	Point velocity measurement
Acoustic Doppler Current Meter (upward-looking)	250-surface	250-surface	Current velocities from ~2.5 mab to sea surface
Acoustic Doppler Current Meter (downward-looking)	--	120-bed	Velocity in 3-cm bins from 1.5 m to seabed
Optical Backscatter Sensor	30, 100, 200	25, 50, 100	Point suspended sediment concentration
Acoustic Backscatter Sensor	0-130	--	Near-bed suspended sediment concentration (1 cm bins)
Conductivity, Temperature, Depth	130	150	Salinity, Temperature, Pressure, Depth
Settling Camera	200	--	Determine floc size and settling velocity
Seabed Camera	200	--	Assess seabed bedforms

Table 2.1 – Instruments deployed on tripod frames for this year-long study.

	NT		ST	
	Bed Building	Bed Eroding	Bed Building	Bed Eroding
Storm duration	longer	shorter	shorter	longer
Wave height	higher	lower	lower	higher
Wave period	shorter	longer	no trend	
Mean currents	weaker	stronger	no trend, but < than at NT	

Table 2.2 – Summary of relative conditions during depositional and erosional events at the NT site, and bed-neutral (no-change) and bed-eroding events at the ST site.

Chapter 3:

In-situ observations of wave-supported fluid-mud generation and deposition on an active continental margin

3.1 Introduction

Small, mountainous rivers (SMR) deliver sediment to the ocean at rates disproportionately high relative to their basin area or water discharge (e.g., Milliman and Meade, 1983; Milliman and Syvitski, 1992; Milliman and Farnsworth, 2011). On active continental margins, the relatively short distance between river mouth and deep-ocean sink allows for the potential of rapid delivery of this fine-grained material – and any associated nutrients or pollutants – to an ocean sink (e.g., Milliman and Syvitski, 1992; Ogston et al., 2000; Traykovski et al., 2000; Islam and Tanaka, 2004).

Recent research has identified gravity-driven sediment flow as the dominant mechanism for seaward transport in many shelf settings and environments including active continental margins (e.g., Gulf of Bohai – Wright et al., 1990; Eel Canyon and shelf - Puig et al., 2000; Traykovski et al., 2000; Waiapu shelf, NZ - Ma et al., 2008). Wave-supported fluid muds (WSFM) are a specific type of gravity flow in which wave energy resuspends, or maintains in suspension, the material in transport (e.g., Wiberg, 2000; Wright et al., 2001; Puig et al., 2004). WSFM have been observed associated along active margins (e.g. Ogston et al., 2000; Traykovski et al., 2000), passive margins (e.g. Jaramillo et al., 2009; Kineke et al., 2006), and in the rock record (e.g. Macquaker et al., 2010). Seabed dynamics can impact chemical (e.g., organic material and porewater) and biological (e.g., infaunal) processes (e.g., McKee et al., 2004; Wheatcroft et al., 2006). Furthermore, the mechanism of transport can impact the sedimentary record and thus its interpretation (Macquaker et al., 2010). The specific environmental

conditions required to generate WSFM are difficult to predict, and the high-sediment concentrations generated are challenging to document using acoustic and optical instrumentation. As a result, the body of literature documenting such flows is small but growing.

This study will investigate a WSFM which occurred on the Waipaoa River shelf (New Zealand) in July 2010, at a mid-shelf location near the 40-m isobath. We will use a combination of observational data and analytical solutions to: 1) understand the conditions in which the WSFM formed and compare them to the theoretical formulations, 2) describe and analyze the resulting deposits, and; 3) predict temporal and spatial patterns of deposition associated with WSFM along a cross-shelf transect.

3.2 Background

3.2.1 Regional setting

The Waipaoa River is a small, mountainous river that drains the Raukumura range on the east coast of the North Island of New Zealand (Fig. 3.1). The relatively small catchment (2205 km^2) is located within the tectonically active Hikurangi margin, and receives considerable rainfall (250 cm yr^{-1} at the headwaters, 100 cm yr^{-1} at the coast; Hicks and Gomez, 2000; Page et al., 2001). River floods are relatively short-lived (<2 days) events, which tend to occur during the austral winter months (July-September). However, major floods (~1900 m^3 s^{-1} water discharge) can occur in any season (e.g., Reid, 1999; Hale et al., 2014). Collectively, these forcings result in an average annual sediment discharge of 15 MT, which puts the Waipaoa among the highest-yield rivers globally (Walling and Webb, 1996; Hicks and Gomez, 2000).

The Waipaoa River delivers water and sediment into Poverty Bay, a relatively small (62 km^2), shallow (<30 m) embayment which opens to the east-southeast (Fig. 3.1). Sediment

discharged during river floods is either temporarily stored within the confines of the bay, or advected offshore (e.g., gravity-driven flow) (Bever et al., 2011; Hale et al, 2014; Kniskern et al., 2014; Walsh et al., 2014). Wave energy has a major impact on the trapping efficiency of Poverty Bay, and as much as half of the sediment from a flood can be stored within the bay when discharge events occur during a period of quiescent oceanic conditions (Bever et al., 2011; Kniskern et al., 2014). The continental shelf seaward of Poverty Bay is relatively narrow (< 20 km) and flat (average slope ~0.14^{o}), and is bounded on its seaward edge by a pair of anticlines (Fig. 3.1). The fastest steady-state sediment accumulation observed on the shelf (~2 cm yr^{-1}) occurs behind these anticlines (Miller and Kuehl, 2010). The mid-shelf region between these features shows significant physical lamination (Rose and Kuehl, 2010) and minimal accumulation on decadal scales (Miller and Kuehl, 2010), suggesting a highly energetic depositional environment. Wave energy is the dominant mechanism controlling sediment resuspension and off-shelf flux from the mid-shelf, with longer-period waves of lower wave height (i.e., not locally generated) typically resulting in seabed erosion, and shorter-period, taller waves more likely to result in sediment deposition on the mid shelf (Hale et al., 2014). In general, river-flood sediment escapes Poverty Bay as the result of sequential oceanic storms, defined herein as extended periods of shear velocity >0.03 m s^{-1}. When storms are of sufficiently long duration (~120 hours), coherence between river discharge and the energetic ocean result in the rapid transport of sediment to and beyond the continental shelf (Hale et al., 2014), a phenomenon observed in similar SMR environments elsewhere (e.g., Ma et al., 2008; Wheatcroft et al., 2010). The large and episodic terrestrial sediment signal, combined with the wide range of oceanic forcing conditions, make the Waipaoa Sedimentary System an excellent location in which to study the fate of sediment from small SMRs.

3.2.2 Fluid muds

Fluid muds moving across an inclined surface are a gravity-driven mechanism that can transport large quantities of sediment across bathymetric gradients. Because of their extreme concentrations, fluid muds have the capacity to transport sediment at greater magnitudes than other advective processes (e.g. Ross and Mehta, 1989; Ogston et al., 2000; Traykovski et al., 2000), and always with a component in the downslope (typically off-shore) direction. The importance of fluid muds for sediment transport has been recognized in estuarine (e.g., Kineke et al., 1986) and shelf environments near mouths of large rivers (e.g., Wright et al, 1992). The mixing of fresh, sediment-laden river water and salty ocean water can form aggregate particles and generate convergent estuarine flow, developing a near-bed layer of very high suspended-sediment concentration (SSC) that can move seaward under the weight of its own gravity (e.g., Kineke et al., 1996; Nichols and Biggs, 1985; Ogston et al., 2008). More recently, fluid muds have been observed where bed stresses resuspend (or maintain in suspension) seabed sediment at sufficiently high concentrations to allow for downslope travel via gravity (~10 g l^{-1}; e.g., Traykovski et al, 2000; Puig et al., 2004; Scully et al., 2002). Examples of these flows on the continental shelf include examples where resuspension is due to currents (e.g., near Huange River, China– Wright et al., 1990), waves (e.g., near Eel River, CA – Traykovski et al., 2000), or a combination of currents and waves (e.g., near Waiapu River, NZ – Ma et al., 2008).

Previous theoretical development has provided the framework with which to predict the behavior of WSFM, which in the simplest form can be described as a momentum balance between a downslope pressure gradient and an opposing bottom stress (e.g., Wright et al., 2001, 2002; Scully et al., 2002, 2003; Friedrichs and Wright, 2004; Wright and Friedrichs, 2006; Ma et al., 2008, 2010). In general, the pressure gradient is controlled by slope (α), gravitational

acceleration (g), weight of sediment in water (s), depth-integrated suspended-sediment concentration (C), and the density of sediment (ρ_S). Bottom stress is controlled by the coefficient of drag (C_D), and the maximum velocity ($|u|$), which is the square root of the sum of wave-orbital velocity (U_w) squared, gravity-driven velocity (U_g) squared, and (depending on theoretical development) current speed at the height of the lutocline (V_c) squared (Eq. 1, 2)(e.g., Scully et al., 2002; Friedrichs and Wright, 2004).

$$U_g = \alpha Ri_b |u| C_D^{-1}, \text{ where} \quad (1)$$

$$Ri_b = gsC\rho_S^{-1}|u|^{-2} \quad (2)$$

Regardless of the specific version of this force balance, a pivotal assumption is that above the critical bulk Richardson number (Ri_c) of 0.25, sediment-induced stratification limits turbulence, which eventually results in particle settling (e.g., Trowbridge and Kineke, 1994; Scully et al., 2002). Below Ri_c, turbulent energy can continue to draw additional seabed material into suspension. When the Ri_c criterion is met, the entire bottom boundary layer is filled to its maximum capacity with sediment (Friedrichs and Wright, 2004).

Acquiring detailed observations of WSFM in field-based studies is challenging, due to their localized and ephemeral nature. Furthermore, using sensitive instrumentation capable of detecting thin, near-bed layers in a harsh ocean environment is difficult. To improve our understanding of the controls of WSFM dynamics, several studies have successfully generated high-density formations in laboratory flumes (e.g., Lamb and Parsons, 2005; Houshmand, pers. comm.), and numerical simulations (e.g., Ozdemir et al., 2010a; Ozdemir et al., 2011). These studies provide the opportunity to control individually the specific drivers of WSFM (e.g., U_w, SSC , α), and to observe their behavior in detail. However, relatively few field-based studies

have evaluated the complexities associated with WSFM formation in a natural setting. The Waipaoa Sedimentary System provides an excellent opportunity to study the formation of fluid muds on the continental shelf, as sediment supply from river floods coincides with strong oceanic forcings (e.g., high waves, strong currents) in some cases, whereas in other events, the river discharges into a quiescent ocean. This variety of conditions allows for useful comparisons of WSFM formation processes.

3.3 Methods

3.3.1 Instrumentation

The data presented here were collected as part of a larger, year-long project on the continental shelf offshore of the Waipaoa River (Hale et al., 2014; Walsh et al., 2014). This study of WSFM generation and deposition focuses on 405 hours (~17 days) of data from early July 2010. Data were collected at two locations in hourly bursts using acoustic and optical instrumentation deployed on tripod frames (Fig. 3.1), which recorded the near-bed and water-column movement of water and entrained sediment, and the concurrent changes to the seabed. Tripod locations were selected based on previous studies of seabed characteristics for the Waipaoa shelf (e.g., Miller and Kuehl, 2010; Rose and Kuehl, 2010), and hydrodynamics within Poverty Bay (Bever et al., 2011). More specifically, hypothesized transport pathways from the river to shelf depocenters were targeted for research. The “inner” tripod (NT in chapter 2) was deployed on the inner mid-shelf at 37-m water depth (Fig. 3.1), where the seabed is characterized by significant physical lamination (Rose and Kuehl, 2010). The “outer” tripod was deployed ~10 km seaward, down bathymetric gradient on the outer-mid shelf at 50-m water depth (Fig. 3.1). This study uses data from optical backscatter sensors (OBSs), acoustic Doppler velocimeters (ADVs), upward-looking acoustic Doppler current profilers (ADCPs), pressure

sensors, and an acoustic backscatter sensor (ABS) with transducers at frequencies of 1, 2, and 4 MHz (shallower tripod only). Data were collected hourly in six-minute bursts, which were then time averaged to produce a single measurement (OBS and ADV) or profile (ADCP and ABS) for each hour. Wave heights were determined by extrapolating from near-bed velocity and pressure fluctuations using linear wave theory. Estimated shear velocities were calculated using the Grant-Madsen model (Madsen, 1994). Current velocities at the top of the lutocline were estimated from single point observations at 1 meter above bed (mab) and extrapolating downwards using the Law of the Wall. Seabed elevation was determined to the nearest 1 cm, based on the strongest acoustic reflection observed below the lutocline. In addition to *in situ* instrument data, wind speeds and directions were extracted from a hindcast climate model (EcoConnect®) operated by the New Zealand National Institute of Atmosphere and Water (NIWA), which uses observational data to predict oceanic conditions at a variety of spatial and temporal scales.

OBSs were calibrated in the laboratory following deployment, in a manner similar to that of Ogston et al. (2000). Sediment from the tripod location was added incrementally to a continually mixed container, and the OBS response recorded. Subsamples were extracted at each sediment increment, and filtered at 0.45 μm to determine total suspended matter. The resulting linear relationship between instrument response and measured SSC was applied to the time-series data. Unfortunately, OBS data from the more seaward tripod could not be calibrated, as the instrument was destroyed by the harsh ocean environment during a subsequent deployment. Data from this instrument are presented in their raw units (volts) instead of calibrated units ($g\ l^{-1}$).

ABS calibration required a multi-step process, modified from Thorne et al. (1993) and Traykovski et al. (2003). The instrument was suspended in a continually mixed 100-l container in the laboratory. For low sediment concentrations (<1 g l^{-1}), calibration was similar to that of the OBS described above, where sediment collected at the tripod site was added to the well-mixed container in small increments, with sub-samples collected and filtered to determine SSC at each concentration and at multiple elevations within the tank. Data were corrected for spherical spreading and distance from acoustic source (after Thorne et al., 1993). As with the OBS, a linear relationship between the acoustic response from the 1-MHz channel and measured SSC was expected (Fugate and Friedrichs, 2002), and when determined, was applied to the time-series data (Fig. 3.2). The 1-MHz channel was used for both seabed elevation and SSC measurements because it is less susceptible to attenuation by elevated sediment concentrations than higher-frequency channels. Despite this advantage, at concentrations >1 g l^{-1}, the material in suspension absorbs sufficient acoustic energy to result in a reduction in backscatter amplitude from distal bins (Thorne et al., 1993). To account for this, and subsequently infer SSC, a recursive algorithm was used, based on distance from the sound source, the observed instrument response, and a sound-absorption parameter specific to the sediment from the study area (eq. 14 in Thorne et al., 1993). Sound absorption was determined by incrementally increasing the SSC in the well-mixed container to >10 g l^{-1}, and calculating the reduction in backscatter amplitude from the instrument in the first (most-proximal) bin to the second bin (Thorne et al., 1993; Traykovski et al., 2004).

The recursive algorithm works by adding the signal reduction due to the concentration of the first bin to the signal in the second bin, accounting for the amplitude reduction as determined by the sound absorption parameter. This process is then repeated for the entire ~1 m of ABS

range. One drawback of this method is that at sufficiently great concentrations, a numerical instability prevents the recursive loop from closing, which results in physically impossible concentration estimates (Traykovski et al., 2004). ABS instruments have been calibrated in a similar manner to this study, using a maximum SSC of 33 g l^{-1}, based on the sound absorption parameters of their specific suspended-sediment distribution (Traykovski et al., 2004). In flume experiments with a similar grain-size distribution to this study, observed SSC maxima were 50-70 g l^{-1} (Houshmand, pers. comm.). In our study, we employ a maximum SSC of 50 g l^{-1} (Fig. 3.2). The sound-absorption parameter is reasonable, if not slightly conservative, based on the favorable comparison of SSCs observed by the 26-cmab OBS and the co-located ABS bin (Fig. 3.2).

3.3.2 Gravity-driven velocity

In this study, we estimate gravity-driven velocity using a combination of equations from Scully et al. (2002) (Eq. 1, 2). Seabed slope was determined from local bathymetry sourced from GeoMapApp (http://www.geomapapp.org), which uses data from previous NSF-funded studies in this region (e.g., Kuehl et al., 2006). Bathymetric data were gridded at 144-m resolution. Constant values were assumed for the density of silicate sediment (2650 kg m^{-3}) and the coefficient of drag (0.003). Current speeds, depth-integrated SSCs and wave-orbital velocities were measured using the instrumentation as described above. Based on calibrated ABS data, the lutocline was typically coincident with the 1 g l^{-1} isocline, and was defined as such in this study (Fig. 3.3). Under the assumption that gravity-driven flow will only occur when the boundary layer is full (e.g., Friedrichs and Wright, 2004), Eq.1 was only solved for time periods when the lutocline was above the height of the predicted boundary layer (Fig. 3.3). A complete list of variables and solutions, and their respective ranges can be found in Table 3.1.

3.3.3 Cross-shelf sediment transport

To address whether material resuspended at the inner tripod site could have exited the continental shelf during a wave-supported gravity-flow event, a simple 2-D numerical experiment was performed. In this experiment, Eq. 1 was sequentially solved for every cell of a cross-shelf transect from the inner tripod location the outer shelf where slope could maintain a WSFM with no additional wave or current energy (0.46^{o}; Friedrichs and Wright, 2004). Initial U_g was calculated for each hourly burst ("packet") of data where WSFM assumptions were met as described above, based on conditions at the inner tripod. Then U_g was calculated at each 144-m cell of the cross-shelf transect, under the assumption that the SSC remains constant in every cell. Due to the lack of oceanographic data between the tripod locations, |u| calculated along this transect neglected V_c. Eq. 1 also required an estimate of U_w for every water depth, which we determined using linear wave theory in a method described by Wiberg and Sherwood (2008) based on significant wave heights and dominant wave periods from the inner tripod. This approach tends to overestimate U_w, though the impacts are likely trivial relative to other assumptions in this method (i.e., constant cross-shelf SSC, and SSC $\leq$50 g l^{-1}). Having established U_g for all cells at each observed SSC, every packet was moved offshore (downslope) based on the product of U_g and time. Each packet is moved offshore for the duration of event conditions observed (i.e. within the 405-hour-long event, packet 1 is subject to 405 hours, of transport; packet 405 is subject to 1 hour). In keeping with the simplicity of our approach, we assumed that SSC remains uniform for each packet, regardless of changes U_w, U_g, or α. Furthermore, we assumed that each packet behaved independently of all other packets (i.e., a faster-moving sediment packet did not combine with a slower-moving packet). The assumptions

of our approach resulted in a conservative estimate for both U_g, and distance traveled by the WSFM.

Having determined the gravity-driven velocity for the duration of the event across a shelf transect, we also investigated the potential temporal and spatial distribution of sediment deposition, based on flux convergence and divergence (e.g., Scully et al., 2002). Convergence typically results in deposition, while divergence can result in either erosion or non-deposition (e.g., Ogston et al., 2000; Scully et al., 2002). At the inner tripod, we used the gradient of flux and the bed slope to predict cumulative deposition (i.e., solved eq. 13 from Scully et al., 2002). Across the transect described in this section, we used the gradient of flux to predict locations of deposition, which were then compared with sedimentological and radiochemical studies of the seabed (e.g., Miller and Kuehl, 2010; Walsh et al., 2014).

3.4 Results

3.4.1 Observed conditions

This study focuses on near-bed conditions during the 405 hours surrounding and including the WSFM event in early July 2010. The transport event was responsible for ~40% of the net-annual cross-shelf sediment flux at 1 mab on the mid-shelf (Hale et al., 2014). The calibrated ABS data in this study confirm that an event in early July generated a WSFM at the inner shelf tripod, with maximum concentrations of ≥ 50 g l^{-1} (Fig. 3.3). The fluid-mud event can be broken down into four phases. Initially, as wave energy increased, sediment was gradually brought into suspension, with the lutocline reaching the height of the wave-current boundary layer after ~20 hours of wave forcing (hours 50-71, Fig. 3.3). Winds during phase I strengthened from 5 to 10 m s^{-1}, and shifted clockwise from the northeast to the southwest (Fig.

3.3). Depth-integrated SSC during the initial phase was < 0.7 g cm^{-2}, and current speeds ranged from 0.05–0.15 m s^{-1}.

Phase II of the fluid-mud event was a period of continued high wave energy (U_w > 0.2 m s^{-1}), from hour 72 to hour 132. The lutocline reached a maximum elevation of 0.26 mab, more than double the height of the calculated boundary layer during the same time period (0.11 mab; Fig. 3.3B). Depth-integrated concentration peaked at 10.8 g cm^{-2}, and V_c was much faster than during phase I, ranging from 0.10-0.45 m s^{-1} (Fig. 3.3). Currents at 1 mab remained in the net-offshore direction continuously, and were generally stronger than currents 3.5 mab, by an average of ~0.08 m s^{-1} (Fig. 3.5). Winds during this period were strong (>10 m s^{-1}), and from the south-southwest (200^o; Fig. 3.3).

During phase III (hours 133-176), U_w and V_c decreased dramatically. Depth-integrated SSC initially reduced to 0.5 g cm^{-2}, until the collapse of the lutocline condensed the suspended material into ~50% of its previous volume, increasing the SSC accordingly (Fig. 3.3). Wind direction remained from the southeast to southwest (~150-200^o, Fig. 3.3), though velocity dropped below 5 m s^{-1}. In phase IV, the final event phase, the boundary layer was periodically filled with sediment until hour 350, when the high-concentration, fluidized layer disappeared entirely (Fig. 3.3). U_w and V_c remained relatively low during this period, and winds were generally light (< 5 m s^{-1}) and directionally variable.

Due to the lack of instrumentation focused within the bottom boundary layer at the outer tripod, observations were somewhat limited. SSC at 0.85 mab increased associated with storm-induced wave and current velocities (Fig. 3.4B). This initial peak in SSC appeared to decrease after ~50 hours, despite continued strong U_w and current velocities. Interestingly, SSC peaked again following a reduction in U_w and current energy. The duration and shape of these SSC

peaks at the outer tripod were similar to peaks in the OBS record from the inner tripod. Cross-correlation of the OBS records from each tripod location (Fig. 3.4B) reveal a relatively strong peak correlation ($r^2 = 0.59$) at a time lag of 23 hours. Current speeds 1 mab and 3.5 mab were similar in both magnitude and direction, and were consistently strong and to the northeast (~50^o) for hours 80-130, with little change in direction (data not presented here).

3.4.2 Empirical solution for downslope velocity

At the inner tripod, U_g was determined both with and without the inclusion of V_c in the calculation of $|u|$. In general, the two compared favorably, though "without" typically resulted in WSFM velocities 0.005-0.01 m s^{-1} faster. The values reported in this section (Table 3.1; Figs. 3.4 and 3.5) represent the more conservative estimate, which include V_c, unlike the cross-shelf transport experiment where V_c was neglected. During phase I of the WSFM, the lutocline remained below the predicted boundary-layer height and therefore the criteria for gravity-driven flow conditions were not likely met. During phase II, calculated, peak, gravity-driven velocities were <0.025 m s^{-1}, coincident with the period of highest SSC at hour 92 (Table 3.1; Fig. 3.4). A brief reduction in depth-integrated SSC occurred around hour 120, which, combined with a period of enhanced U_w, had the net effect of slowing U_g to <0.01 m s^{-1}. While conditions for gravity-driven flow were met during phase III, the depth-integrated SSC appeared to decrease drastically, resulting in slower U_g (<0.02 m s^{-1}). During phase IV, the boundary layer was filled only periodically, and when criteria were met, U_g approached a maximum of 0.01 m s^{-1} (Table 3.1; Fig. 3.4).

3.4.3 Cross-shelf transport

Predicted gravity-driven velocity tended to increase in the offshore direction due to the generally increasing slope, for all sediment packets examined in our numerical experiment. The maximum gravity-driven velocity (0.26 m s^{-1}) occurs during phase II of the WSFM (hour 92; depth-integrated SSC = 10.8 g cm^2), 10 km seaward of the inner tripod, near the outer tripod and shelf break (Fig. 3.4). Of the 405 modeled sediment packets that we initiate tracking at the inner shelf tripod, 90 were capable of reaching the region of self-sustaining flow in the time available (Fig 3.5). The sediment associated with these 90 packets (22% of total event time) represents 75% of the total sediment flux that passed the inner-shelf tripod, below the lutocline, over the course of the event (Figs. 3.4, 3.5). The time for a packet to travel from the inner tripod to the shelf edge (~12 km), under the influence of gravity alone, ranged from 50-300 hours, with an average of 132 hours (Fig. 3.4). Because the required baseline conditions for fluid mud generation were not met during phase I, no packets from this time period exited the shelf due to gravity-driven flow. Over the same time period, cross-shelf currents were capable of moving sediment a net distance of 3 km offshore.

Cross-shelf current velocities (1 mab) were consistently offshore only during phase II of the WSFM; all other phases of the event exhibited flow reversals consistent with semi-diurnal tidal fluctuations (Fig. 3.5). Similarly, the height of the lutocline remained well above the top of the predicted bottom boundary layer. Maximal SSC values were observed in the OBS data at both the inner and outer tripod locations during this second phase (Fig. 3.6). Furthermore, of the 60 packets generated during phase II, 54 were able to exit the shelf environment over the course of the event (Fig. 3.5). Cross-shelf currents during this same period moved 18 km in the offshore direction, reaching the shelf edge in approximately 50 hours, which was similar to the travel time of the fastest-moving gravity-driven sediment packets.

During phase III, waning oceanic conditions (and the corresponding reduction in SSC) resulted in only 20 of 43 packets escaping the shelf environment (Fig. 3.4). Because the ambient cross-shelf currents experienced periodic flow reversals during this phase (Fig. 3.5), the net off-shelf travel distance due to currents was only 2 km. Phase IV exhibited a continued reduction in gravity-driven export, with only 16 of 173 packets exiting the shelf. Similar to phase III, cross-shelf transport due to currents in phase IV was affected by tidal reversals, resulting in a net distance of ~5 km.

Cumulative deposition, predicted using the gradient of flux and bed slope at the inner tripod, was highest during phase II (~0.04 m; Fig. 3.6). There was also minor deposition (<0.005 m) predicted during phase III. Seabed elevation as measured by the ABS increased by 0.03 m in phase II, 0.05 m in phase III, and 0.02 m in phase IV (Fig. 3.6). Because seabed elevation from acoustic instruments can change due sediment deposition and erosion, as well as the instrument package settling into the seabed, we examined the time-averaged, tidally filtered water pressure, which increased by ~7 cm over the course of the event (Fig. 3.6). Deposition was predicted between transect km 4-6, and immediately seaward of the outer tripod, for all bursts in the cross-shelf dimension (Fig. 3.4).

3.5 Discussion

WSFM are localized and ephemeral, and documenting them *in situ* remains a challenge. Detailed observations of near-bed conditions allow us to develop an understanding of at least some of the processes responsible for WSFM formation, development, and collapse. The differences in driving forces between the four event stages have dramatic consequences in the behavior of the WSFM, with implications for sediment accumulation and off-shelf transport (Table 3.1). Comparisons between the different phases for WSFM, as well as the likely behavior

of the WSFM across the shelf, allow us to understand better the depositional environments described in previous research (e.g., Miller and Kuehl, 2010; Rose and Kuehl, 2010).

3.5.1 Evolution of the fluid mud event on the mid-shelf

During the initial phase of WSFM generation on the inner shelf, the gradually strengthening wave climate resuspended local seabed material to concentrations >1 g l^{-1}. Though there had been a series of smaller (<600 m^3 s^{-1}) floods in May and June prior to this event, there was insufficient sediment available to overcome the frictional forces in the balance from eq. 1. While the sediment in suspension may have been transported to the site at relatively low concentrations, shear velocities during this phase were in excess of the threshold for resuspension, (0.008 m s^{-1}; Hale et al., 2014). SSC profiles exhibited a logarithmic increase toward the seabed (Fig. 3.2F).

In the second stage of the event, the SSC profile also increased logarithmically toward the seabed, but reached an inflection point near the wave-current boundary layer, below which concentrations remained relatively uniform down to the seabed, assuming a shape described by Ozdemir et al. (2011) (Fig. 3.2). In fact, the lutocline appeared to be as much as 0.15 m above the top of the predicted wave-current boundary layer during this stage, and this was coincident with an increase in current speeds (and, correspondingly, U_{*wc}), and SSC >>10 g l^{-1} (Fig. 3.3). Numerical and physical modeling experiments suggest that at large values for SSC, standard estimates of boundary-layer thickness may be inaccurate due to turbulence damping (e.g., Lamb et al., 2004), and possible laminarization of the fluidized layer (e.g., Trowbridge and Kineke, 1994; Winterwerp and Kessel, 2003; Ozdemir et al., 2011). During this second phase, Ri_b was well in excess of the critical value of 0.25, indicating that gravity-driven transport should have occurred (Table 3.1) (e.g., Trowbridge and Kineke, 1994; Scully et al., 2002). Traykovski et al.

(2000) observed gravity-driven velocities >20 cm s^{-1} on the Eel shelf during an event in 1998, which Scully et al. (2002) subsequently modeled accurately using the same formulations employed in this study. On the Waipaoa shelf, we observed relatively slow gravity-driven velocities at the inner shelf tripod (<0.03 m s^{-1}; Fig. 3.4; Table 3.1). This difference in downslope velocities between the Waipaoa and Eel systems likely results from a combination of our conservative estimate of the depth-integrated SSC, and the extremely shallow slope of the mid-shelf on the Waipaoa margin (0.14^{o}) relative to the Eel margin (0.34^{o}).

During the third phase of WSFM, SSC decreased rapidly around hour 130, coincident with a rapid reduction in U_{*wc} (Fig. 3.3). This brief period of relative calm likely allowed for the deposition of sand and coarser silts, leaving only the finer grains in suspension. Fine-grained sediment is more acoustically transparent than coarser material (Cartwright et al., 2013), and the relatively low SSC observed from hours 133 – 155 was a reflection of this; the absence of sand grains prevented the complete absorption of the acoustic energy, and precluded the occurrence of the numerical instability described in section 3.2.3. During the brief increase in current speed around hour 145, there was a corresponding increase in near-bed SSC, suggesting that additional material was resuspended from the bed, though not enough to completely attenuate the acoustic signal within the layer (Fig. 3.3). The continued decrease in the elevation of the lutocline at hour 155 resulted in a concurrent increase in SSC (Fig. 3.3), and may be attributed to two causes. First, sediment suspended in the combined wave-current boundary layer collapsed into the wave boundary layer, as both current and wave energy decreased. Theoretically this would increase the mass of sediment per unit volume (e.g., Traykovski et al., 2004). In addition, fluid-mud concentrations should have resulted in a condition where the sediment fall velocity was hindered, which serves to maintain elevated SSC within the WSFM layer (Fig. 3.3; e.g., Mehta et al.,

1986). This combination of hindered settling and moderate wave energy and tidal currents was responsible for maintaining particles in suspension for the final phase of the event, which lasted for an additional 175 hours (hours 175-350; ~7.25 days). The lutocline height was coincident with the height of the predicted bottom boundary layer periodically, corresponding in time with tidally driven current-speed maxima (Fig. 3.3), which suggests the potential for modest gravity-driven flow. Gravity-driven flux during this portion of the flow was correspondingly low, when compared with the periods of higher SSC (Fig. 3.6).

3.5.2 Implications for cross-shelf sediment transport

Our observations demonstrate that a WSFM occurred during this event at the inner-shelf tripod location. In addition to our measurements on the inner shelf, a near-bed OBS on the outer shelf tripod showed a SSC peak following the reduction of local wave and current energy, suggesting the arrival of gravity-driven flow initially generated elsewhere. WSFM was not the only mechanism by which sediment could be advected to the outer tripod site during this event. Winds during the entire second and third phase of the WSFM were strong and from the south to southwest, creating downwelling-favorable conditions (Fig. 3.3). At the inner tripod, downwelling was observed in the upward-looking ADCP velocity data ~50 h following the onset of these conditions, and distinct water-column shear existed between hours 118-239 (Fig. 3.5). Downwelling currents, however, would require ~50 h to traverse from the inner tripod to the shelf edge, based on a cumulative summation of the average current speed at the inner tripod site (1 mab) during the period of enhanced downwelling. The enhanced near-bed currents prior to and during this time period indicate that downwelling occurred in addition to, rather than in lieu of, gravity-driven flow. As such, it is unlikely that wind-driven downwelling currents were the sole responsible mechanism for the initial pulses of suspended sediment observed.

Currents 1 mab were stronger in the offshore direction than currents 3.5 mab throughout phase II, a condition that began well before downwelling was observed in the upward-looking ADCP data (e.g., hour 76 vs. hour 118; Fig. 3.5). Furthermore, currents 1 mab were exclusively in the offshore direction throughout phase II (i.e. no tidally induced direction reversal), while currents 3.5 mab and higher in the water column exhibited periodic velocity modulation or complete flow-direction reversals due to tidal forcing (Fig. 3.5). The enhancement of seaward-directed currents via gravity-driven flow has been demonstrated in other shelf environments (e.g., near the Huanghe River, China – Wright et al., 1990; near the Fly River, Papua New Guinea – Martin et al., 2008), and was likely occurring throughout phase II and into phase III of the WSFM event (Fig. 3.5).

Assuming that the calculated gravity-driven velocity was the only influence on transporting sediment within the fluid-mud layer, we can make a conservative estimate of sediment flux below the lutocline, and compare it with flux estimates in the overlying near-bed (<1.2 mab) region. Data indicate the potential for substantial sediment to have escaped the shelf in the WSFM layer during this event, despite the modest gravity-driven velocities (<0.03 m s^{-1}) at the inner tripod site, and relatively short duration over which they operated. At the inner tripod, the cross-shelf cumulative sediment flux within the WSFM layer was ~1900 g cm^{-2} over the course of the event (Fig. 3.6). This is nearly an order of magnitude greater than the cumulative flux between the top of the WSFM layer and ~1.2 mab (~200 g cm^{-2}; Fig. 3.6). What is more notable, flux during the WSFM event was almost exclusively during phase II, when flux in the overlying layer was minimal, totaling only ~120 g cm^{-2} (Fig. 3.6). Flux above the WSFM layer was controlled by shelf currents that were at least partially driven by coastal downwelling during phase II, which highlights the relative importance of WSFM in exporting sediment from

the shelf environment. This has not been documented previously for the Waipaoa margin, although cross-shelf transport in this manner as has been observed elsewhere (e.g., Ogston et al., 2000; Traykovski et al., 2000; Jaramillo et al., 2009). Furthermore, despite the relatively low velocities at the inner shelf tripod location, the WSFM has the potential to accelerate as the seabed steepens offshore.

Our analytical solution suggests that the fastest-moving packets (i.e. largest negative buoyancy due to sediment loading) would require ~50 h to travel from the inner tripod to the region of self-sustaining flow (Fig. 3.5). The second pulse of elevated SSC observed at the outer tripod occurred during a period of waning oceanic conditions, suggesting the arrival of material from farther inshore. The specific timing of the peaks observed within this second pulse resembles that of the OBS record at the inner tripod (Fig. 3.4), with a 23-h delay. Also, SSC does not correlate with U_{*wc} at the outer tripod during this period, indicating that material arrived via an advective process rather than local resuspension. These results agree with observations drawn by a numerical model associated with this research (Moriarty et al., 2014). During the initial model simulation, which did not include gravity-driven flow, all river-flood material was deposited in or near Poverty Bay. With the incorporation of a gravity-driven flow module, their model accurately recreated the pattern of river-flood deposition observed by Walsh et al. (2014). It is clear, therefore, that while downwelling occurred during this event, and likely played a role in cross-shelf sediment transport, WSFM was responsible for an important, and likely dominant, component of the sediment flux.

3.5.3 Sediment deposition in time and space

Shelf sediment deposition, to a first order, is controlled by convergence or divergence of flux (e.g., Ogston et al., 2000; Scully et al., 2002). Ideally, the gradient of flux, therefore,

indicates where we can predict temporal or spatial trends in sediment deposition (e.g., Traykovski et al., 2000; Scully et al., 2002). In the case of our analytical solution for gravity-driven velocity, SSC exerts a first-order control over both terms comprising flux (velocity and concentration) and as such, gravity-driven flow and flux are covariant. We are therefore able to examine the spatial derivative of gravity-driven velocity, rather than flux, to predict convergence along the transect described in our analytical solution for U_g. Predicting seabed change in systems where sediment transport is driven by more classical advective mechanisms, and flux and flow do not necessarily vary together is a difficult process, which would require a different and more complex method (e.g., Ogston et al., 2000; Puig et al., 2001; Ogston et al., 2008). On the Waipaoa shelf, gravity-driven velocities tend to slow as the slope decreases between transect-km 4-6, suggesting the possibility of enhanced deposition in this region (Fig. 3.4). This correlates well with the findings of Miller and Kuehl (2010), who observe enhanced sediment accumulation rates >5 mm yr^{-1} in this region of the mid-shelf (Fig. 3.1). The seabed radiochemical data from Walsh et al. (2014) also show signs of recent deposition of terrestrial-sourced material in samples collected in this region during September 2010, ~2 months after the WSFM event.

We can also predict deposition through time, by examining flux convergence and divergence at the inner tripod site. Here, cumulative deposition estimated from the gradient of wave-orbital velocities and shelf slope (eq. 13 in Scully et al., 2002) compares favorably with the depositional pattern observed in the ABS data (Fig. 3.6). When the 5-cm change in observed seabed elevation associated with a pressure change due to tripod settling (Hale et al., 2014) is accounted for, the similarity becomes even more obvious and the prediction of deposition is accurate to within 1 cm, which is the resolution of the ABS (Fig. 3.6).

Despite the limitations of our field instrumentation and the assumptions necessary for predictions of deposition, we can draw reasonable estimates of seabed change due to oceanic processes, both spatially and temporally (Figs. 3.4 and 3.6, respectively). We did not extend our transect off the shelf, but it is not unreasonable to predict sediment accumulation locally on or at the toe of the morphologically complex slope (Fig. 3.1; Alexander et al., 2010). This work builds on earlier studies, highlighting the importance of sediment-gravity flows in the transfer of sediment from river source to ocean sink, as well as the inter-related nature of transport processes and seabed morphology (e.g., Traykovski et al., 2000; Scully et al., 2002).

3.6. Conclusions

In July 2010, high waves and elevated river discharge combine to rapidly export substantial material from the inner shelf across the margin. Through wave resuspension and advection from neighboring areas, near-bed SSC at 37-m water depth offshore of the Waipaoa River exceeded the threshold for gravity-driven flow. We observe SSC >50 g l^{-1}, below a lutocline whose height is greater than that of the predicted wave-current boundary layer. Using instrument data from the inner shelf, including calibrated SSC from ABS, we can solve force balances to estimate gravity-driven velocity, and the potential for off-shelf transport. Even with conservative SSC values, we predict that 75% of the material transported past the inner tripod would have escaped the shelf. We are also able to use the gradient sediment flux to make simple predictions of where we might expect sediment to accumulate in time (at one location), or in space (over the duration of the event), with reasonable agreement to previous seabed studies. Given sufficient time during which the boundary layer is filled with fine-grained sediment, WSFM flows can be an immediate link for terrestrial material to the deep ocean. During this entire study year, Hale et al. (2014) observed several large river floods, and several strong ocean

storms, however only this single event was capable of immediately transporting river-derived sediment off the continental shelf. Considering that the majority of transport during this event occurred in the bottom 10-20 cm of the water column highlights the importance of WSFM in this, and likely other event-based systems.

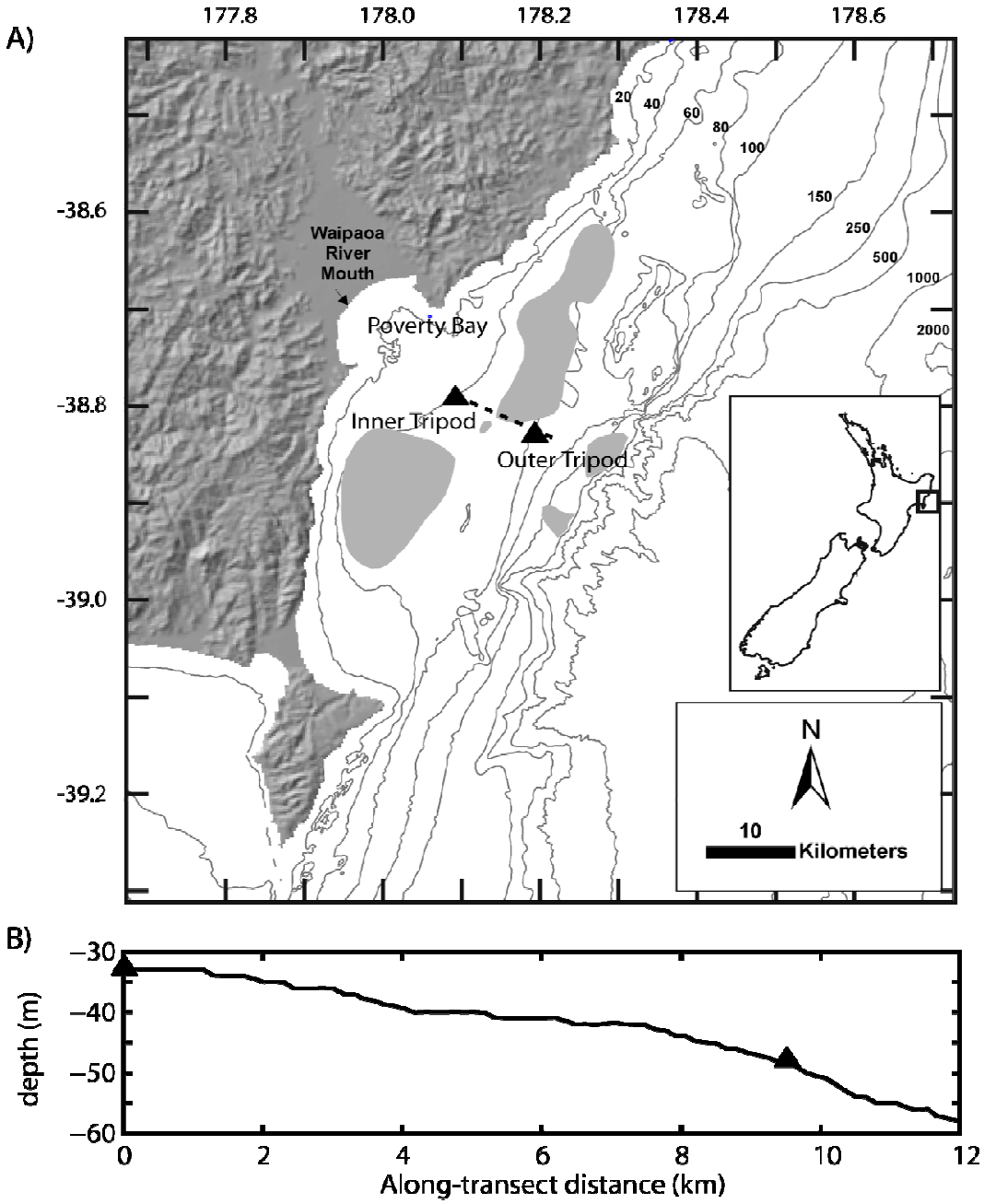

Figure 3.1 – A) Map of study area, including tripod locations (black triangles). Shaded regions are areas of enhanced accumulation (from Miller and Kuehl, 2010). Dashed line is the cross-shelf transect used for the numerical experiment. B) Cross-shelf profile used for numerical experiment. Tripods locations shown with triangles.

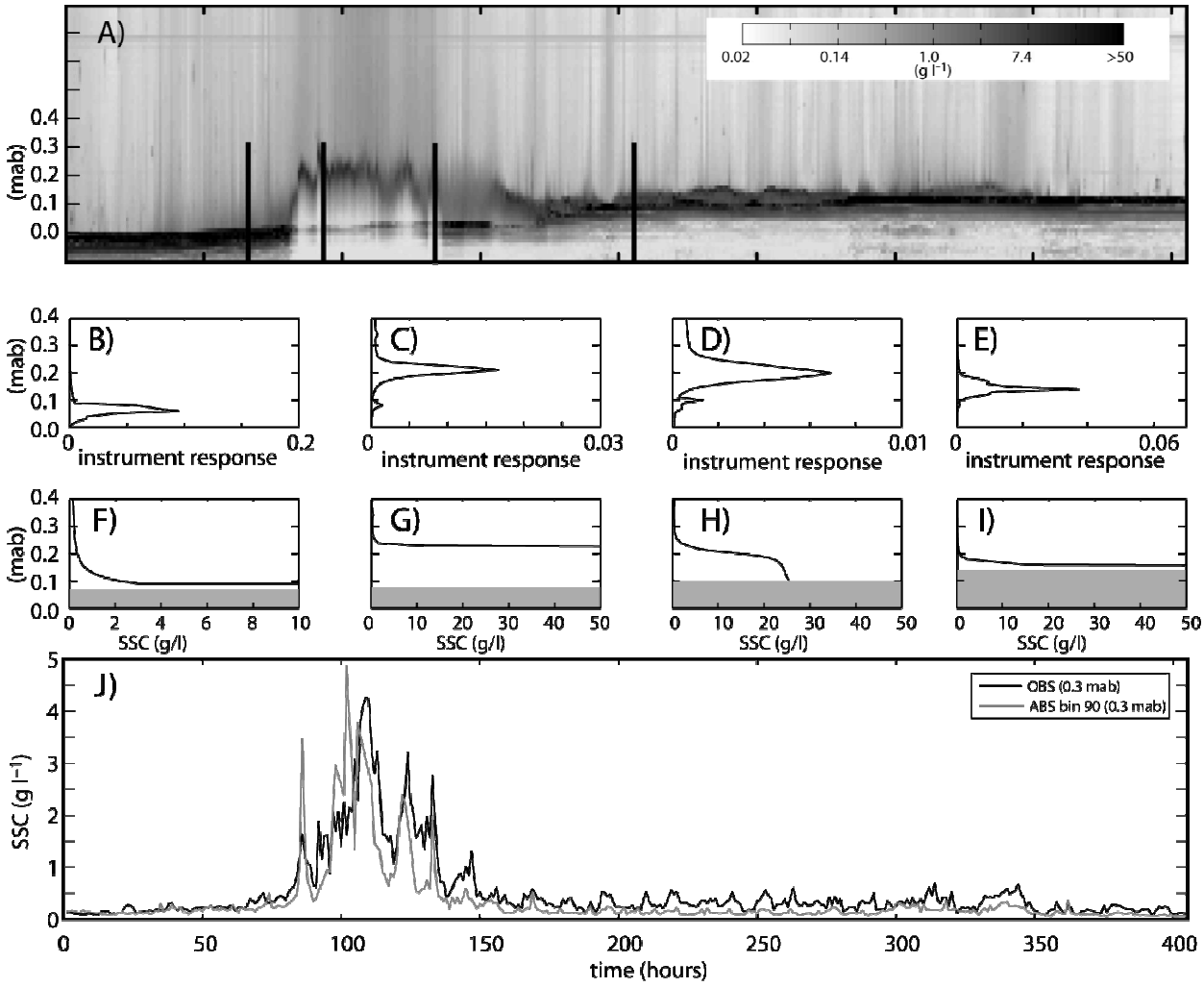

Figure 3.2 – ABS data during event, and example profiles showing results of ABS calibration. Panel A) shows ABS data calibrated to SSC <1 g l^{-1}. Panel B-E show the raw instrument response from four representative profiles identified with black lines in A). Panels F-I demonstrate the effectiveness of the recursive algorithm depending on instrument response, and the grey areas indicate the interpreted seabed. Panel J compares SSC from the OBS at 0.3 mab with ABS data at the same elevation.

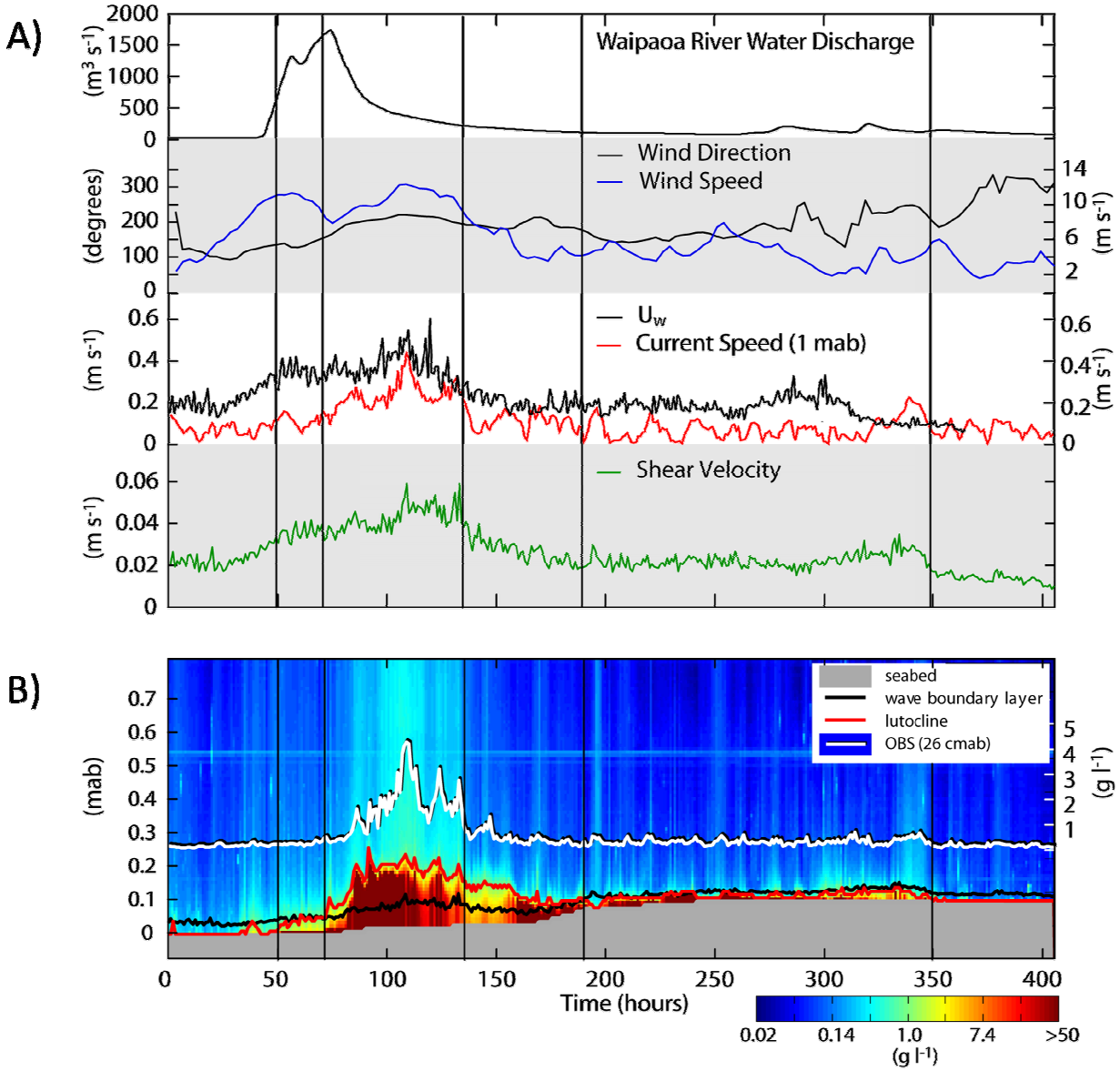

Figure 3.3 – A) Time series of Waipaoa River water discharge (black), wind speed (blue), wind direction (black), wave-orbital velocity (black) current speed (red), and U_{*wc} (green) at inner shelf tripod. B) Near-bed suspended sediment during WSFM event with the event phases identified. Notice the lutocline thickness relative to the wave-boundary-layer thickness.

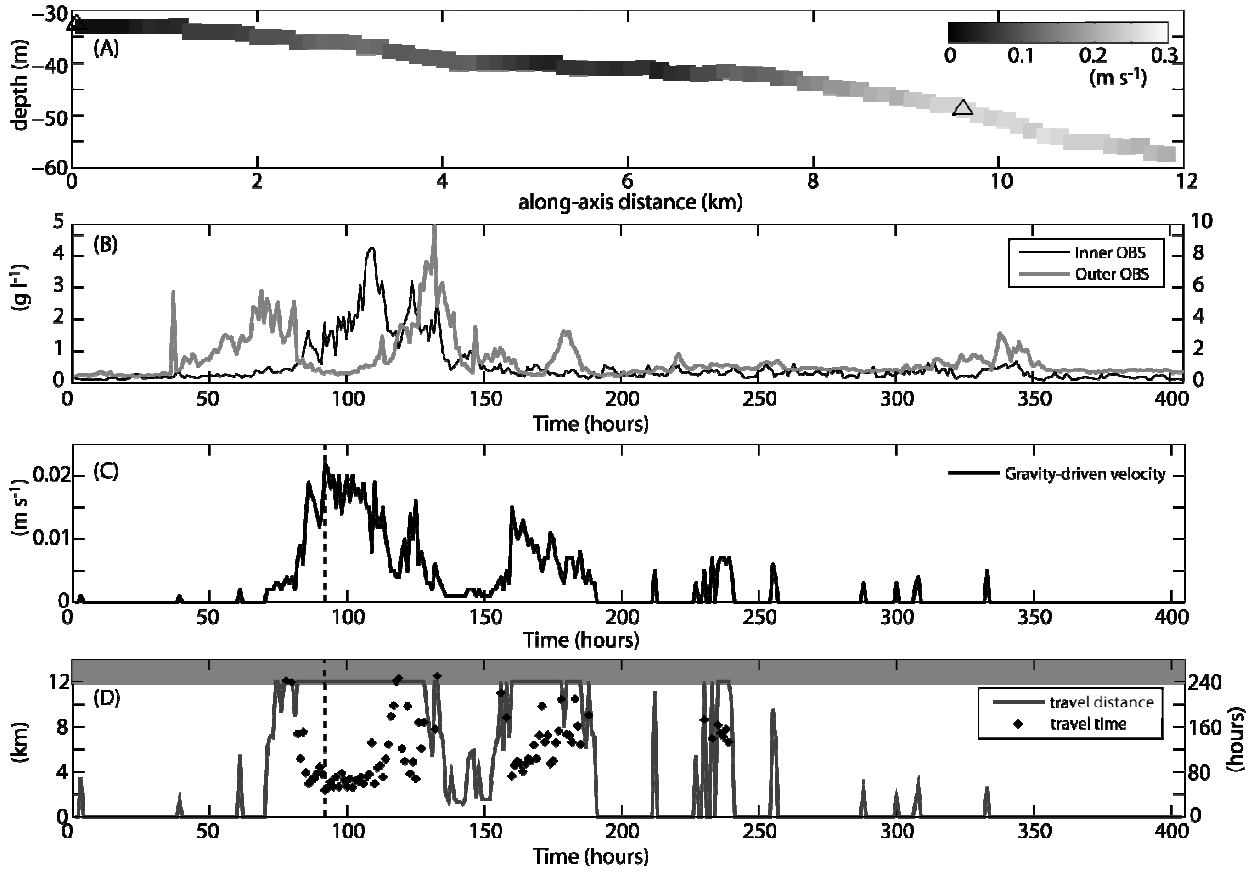

Figure 3.4 – Observational data and results of the analytical solution to the Friedrichs and Wright (2004) model for gravity-driven velocity. Panel A) shows U_g at all locations during the fastest-moving event period (hour 92). Shaded regions indicate areas of predicted deposition based on the gradient of U_g. B) OBS data from the inner (black line) and outer (gray line) tripod locations, demonstrating the 23-hour offset between peaks C) U_g at the inner shelf, for each burst of event data. The dashed line depicts when the velocities in panel A) were computed. D) total distance travelled (gray line) and time required to cross shelf (black dots, when applicable) for each burst. Beyond 12 km, flow becomes self sustaining and is no longer in the realm of our analytical solution.

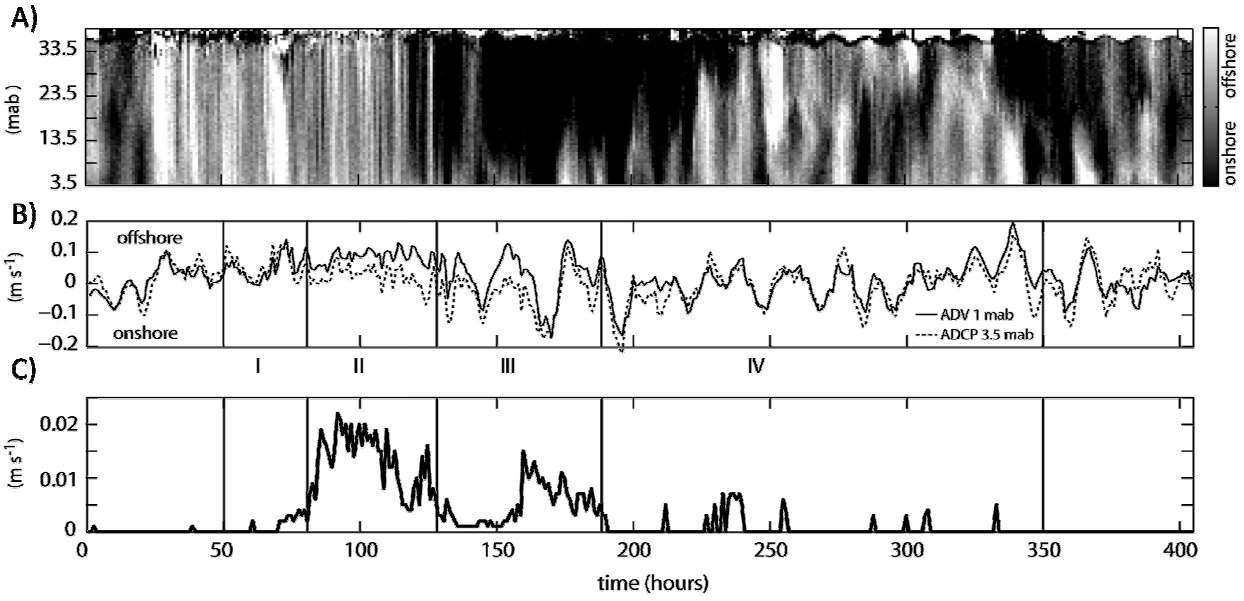

Figure 3.5 - Cross-shelf velocity from inner tripod (A) water-column ADCP, (B) currents at 1 mab from single-point ADV (solid line), and at 3.5 mab from the ADCP (dashed line), (C) and estimated U_g, with WSFM phases identified by vertical lines. Black in panel A) shows landward flow, while white represents seaward flow. Notice that currents 1 mab (panel B) are directed strongly seaward prior to the onset of downwelling (observed in panel A), during the period of strongest gravity-driven velocity.

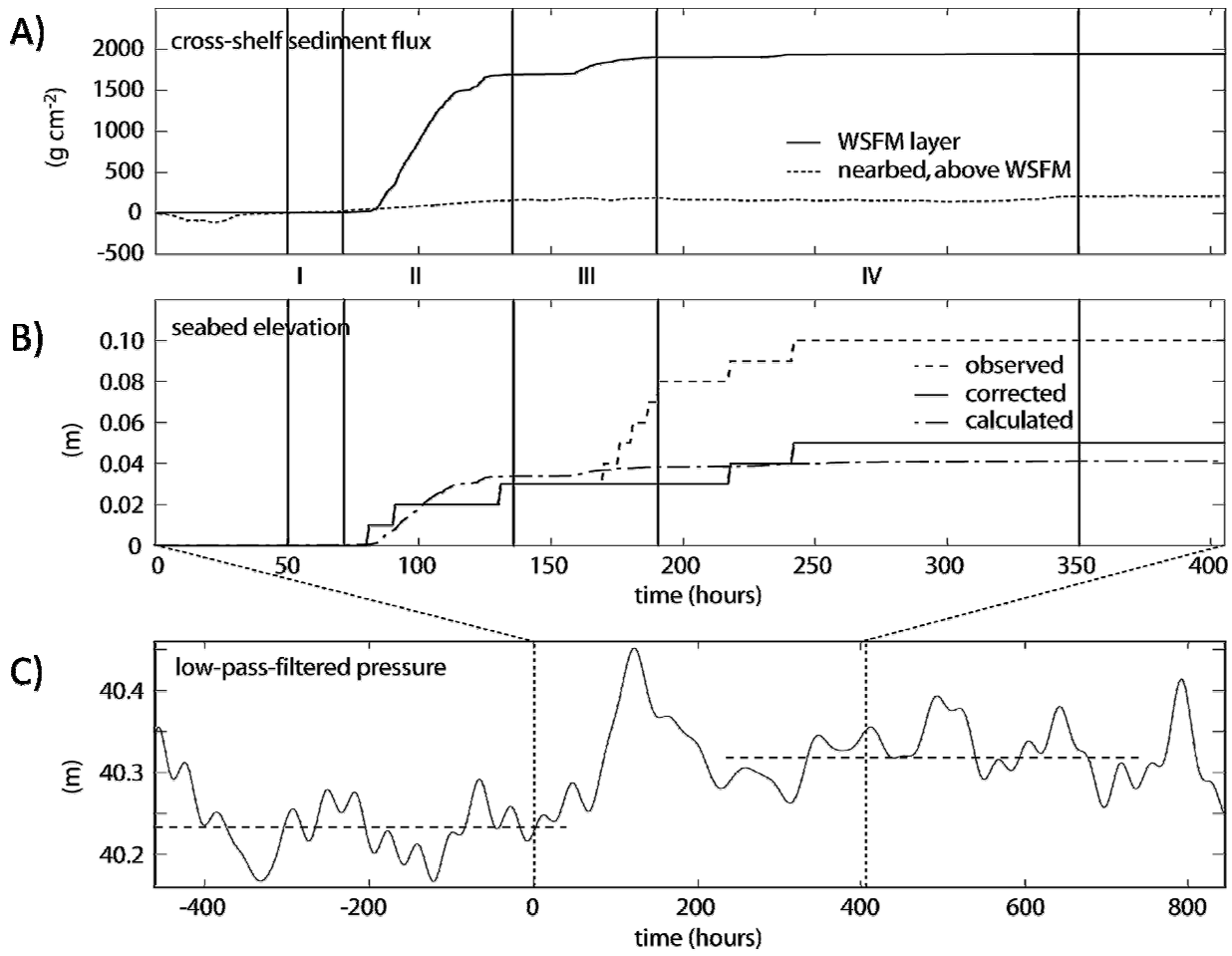

Figure 3.6 – A) Cross-shelf sediment flux within the WSFM layer (solid line) and between the lutocline and ~1.2 mab (dashed line). Flux within the WSFM layer is >11 times greater than flux in the overlying near-bed region. B) Observed seabed elevation from the ABS (single dashed line), seabed elevation with a correction due to tripod settling (solid line), and predicted deposition based on Scully et al. (2002), eq. 13. The corrected and predicted deposition agree in both space and time, within the resolution of the instrumentation. C) Low-pass-filtered pressure data, showing the change in pressure measured by the instrumentation, associated with tripod settling (Hale et al., 2014), which is partially responsible for the apparent deposition in the observed seabed data from panel B).

WSFM Phase (h)	C (g cm^{-2})	$\|u\|$ (m s^{-1})	Ri_b	U_g (m s^{-1})
Phase I (50-71)	0.30 – 0.78 (0.69)	0.26 – 0.42 (0.34)	0.01 – 0.05 (0.03)	0.000 – 0.002 (0.000)
Phase II (72-132)	0.93 – 10.8 (5.59)	0.28 – 0.60 (0.42)	0.02 – 0.39 (0.15)	0.002 – 0.022 (0.011)
Phase III (133-176)	0.43 – 4.10 (1.57)	0.15 – 0.62 (0.28)	0.02 – 0.63 (0.14)	0.001 – 0.015 (0.005)
Phase IV (177-350)	0.08 – 2.09 (0.67)	0.12 – 0.34 (0.19)	0.01 – 0.41 (0.10)	0.000 – 0.008 (0.001)

Table 3.1 – Ranges and mean values for the variables and products of Eqs. 1 and 2. Mean values (in parentheses) are always highest during phase II.

Chapter 4:
A method for estimating down-core variability on multiple time scales using x-radiographs

4.1 Introduction

Continental shelves serve as sediment traps for material being delivered to the ocean on both active and passive margins (e.g., Nittrouer, 1979; Kuehl et al., 1985; Sommerfield et al., 1999). Physical delivery and reworking of sediment are known to cause variations in the textural properties of the seabed on the continental shelf (e.g., Sommerfield and Nittrouer, 1999; Hill et al., 2000; Wheatcroft and Borgeld, 2000; Palinkas et al., 2005). A variety of techniques are used to quantify these variations, with the goal of understanding the processes responsible for the formation of a specific deposit, or the general conditions during the time period of strata formation (i.e., were storms and floods more or less energetic than at present). Sediment properties used to establish conditions during deposition include grain-size distribution, porosity, bulk density, and sedimentary structures (e.g., Nittrouer, 1979; Kuehl et al., 1986; Jaeger and Nittrouer, 1995; Bentley and Nittrouer, 2003), however the methods used to extract these data typically require considerable time and/or resources to investigate. In the interest of maximizing spatial coverage, data is typically incorporated from cores in as many locations as possible. As a result, down-core resolution is typically somewhat coarse, with subsamples 1-2-cm thick collected at intervals of 1-5 cm. In shelf areas where storm-generated strata are commonly ~1 mm to many cm in thickness with complex internal structure, coarse sampling presents the possibility of missing potentially important events or details in the strata. X-radiography is often used a proxy for sediment bulk density and benefits from fine-scale resolution (~0.1 mm) (e.g. Hamblin, 1962; Howard, 1968; Wheatcroft and Borgeld, 2000; Wheatcroft et al., 2006; Drexler and Nittrouer, 2008). Unfortunately, image acquisition and processing often result in bulk-density observations and measurements that are core-relative, and core-specific (i.e., the absolute

value of x-ray attenuation from one core does not typically apply to other cores), which makes direct comparisons difficult. As a result, x-radiography has been mostly used as a qualitative tool for assessing seabed character (e.g., Wheatcroft and Borgeld, 2000; Wheatcroft et al., 2006; Palinkas et al., 2005; Drexler and Nittrouer, 2008; Rose and Kuehl, 2010).

In this study, a method using x-radiograph images to quantify the degree of physical lamination preserved in the seabed is developed, and employed to assess stratigraphic changes on continental shelves associated with major oceanic and river discharge events. Using cores collected on the Waipaoa shelf (Rose and Kuehl, 2010; Walsh et al., 2014) and the Rhône shelf (Drexler and Nittrouer, 2008), quantitative estimates of the degree of physical lamination preserved on a decadal-to-century scale are made, and utilized to investigate seasonal changes due to known physical forcings. Selecting this pair of study locations provides the opportunity to test our method across a variety of depositional environments. On the Waipaoa margin, shelf sedimentation near a small, mountainous river system was examined, where wave events are the dominant force in shelf reworking (Hale et al., 2014). In contrast, deposition associated with the Rhône River occurs on and near the subaqueous delta of a large river, where flood events are critical to strata formation (Drexler and Nittrouer, 2008). This range of conditions allows for an examination of the strengths and weaknesses of this method for rapid core characterization using x-radiograph images.

In each of these study locations, substantial previous research has been undertaken to investigate the processes responsible for sediment transport and deposition. The Waipaoa study benefits from the analysis of time-series tripod data collected during the same time period as the cores analyzed (Hale et al., 2014), a numerical model of the shelf hydrodynamics (Moriarty et al., 2014), and geochemical and textural data for the region (Miller and Kuehl, 2010; Rose and

Kuehl, 2010; Walsh et al., 2014). The processes affecting the properties that characterize the surficial deposits are reasonably well understood. Similarly, the Rhône region has been studied extensively from both sedimentological (e.g., Drexler and Nittrouer, 2008), and process-based standpoints (Durrieu de Madron et al., 2008; Ferre et al., 2008; Ogston et al., 2008; Ulses et al., 2008; Marion et al., 2010). By developing a method to rapidly quantify down-core sediment variability using existing data, questions regarding small-scale spatial variability and the potential impact of individual events on the longer-term geologic record are addressed

4.2 Background

4.2.1 Study locations

4.2.1.1 Waipaoa margin

Sediment cores from the shelf seaward of the Waipaoa River were collected in 2005, and again in four cruises during 2010-2011 (Fig. 4.1). These cruises were part of the larger NSF-funded Margins Source-to-Sink program, with the goal of characterizing the sediment transport and deposition within the Waipaoa Sedimentary System (WSS) over a variety of time scales (Alexander et al., 2010; Gerber et al., 2010; Miller and Kuehl, 2010; Rose and Kuehl, 2010; Kniskern et al., 2014; Walsh et al., 2014). Cores were analyzed using geochemical and textural techniques, including x-radiography. Previous studies examining x-radiograph images from this area describe a radial pattern of decreasing physical lamination with increased distance from Poverty Bay, the point source of sediment to the region (Rose and Kuehl, 2010; Walsh et al., 2014). The clay fraction within the seabed tends to increase with distance from Poverty Bay, while the variance about this mean decreases (Walsh et al., 2014). Even though sediment reaches these distal regions episodically, mechanical sorting has resulted in similarly sized particles which are rapidly mixed by physical and biological reworking. A similar pattern is

observed in ^{210}Pb profiles, where cores proximal to the sediment source show low activity and non-steady-state profiles indicative of event-based sedimentation, while distal cores exhibit steady-state accumulation, which suggests that mixing is able to rapidly destroy evidence of episodic sediment delivery (Miller and Kuehl, 2010).

In addition to the coring studies, acoustic and optical instrumentation deployed within Poverty Bay in 2006 (Bever et al., 2011) and on the mid-shelf in 2010-2011 (Hale et al., 2014) monitored sediment and water movement. These investigations demonstrate that sediment transport on the Waipaoa margin is event driven. In the case of the 2010-2011 study year, ~40% of the near-bed, cross-shelf sediment transport at one mid-shelf location occurred during a single event in July 2011 (Hale et al., 2014). Cores collected from the shelf in September 2010 show a deposit of ~1-12 cm with evidence of wave resuspension and early signs of bioturbation (Walsh et al., 2014). This corresponds well with the observation of a wave-supported fluid mud associated with the July event (Chapter 3). In October 2010, between the coring events in July and September, the region was subject to only one additional river flood >1900 $m^3 s^{-1}$; the threshold for a "major flood" as defined by Reid (1999). Bed elevation increased slightly (~1 cm) on the mid-shelf as a result of this flood and the ensuing wave event, but in general, the Austral spring and summer months were quiescent and subject to relatively few resuspension events (Hale et al., 2014). A qualitative comparison of x-radiographs reveals a general decrease in the degree of physical stratification for the surface layer between September and February (Walsh et al., 2014).

4.2.1.2 Rhône River mouth

Sediment cores were collected on the shelf seaward of the Rhône River in October 2004 and April 2005 (Fig. 4.1), as part of a study characterizing sediment transport and deposition in

the Gulf of Lions (DeGeest et al., 2008; Drexler and Nittrouer, 2008; Ogston et al., 2008; Ulses et al., 2008; Marion et al., 2010)(Fig. 4.1). Sediment delivery in this system is episodic and event-driven, with 80% of the annual sediment load delivered during river floods (Drexler and Nittrouer, 2008). Cores collected in October 2004 showed a ~5-cm-thick bioturbated surface layer, resulting from a period of ~ 6 mos of near-average discharge conditions (Drexler and Nittrouer, 2008). The relatively fine-grained composition of this layer, combined with its radiochemical signature, indicates that despite the lack of preserved physical stratification, this layer was recently emplaced. X-radiographs of cores collected in October 2004 were described qualitatively, and placed in one of three categories: physically stratified, partially stratified, or bioturbated, and showed progressively more biological mixing with distance from the river mouth (Drexler and Nittrouer, 2008). Between October 2004 and the April 2005 coring event, a series of discharge events occurred, including two longer-duration (>11 day) floods. The second of these floods had a peak discharge of ~4000 m^3 s^{-1}, and was waning during the April 2005 sampling event (Drexler and Nittrouer, 2008). There was also a ~week-long period of elevated wave heights (>2 m) in late January 2005.

X-radiographs of cores collected in April 2005 were qualitatively described by Drexler and Nittrouer (2008), and show a distinct, physically stratified surface layer of 1-6 cm. This layer was characterized by a low sand content (<10 %), the presence of the radionuclide ^{7}Be, and relatively low ^{210}Pb activity, indicating recent and rapid deposition of riverine material. Three core locations in April 2005 were repeat occupations of stations from October 2004, allowing for the direct comparison of physical properties and x-radiograph images. In these three examples, the surface layer (3-6 cm thick) of physically stratified sediment overlays a region of bioturbated sediment, representative of the October 2004 seabed surface (Drexler and Nittrouer, 2008).

4.2.2 X-radiography

X-radiographs of sediment cores have been analyzed for over fifty years to describe changes in bulk density, which reflect changes in the conditions under which a specific deposit was formed (e.g., Hamblin, 1962; Howard, 1968; Algeo et al., 1994; Wheatcroft et al., 2006; Drexler and Nittrouer, 2008). X-radiographs present a non-invasive mechanism by which to procure highly detailed information about sediment cores. X-radiographs have been used to evaluate bioturbation (e.g., Wheatcroft et al., 2006), to document the presence of flood-derived material (e.g., Wheatcroft and Borgeld), and to evaluate the specific processes likely responsible for the formation of a deposit (e.g., Drexler and Nittrouer, 2008; Martin et al., 2008). According to Beer's Law (eq. 1), received x-ray intensity (I) is dependent on initial intensity (I_0), material thickness (D), and a linear attenuation coefficient (μ), which is controlled by electron density, radiation energy, and packing density of the x-rayed material (e.g., Aylmore, 1993).

$$I=I_0\exp(-\mu D) \qquad \text{- Equation 1}$$

Previous studies have compared discrete measurements of porosity with the corresponding x-ray attenuation in order to infer bulk density, which is related to sediment grain size (e.g., Orsi and Anderson, 1999; Migeon et al., 1999; Kowalczk, 2005; Wheatcroft et al., 2006). Assuming constant values for sediment grain density and water density, porosity (ϕ) relates to bulk density with the relationship described in Eq. 2.

$$\phi = 1 - \rho_{bulk}/\rho_{sediment} \qquad \text{- Equation 2}$$

Though x-ray intensity is used as a proxy for bulk density (and therefore sediment grain size), images are most commonly analyzed and compared qualitatively, a seemingly necessary by-product of the variability inherent in every specific application. Possible inconsistencies inherent to all systems include distance from source to x-ray receiver panel, slab thickness, and x-ray

exposure intensity, each of which has the potential to affect the intensities produced in the resulting image. Even more importantly, images are often manipulated after acquisition, to highlight changes in density that are not immediately obvious, using adjustments to the image window and level (e.g., Wheatcroft et al., 1997). The image window is the range of pixel intensities, while the level is the midpoint. A narrower window increases contrast, while adjusting the level highlights either the darker (lower-bulk-density) or lighter (higher-bulk-density) regions of a core. Through image manipulation, features such as erosional contacts (e.g., Drexler and Nittrouer, 2008), cross-stratified silts (e.g., Wheatcroft et al., 2006), and parallel-laminated silts (e.g., Jaeger and Nittrouer, 1995) become obvious.

Recently, several studies have employed image processing techniques and software to quantify x-radiographs in a variety of ways (e.g. Lofi and Weber, 2001; Wheatcroft et al., 2006). In physically laminated settings such as varved lakes, software can detect individual stratum (e.g., Saarinen and Petterson, 2001). In another example, the contrast in density between a recently deposited flood layer and the underlying seabed was sufficiently stark for the deposit thickness to be estimated automatically (Wheatcroft et al., 2006). Other attempts have been made to quantify grain density, as well as the presence of biological burrowing (e.g., Wheatcroft et al., 2006). Unfortunately, outside of a very specific set of conditions, where cores contain nearly perfect horizontal strata with minimal bioturbation, these sorts of quantitative measurements become increasingly difficult to employ.

4.3 Methods

4.3.1 Field Data

Waipaoa shelf sediment cores were collected on two cruises using an Ocean Instruments® multicorer. Individual casts returned as many as eight core barrels, at a maximum

horizontal spacing of 2.5 m. Cores were examined from within the same cast, as well as repeat occupations of the same location, to address how local variability affects the ability to monitor temporal change. In all, 37 cores from 36 locations were collected and imaged in September 2010, and a total of 51 cores (36 repeat occupations of September cores) were collected in February 2011. Small-scale spatial variability was examined, using as many as 3 cores from 8 locations in February. Cores were imaged in polycarbonate trays (8W x 2.5D x 60L cm), using a Varian PaxScan 4030E flat panel digital imaging system and an Ecotron EPX-F2800 portable veterinary x-ray generator. Typical generator settings were 50 kV and 25 mA.

Cores from the Rhône were collected in two cruises using a box-corer, and were sub-sampled using polycarbonate trays (12W x 2D x 60L cm). These constant-thickness slabs were imaged using a Madison Medical Corporation Model VR 1020 portable X-ray system, with variable exposure recorded on a Flashscan 35 digital X-ray imaging subsystem. In total, 23 cores were collected in October 2004, with 19 cores collected in April 2005. In this study, only three cores were repeats from the same station, all of which were proximal (2-3 km) to the river mouth, and in ~30-m deep water.

4.3.2 Porosity measurements

In each study, porosity was examined based on a subset of samples, which were subsequently compared to their associated x-ray intensity. Herein, we examine a total of 17 cores from the Waipaoa (7 from July, 10 from February), which were extruded at 1-2-cm increments immediately following their collection. Samples were refrigerated until examination in the laboratory, where porosity was measured by weighing, drying, and reweighing 5-15 g of homogenized sediment, to determine the water content. In most cases, the subsampled core was collected in the same cast and adjacent to the x-rayed core, and we directly subsampled two x-

ray trays for porosity. Because the absolute depths of specific strata varied between cores used for x-radiography and cores used for laboratory measurements, corresponding peaks of high pixel intensity and low porosity were matched.

4.3.3 X-radiography

For the analysis of sedimentary structures, cores from each study area were digitally imaged and exported from their respective acquisition software with adjustments to the window and level similar between individual cruises. All images presented herein are x-ray negatives, where lighter colors correspond to higher-bulk-density sediment. In addition, to test the sensitivity of the method to discrepancies in image manipulation, a series of images of Waipaoa cores were exported with a wide-range of values for both window and level. To compute the down-core variability (DV), window and levels were optimized to enhance visible structure across the widest-possible range of pixel intensities. Different acquisition software was used for the respective systems, and the digitization values used for image optimization varied accordingly. For the system used in the Waipaoa, window and level were each typically 3000-4000. For the Rhône software, window width was 300-1100, while the level was always 1 (the midpoint). Following optimization, x-ray images of cores from both cruises were inspected qualitatively, to estimate the degree of physical reworking in the surface layer, and to measure the deposit thickness. These visual comparisons were used to determine the accuracy of the automated method of core characterization described below.

Images were imported into image-processing software. To minimize the effects of core barrel edges, the mean intensity value of the 400 center-most pixels (~5 cm) was determined for each row within the x-radiograph. Qualitative examination indicates that in this region, strata remain relatively unaffected by friction along the edge of the core barrel (i.e., no obvious edge

effects). An algorithm was employed to automatically pick the top and bottom of the sediment within each core barrel, and all cores had a similar length, within 10 cm. The resulting x-ray intensity profile was smoothed using a Gaussian filter, with a window of 80 pixel, which corresponds to a length of ~1 cm. This width was selected to optimize noise without removing the variability of interest from the signal. To compute DV, the mean of the absolute values of differences between the x-ray intensity and the filtered data was calculated for every row of pixels. This method does not effectively identify variability in cases where event layers are consistently >>1 cm, because the smoothed data vary concurrently with the raw signal. The windowed filter should prevent disproportionately high DV due to persistent trends from external forces (e.g. sediment compaction, uneven x-ray exposure).

Having characterized the DV for each core, spatial patterns across the shelf were examined. To do so, DV values were interpolated using a natural-neighbor technique, which was selected because the dataset is irregularly spaced. Interpolated contours were drawn at one standard deviation using ArcGIS® software. In cases where multiple cores were collected at the same location, all values were included when interpolating. Interpolations were made for both September 2010 and February 2011 on the Waipaoa shelf, as the spatial coverage was similar enough between the two cruises to allow for direct comparison. For the Rhône, only the October cores were interpolated due to a lack of sufficient repeat occupations.

To examine changes in surface strata due to environmental factors between cruises quantitatively, the fraction of total down-core variability (FV) in the surface layer was determined. The fraction of total variability was determined at averaging intervals of 1, 3, 5, and 10 cm, corresponding to observed event-layer thicknesses. FV was normalized by the total number of pixels in each core, to remove the influence of core length (i.e., longer cores would

tend toward lower fractional variability if not normalized). Emplacement (or destruction) of an event layer should have the effect of increasing (or decreasing) FV accordingly. By determining the FV, contrasts can be drawn between cores from multiple cruises without the need to compare the exact value of x-ray intensity.

4.4 Results

4.4.1 Physical properties of Waipaoa cores

Cores collected on the Waipaoa margin demonstrate a wide range of porosities (Fig. 4.2). Assuming constant values for water and particle density, porosity and bulk density can be directly related. A negative correlation exists between pixel intensity and porosity in September and February cores (Fig. 4.2). The overall relationship was relatively strong for most cores (Sept: mean r^2=0.74; Feb: mean r^2=0.75). If three cores (s319, s324, s405) with exceptionally low r^2 values (<0.50) are excluded, the correlation improves to 0.88 in September, and 0.78 in February. The slope of the linear relationship was similar for all cores, across both cruises (Sept: mean=-0.0012, std-0.00029; Feb: mean=-0.0011, std=0.00025). Although all cores exhibited nearly the same slope, the y-intercept (or maximum porosity at 0 intensity) ranged considerably (Fig. 4.2, Table 4.1). In September, the mean was 0.50, with a standard deviation of 0.03, while in February, the mean was 0.47 with a standard deviation of 0.05 (Fig. 4.2, Table 4.1).

4.4.2 Inherent-variability analysis

Image window and level are commonly manipulated to highlight specific core features when visually inspecting x-radiographs. Not surprisingly, therefore, these same tools can have a major impact on the value of the DV parameter. Images imported with no manipulation had the lowest DV values, typically on the order of 1 for all cores. As contrast increases, DV tends to increase (Fig. 4.3). The rate at which DV increases depends on the degree of physical lamination

within the core. This suggests that while it is possible to artificially generate a core image with high DV value despite minimal physical lamination, physically laminated cores almost always show higher DV than mottled cores. Most importantly, the difference in DV due to small changes in either window or level within a single core is minimal, suggesting that if the operator uses "reasonable" values for each and is not intentionally generating high contrast, the resulting DV will be related to physical patterns of density change.

The Waipaoa study benefits from the use of repeat cores at the same location, during the same cruise. In some cases, these cores were collected in the same cast (<2.5 m apart), and in others, cores were collected as close as possible to one another given the accuracy of GPS, ability of captain to occupy and hold station, and a ship that does not have dynamic positioning (~300 m). The DV of cores at the same location – even those collected on the same cast – can vary by as much as a factor of two (core s445ii: DV=4; s405ii: DV=9.02), with the average difference being 30% (Table 4.2). The difference tends to be particularly large in higher-DV cores (Table 4.2). While higher-DV core locations (mean DV >4) tend to exhibit more difference between individual cores, and with only one exception the maximum DV from a low-DV location is smaller than the minimum DV from a high-DV location (Table 4.2).

4.4.3 Spatial patterns of down-core variability (DV)

At the finest scale (mm), raw pixel intensity does not typically fluctuate drastically around the low-pass filtered data. In cases of abrupt changes in density – like those differentiating a low-bulk-density flood deposit from the previously existing seabed – the raw intensity signal and the smoothed data can differ substantially (Fig. 4.4). As expected, the smoothed data correlates with the raw intensity in strata >1 cm thick, where inflection points

correlate well with observed bed changes. To better understand controls on DV, spatial and temporal patterns at both study sites are investigated.

4.4.3.1 Waipaoa margin

In the case of the Waipaoa, DV decreases radially with distance from the sediment source. DV ranged from 1.8 to 10.2 in September 2010, with the highest values observed on the mid-shelf. The absolute DV values are typically slightly lower in February 2011 than September 2010 (Sept: mean DV=4.93; Feb: mean DV=4.73), however the overall spatial trends observed are similar (Fig. 4.5). Cores collected near and within Poverty Bay show consistently high DV (> 6.4), corresponding to their physically laminated nature (Figs. 4.4-4.5). In general, the trend is for higher DV north of the mouth, rather than the south, for both the September and February cores (Fig. 4.5). The lower DV observed in cores collected on the northern portion of the mid-shelf in February is partially due to interpolation around the low DV observed in a single core (Fig. 4.5). Moderate DV south of the mouth is observed in the shallower water depths for cores collected on both cruises.

4.4.3.2. Rhône River mouth

Cores collected near the Rhône River display a sharp decrease in DV as water depth increases seaward of the river mouth (Fig. 4.6). The decrease in DV is gradual to the west, with relatively high values observed >5 km from the river mouth. Due to the lack of cores collected east of the river mouth, the rate of change in this direction cannot be assessed. DV values from the Rhône are several orders of magnitude higher than the Waipaoa, which reflects a difference in the software and digitization used for image acquisition and export, not the actual variations in density within the cores.

4.4.4 Seasonal change (FV)

4.4.4.1 Waipaoa margin

To quantitatively evaluate seasonal change in surface deposits, the FV of the surface of every core is examined across a range of length scales (Fig. 4.7). To test the accuracy of the method relative to previous qualitative efforts, cores were first examined visually. Based on visual inspection of the x-radiographs, the average thickness of the physically stratified surface layer was 2.7 cm in September (max = 12 cm), and slightly thinner in February (mean = 2.3 cm; max = 10 cm). In general, the layer on the mid-shelf and northern regions tended to be thicker in September, while the shallow and southern regions showed a thicker deposit in February (Fig. 4.8). Visual inspection to compare with the automated method of this study reveals that of the 33 unique core locations, only 16 are visibly different between the two cruises. Of these, 11 cores showed a more-distinct surface layer in September than in February (i.e., negative change in FV), while 5 showed the inverse (Fig. 4.8). Changes in the surface deposit (both positive and negative) were observed mostly on the mid-shelf, with a few exceptions along the perimeter and within Poverty Bay. Sites where a surface deposit was more evident in February (i.e., positive change in FV) are mostly located in the southern half of the mid-shelf region (Fig. 4.8).

Depending on the length scale over which the FV was calculated, this method was able to correctly identify a change in surface structure in 15 of the 16 locations where the surface deposits were visibly different between the two sampling events. In fact, there was only one core site(cores s337/s422) in which the method could not detect the visibly identified change at any length scale (Fig. 4.8). While the direction of FV change was correctly identified in a similar number of cores at each averaging length, the specific cores that were correctly identified were not the same (Fig. 4.8). For example, the locations where FV correctly identified surface change

using 10 cm and 5 cm averaging lengths were identical, except that the 10-cm average also correctly identified the direction of change in a core collected within Poverty Bay (cores s339/s439). In general, highest accuracy was observed in the northern half of the mid-shelf region; a region where the thickness of the physically stratified deposit changed dramatically according to visual inspection (Fig. 4.8).

4.4.4.2 Rhône River mouth

The FV parameter was successful in predicting temporal surface changes at each of the three examples of repeat cores collected near the mouth of the Rhône River (Fig. 4.9). Each core was previously classified as "physically stratified" despite an obvious biologically mixed surface layer in the October x-radiographs (Drexler and Nittrouer, 2008). In every core collected in April 2004, a bioturbated layer beneath the 3 to 6 cm of new deposition is observed (Fig. 4.9). The surface layer was the thickest in core G31 (6 cm). Cores E33 and F32 show higher FV in April for each of the 1, 3, and 5-cm length scales. FV is higher when examined across the upper 10-cm of the core. Core G31 shows higher FV in April at only the 3, 5, and 10-cm length scales.

4.5 Discussion

In this study, the method described above is developed to quantify the density variability of ~50 cm cores (~100-year timescale) using x-radiographs, and subsequently employed to evaluate how this variability changes on seasonal time scales. To test the wider-scale applicability of this method, down-core characteristics and seasonal change were examined in two environments, each subject to a unique set of driving forces: the Waipaoa margin and the region near the mouth of the Rhône River. In the Waipaoa example, cores are compared from across the shelf, ranging from constantly reworked cores within Poverty Bay, to highly bioturbated cores near the shelf edge (Walsh et al., 2014). Repeat cores separated by five

months are used to observe the destruction of a surface layer emplaced by a powerful event in July 2010, responsible for the generation of a wave-supported fluid mud and 1-5 cm of deposition on the mid-shelf (Hale et al., 2014). Near the Rhône River mouth, observations were used study changes in seabed characteristics following the implementation of a flood layer in April 2005 (Drexler and Nittrouer, 2008). Together, these results provide examples where a quantitative interpretation of x-radiographs can be used to identify specific products of physical processes.

The method used to estimate DV is not entirely quantitative, as subtle differences in the exact physical setup of the x-ray system, or in how images are manipulated, can have implications for the absolute variability. On the ~100-year timescale of the Waipaoa cores, the range of differences in down-core density variability at a single location between cruises is comparable to the difference in cores collected at the same location in the same cruise. However, by examining the depths at which the most density variation occurs within each core, attempts can be made to distinguish between small-scale spatial variability, and a tangible change in the observed preservation of an event layer. The expectation, therefore, is a reduction in the FV observed in the surface of the core over time, as bioturbation and erosion remove traces of previous flood deposits.

4.5.1 Pixel intensity, porosity, and bulk density

Using changes in bulk density to infer depositional history has been employed by sedimentologists for decades (e.g., Nittrouer, 1979; Kuehl et al., 1985; Jaeger and Nittrouer, 1995; Sommerfield and Nittrouer, 1999). Previous studies have relied on the time consuming, relatively low resolution (≥1 cm) method of drying and weighing subsamples, as described in section 3.2. For example, the high-porosity layer located at 7-9-cm depth in core s324 (Fig. 4.4)

may have gone unnoticed were it not for the x-radiograph image, as the subsamples examined in the laboratory were collected immediately above and below this stratum. Alternatively, high-resolution multi-sensor core loggers can be used, however these require full-length core barrels, and are difficult to utilize in the field due to technical and spatial constraints. In this study, x-radiograph images are employed, which are otherwise used to examine specific sedimentary structures invisible to the naked eye. From these images, meaningful information regarding decadal to century depositional patterns can be extracted, along with an understanding of seasonal changes in surface variability.

In the case of the Waipaoa margin, the slope of the relationship between pixel intensity and porosity is relatively well constrained, with only one or two outlying cores (319, 324, 405) on either cruise (Fig. 4.2). Each of these outlying cores was collected at an area where small-scale spatial variability is particularly high, which results in additional challenges when comparing samples from one core to an x-radiograph image of an adjacent core within a multicore set. Given that the attenuation coefficient (μ) is expected to behave linearly (Eq. 1), the relationship between pixel intensity and porosity may not appear surprising. However, given the number of variables and degree of discrepancy inherent in this type of system, the correlation is encouraging for several reasons. One interesting conclusion drawn from this similarity is that, after establishing this relationship, only a single porosity value for any core is required to infer porosity at all depths of x-rayed cores. Furthermore, based on the similarity in the relationship of pixel intensity to porosity between cruises (Fig. 4.2), the potential DV is the same for all cores, in both cruises. While there exists the possibility for bias due to either image processing or instrument setup (Fig. 4.3), the range of observed pixel intensity values varies in a repeatable,

predictable manner, indicating that this bias does not affect the interpretations made using this methodology.

Stark contrasts between layers of differing bulk densities control DV in our system. This seems to contradict the findings of Wheatcroft et al. (2006), who observe the highest variability in bulk density within bioturbated layers. The difference in these results stems from a difference in method: our study averages pixel intensity across horizontal lines, and compares between these averages to determine DV (Fig. 4.4), and therefore is focused towards the horizontal physical layering. Their study, on the other hand, compares the range of pixel intensities in a given area, which is designed to highlight the complex matrix of small-scale borrows made by benthic organisms.

4.5.2 Interpreting decadal and seasonal patterns on the Waipaoa margin

In general, the spatial pattern observed in the DV on the Waipaoa margin compares well with observations made in previous studies (Rose and Kuehl, 2012; Walsh et al., 2014). Similar to these past studies, a radial pattern of decreasing DV with distance from Poverty Bay is observed (Fig. 4.5). The degree of physical lamination (both DV-interpreted and qualitatively assessed) decreases over a shorter distance to the south than the north, which may be due to the effects of Coriolis forcing on the river plume, as observed in a numerical simulation of the region (Moriarty et al., 2014). Interestingly, water-column observations of sediment flux near the mid-shelf show a general trend to the northeast, but currents indicate that there also exists the capacity for transport to the southwest (Hale et al., 2014), indicating that event-based sediment transport (i.e., correlated velocity and suspended-sediment fluctuation) may behave differently than the mean components. DV from February is actually reduced in the northern shelf (Fig. 4.5), corroborating the observations of Walsh et al. (2014), who examined x-radiograph images

qualitatively. The destruction of surface strata and associated reduced DV is possibly due to seabed erosion and transport under relatively quiescent conditions, bearing in mind that the threshold for resuspension in this region is exceeded during ~80% of the study period (Hale et al., 2014). Thus, seabed density changes characterized by DV are affected by processes operating on both short-term (daily to monthly) and long-term (decadal) time scales. To quantify seasonal change in surface variability the FV parameter is examined (Figs. 4.5, 4.7, 4.8).

Because the contrast in density between event layers and the underlying seabed is the source of most DV in this system, and because bioturbation tends destroy strata, surface FV should decrease in the months following event-layer emplacement, assuming no subsequent events (e.g. Wheatcroft et al., 1997; Walsh et al., 2014). When examined qualitatively (i.e., visual examination), cores from 24 locations on the Waipaoa shelf display physically laminated strata near the surface (Fig. 4.8). In 18 of these cores, mostly on the northern half of the mid-shelf, the layer is more distinct (i.e., less bioturbated) in the cores collected in September than those collected in February 2011, reflecting the emplacement of a WSFM deposit in July 2010, and its subsequent deterioration. Depending on the length-scale used, the method for determining FV correctly identifies changes in the degree of physical lamination in the surface of as many as 20 cores (Fig. 4.8). The most accurate length scale over which to average to identify surface change is 3 cm, similar to the average deposit thickness of 2.3-2.7 cm. This indicates that the density contrast between the surface layer and the previously existing seabed has been modified; either reduced via bioturbation (where FV is reduced in February), or enhanced due to physical reworking (where FV is increased in February)(Fig. 4.8). Results were similar when using the 5-cm and 10-cm length scales (Fig. 4.8). This is likely due to the fact that at these length scales, both the higher-than-average surface FV, and the underlying region of low FV are

included. At greater averaging length scales, the FV is no longer successful at predicting surface change. At the farthest-offshore location (s321/s433), visual inspection of the x-radiograph indicates wave resuspension in the upper 1-cm in September 2010, but not in 2011. FV is correspondingly higher in September 2010 than February 2011, when examined on the shortest FV length scales (1, 3 cm; Fig. 4.8). At 5 and 10 cm, the enhanced surface FV is averaged out by the underlying low FV layers, and the trend in FV observed at the shorter lengths disappears (Fig. 4.8). This highlights the importance of using a range of length scales and a moderate understanding of the system, to determine the most appropriate averaging length for a given sedimentary environment. Future research will focus on extracting information regarding deposit thickness based on changes in the surficial FV at varying length scales.

4.5.3 Interpreting decadal and seasonal patterns near the Rhône River mouth

The distribution of DV near the mouth of the Rhône River resembles the pattern of physical stratification described by Drexler and Nittrouer (2008)(Fig. 4.6). DV decreases rapidly seaward of the river mouth, as water depth increases (Fig. 4.6). The reduction is more gradual to the west, as water depth remains relatively constant. Sediment is transported predominantly to the west in this system (Durrieu de Madron et al., 2008), but cores were not taken east of the mouth to illustrate the drop-off in DV that is likely observed in this direction.

While the sample size is smaller here, each of the three repeat cores can successfully identify the increased FV in the surface layer over time (Fig. 4.9), assuming that an appropriate averaging length scale is employed. For the relatively thin surface layers at E33 and F32 (3 and 5 cm, respectively), FV is greater in April 2005 than October 2004, at 1, 3, and 5-cm lengths, but lower at the 10-cm length. FV is controlled by the parallel laminae observed in the internal structure of this recently emplaced, river-generated flood deposit. Inspection of the x-

radiographs from October 2004 reveals that the most dramatic density contrast occurs at 8-10 cm in each of these cores, between bioturbated sediment and older, physically stratified sediment (Fig. 4.9). As a result, FV appears higher in October 2004 than April 2005, but only when this deeper layer is included (i.e., with the 10-cm averaging length). Alternatively, for the thicker, 6-cm event layer observed in core G31 from April 2005, averaging over the shortest interval (e.g., 1 cm) suggests that FV is greater in October 2004 (Fig. 4.9). FV at site G31 between the two cruises is very similar at the 3 and 5-cm length scales, and it is not until the obvious boundary between recent flood sediment and older, bioturbated sediment is incorporated (i.e., the 10-cm averaging length) that FV is clearly greater in April 2005 than October 2004 (Fig. 4.9). If the approach assumed a characteristic deposit thickness and only examined FV at that averaging length, the importance of the deposit at this location may have been overlooked. However, by using a range of length scales, this method is capable of identifying the observed spatial variations in the deposit thickness.

4.5.4 System Comparison

That our method is able to characterize the style of seabed deposition accurately in each of these systems is encouraging, given the differences in their environmental conditions. In the Waipaoa, the distance between sediment source and the mid-shelf (>15 km) allows for sediment sorting based on depositional energy. As a result, both DV and FV here are controlled by the strong contrasts between layers of relatively high and low bulk density (Figs. 4.4, 4.5, 4.7). The density contrasts observed between strata seem to control DV in most of the system, more so than minor laminae within an event layer. The corollary here is that cores collected within Poverty Bay (the initial site of rapid, temporary deposition), despite being subject to continuous wave reworking, actually have lower DV values than those on the mid-shelf in September 2010

(Fig. 4.5). The internal structure of the deposit plays a more important role here, as deposits are generally thicker, and the density variation between deposits is minimal. This result is similar to the pattern observed in the textural data from Walsh et al. (2014), where cores collected within Poverty Bay and on the outer shelf have a relatively uniform clay fraction (and therefore similar bulk density), whereas the mid-shelf exhibits a high degree of variance about the mean clay fraction. Thus, at this point, some *a priori* knowledge is required to infer the potential cause of reduced down-core density, as well as to establish the length over which to examine FV. The true value of this method is that it can rapidly and accurately quantify spatial patterns and seasonal change in seabed density, using data that is currently being collected for qualitative assessment.

Cores with the highest DV on the Rhône were mostly collected within 5 km of the sediment source (Fig. 4.6), as is typical of larger rivers discharging into relatively calm, semi-enclosed environments (e.g., Palinkas et al., 2005; Wheatcroft et al., 2006). The density contrast between bioturbated and physically laminated sediment can be important, as observed in FV at longer length scales in the shallow cores. That said, the dominant control on DV in this river mouth deposit is minor density fluctuations within strata, which reflect changes in grain size. In the case of the western-most transect on the Rhône delta, grain-size distributions show that cores in water deeper than 30 m have minimal sand content and have a nearly constant clay and silt distribution (Drexler and Nittrouer, 2008), which corresponds well with our observations of higher DV in shallow water relative to deep. This observation is similar to the observations from within Poverty Bay, and lends credence to the wider-scale applicability of our method.

4.6 Conclusions

Textural data from shelf sediment cores provide important information regarding system behavior on a variety of time scales. Generating these data in a laboratory can be a time-consuming, resource-intensive prospect. In this study, a method is developed using commonly collected x-radiographs that are typically examined qualitatively, to examine the spatial variability of a region's depositional history on a decadal scale, and to quantify seasonal changes in the seabed based on strata implementation and destruction. Extracting quantifiable data from x-radiographs is rapid, non-destructive, and relies on existing technology, without the need for additional equipment that is both expensive, and bulky. Our method is not perfect, and at present has only been proven effective in areas with distinct spatial patterns and strong seasonal signals. That being said, the interpretations enabled by the methodology developed in this study compare favorably to those of previous studies which used a broad suite of textural and radiochemical tools. DV quantifies the longer-term depositional history at an individual location, and through spatial interpolation can address questions regarding shelf dynamics, and the interaction between short-term deposition and long-term accumulation. FV further quantifies this change on a (e.g., seasonal) scale, normalizing DV to examine changes in the surface layer over time. The previous studies against which this methodology is tested were conducted in very different depositional environments, yet the accuracy of the technique is similarly high in both.

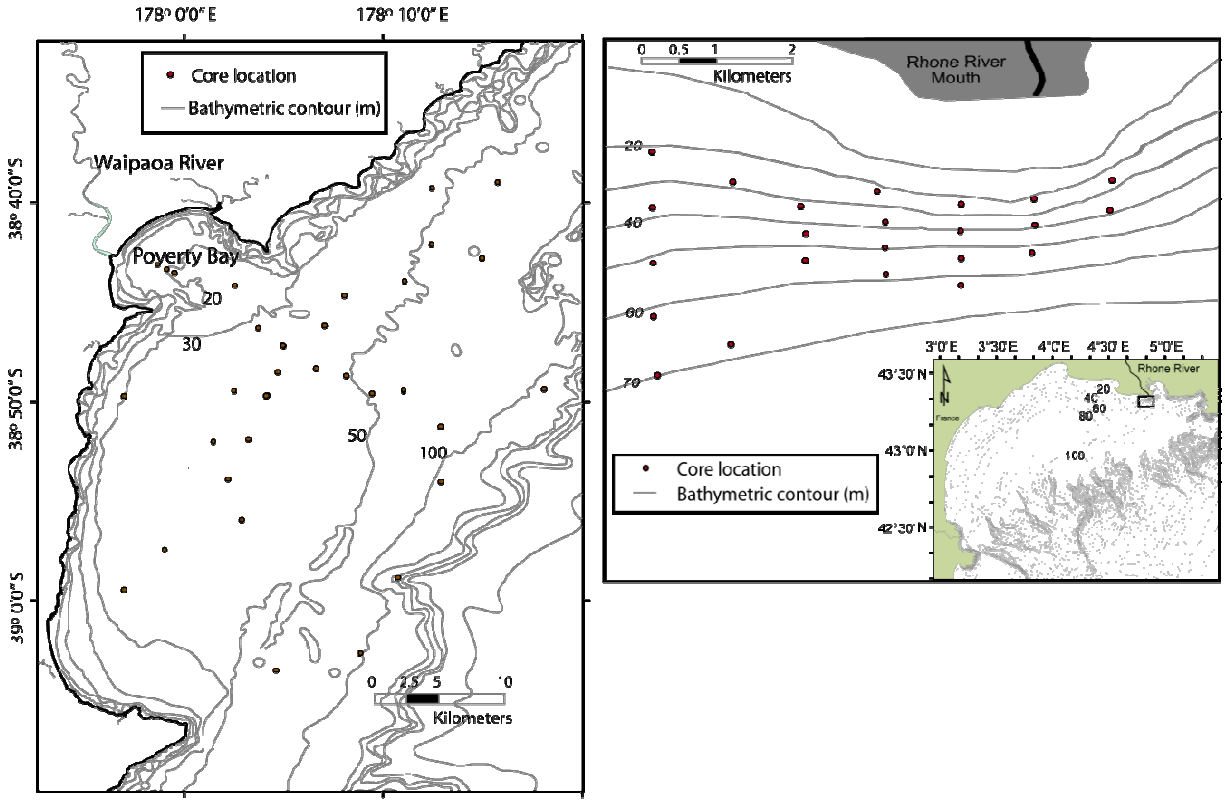

Figure 4.1 – Core locations for the Waipaoa margin, NZ, and region proximal to the Rhône River mouth, FR. Note the difference in length scales, where the cross-shelf distance of the Waipaoa is ~20 km, versus <10 km on the Rhône.

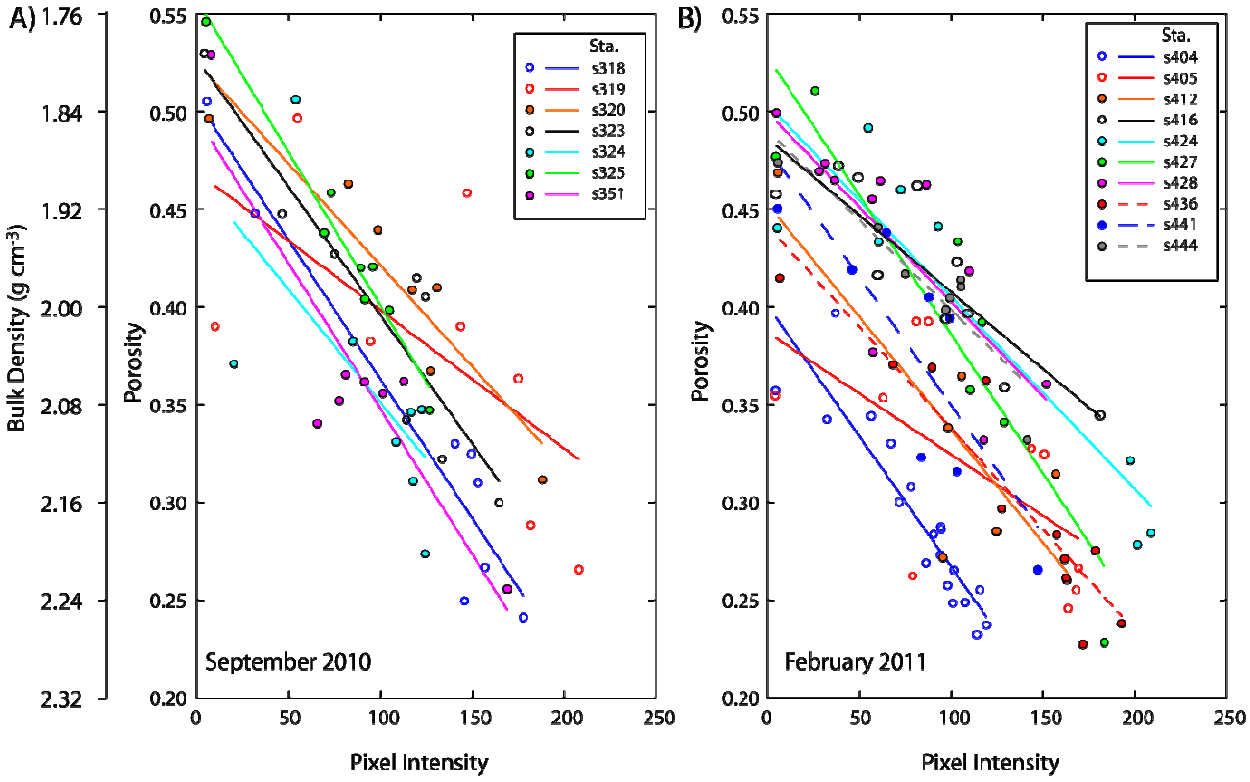

Figure 4.2 – Comparison of porosity and pixel intensity for samples collected on the Waipaoa margin in a) September 2010, and b) February 2011. The relationship is similar between cores, and between cruises, suggesting that total down-core density can be estimated from the highest porosity value, typically located at the core surfaces.

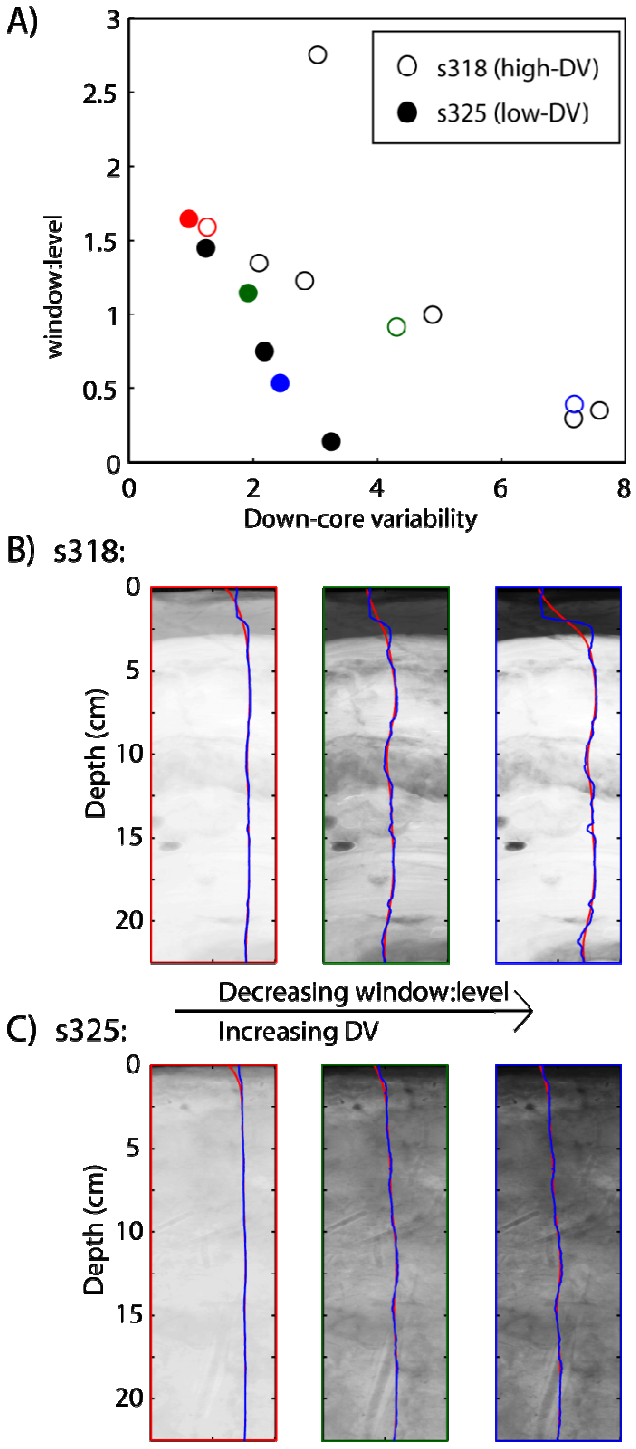

Figure 4.3 – The relationship between window/level and the ensuing DV, within cores of low (s325, solid points) and high (s318, empty points) physical lamination. The points in panel a) represent three unique windo:level combinations, where the color corresponds to the box outlining the x-radiograph image in panels b) and c). Blue curves correspond to average, raw pixel intensity for each row of pixels, red curves are smoothed with a low-pass filter.

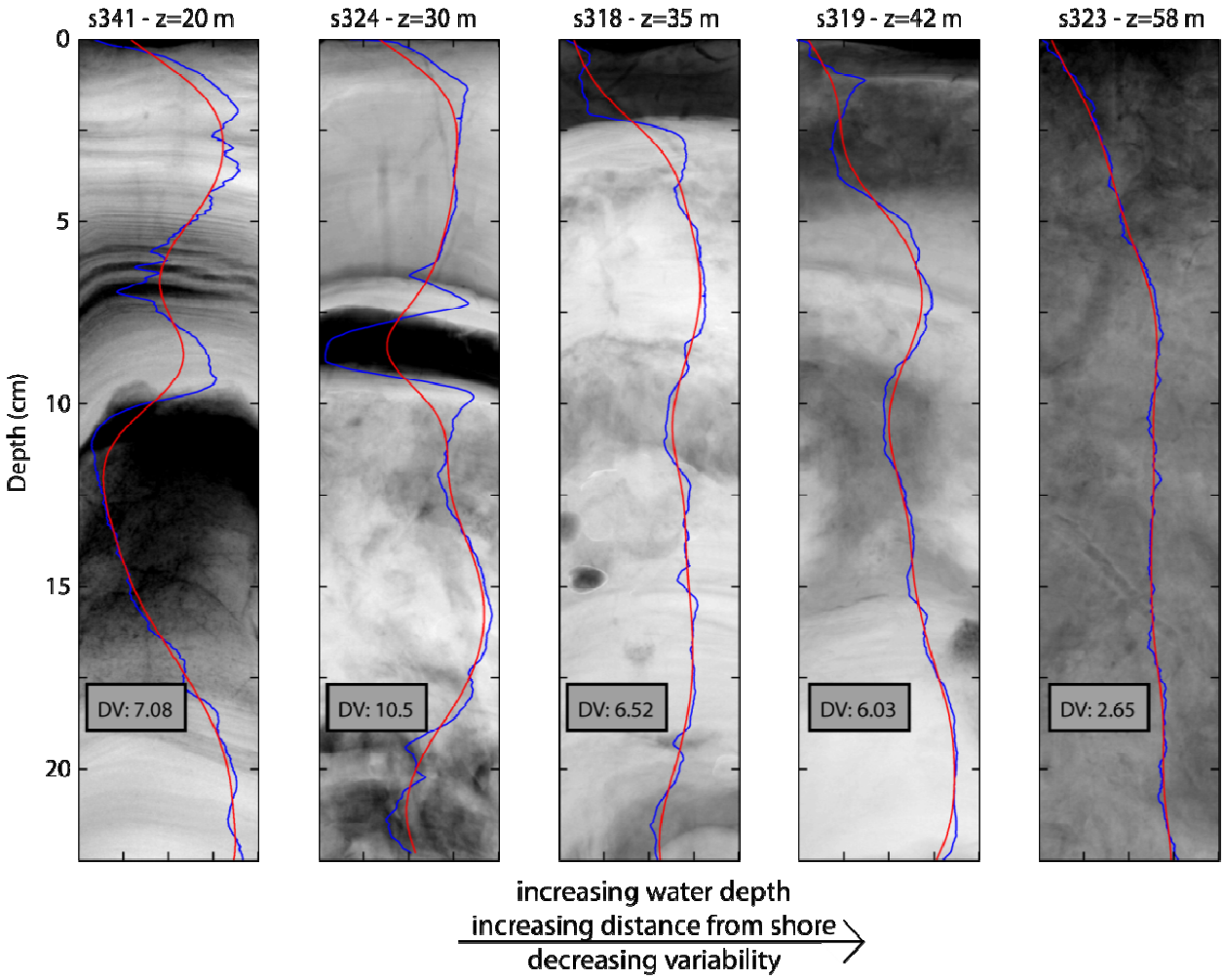

Figure 4.4 – X-radiograph negatives and their associated DV from cores collected on a shore-perpendicular transect. Blue curves correspond to average, raw pixel intensity for each row of pixels, red curves are smoothed with a low-pass filter. Preservation of physical structures, and their thickness, decreases as water depth and distance from the sediment source increases.

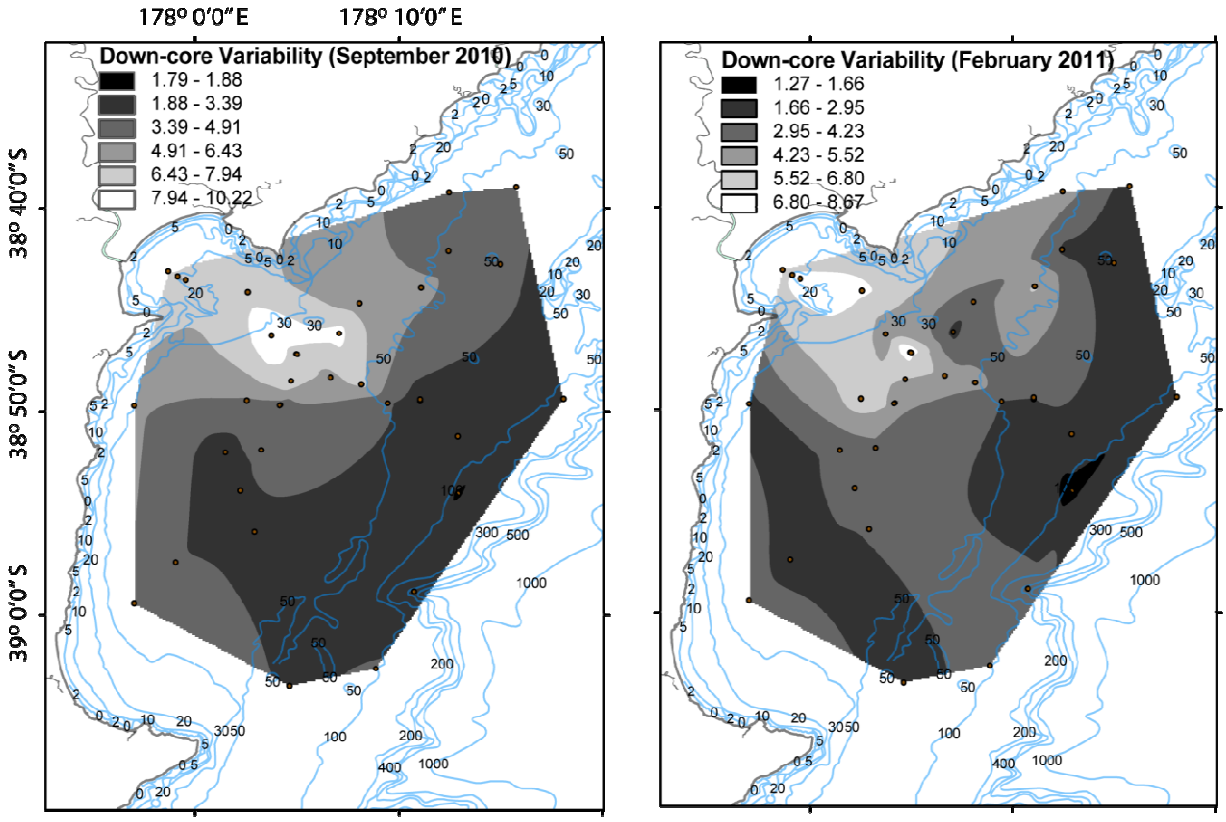

Figure 4.5 – Century-scale down-core variability (DV), based on cores collected in September 2010 (left) and February 2011 (right). While not identical, both images do a reasonable job of replicating the observations of previous studies (Rose and Kuehl, 2010; Walsh et al., 2014). The reduced variability in the northern half of the right-hand image is likely due to physical reworking, but is especially dramatic due to interpolation about a single core on the northern mid-shelf.

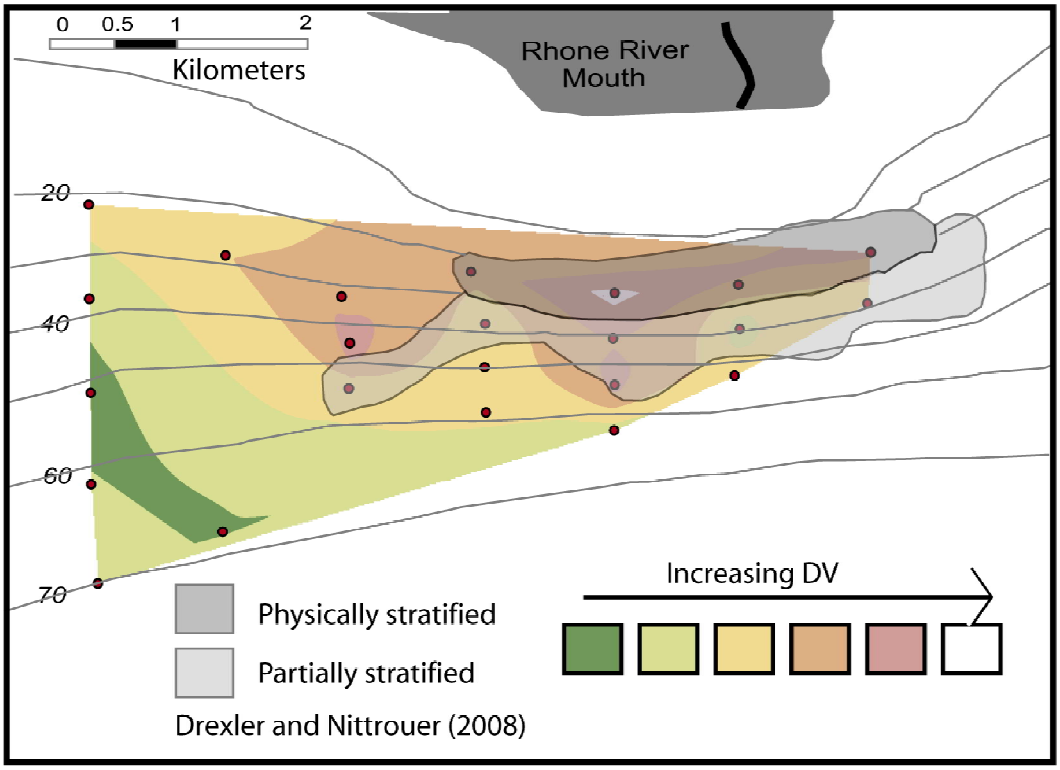

Figure 4.6 – Down-core density variability and visual analysis of sedimentary structures of cores collected on the Rhône margin, originally collected and analyzed by Drexler and Nittrouer (2008). Shaded regions correspond to those author's qualitative assessment of physical stratification. Colored shading represents this study's analysis, with cooler colors corresponding to cores of lower DV.

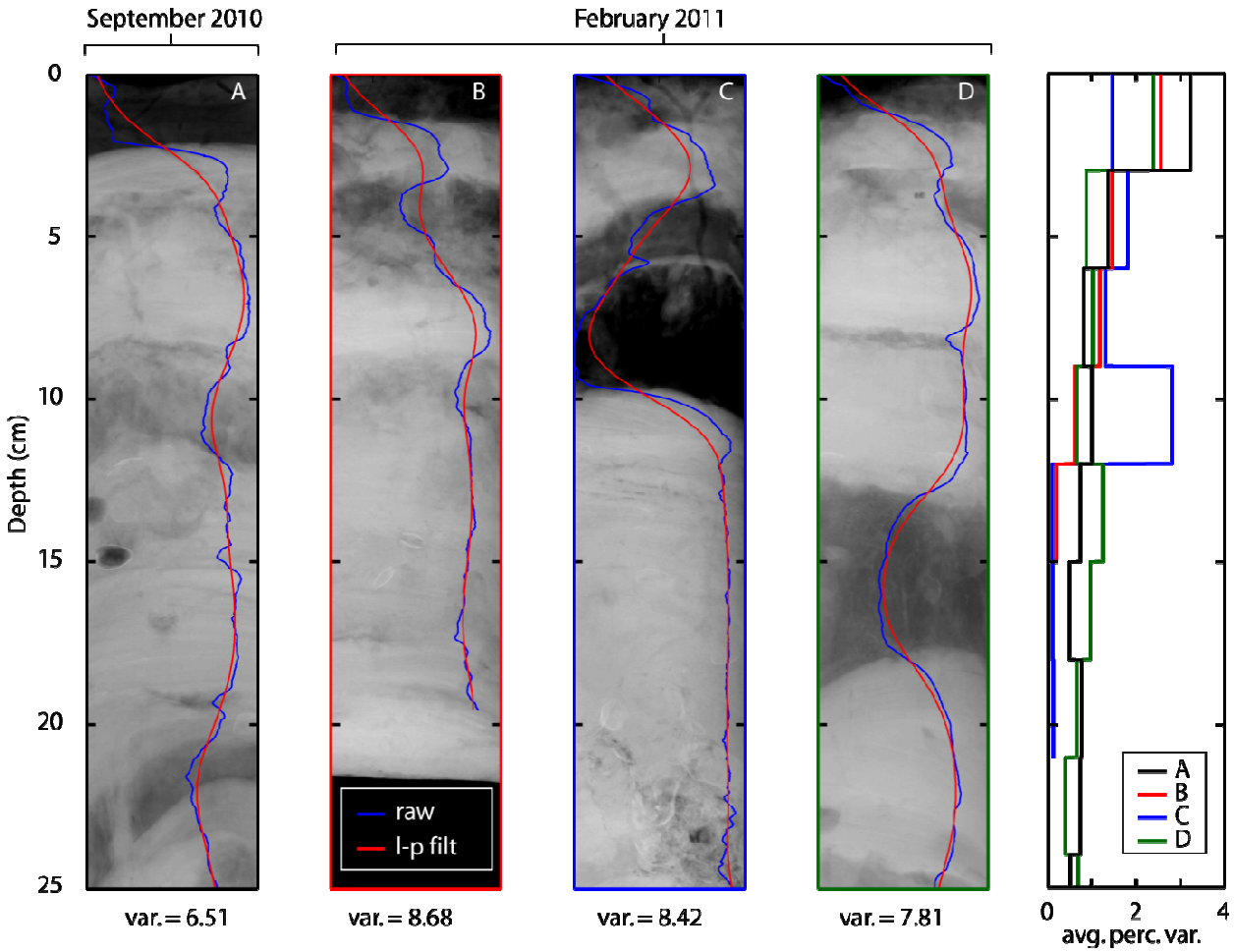

Figure 4.7 – Comparison between the raw intensity data and low-pass-filtered data for a mid-shelf location from September 2010 (A), and February 2011 (B-D). Panel E demonstrates that in all cases (to varying degrees), FV averaged over 3-cm is higher in September than in February.

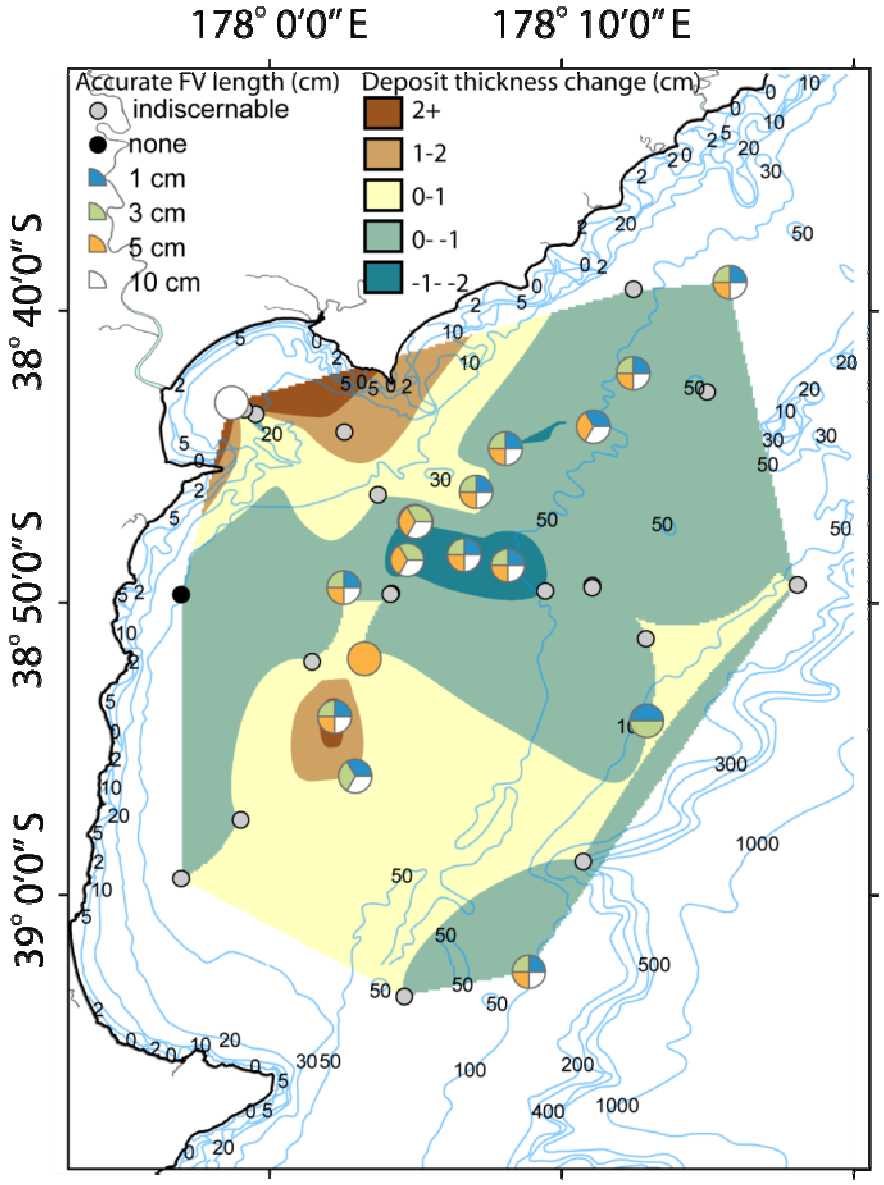

Figure 4.8 – Cores collected and analyzed on the Waipaoa margin as part of this study. Colored contours represent the change in observed surface deposit thickness, with cooler colors representing a thicker deposit in September. Inset pie charts demonstrate the length scales over which FV correctly identified the type of surface variability change.

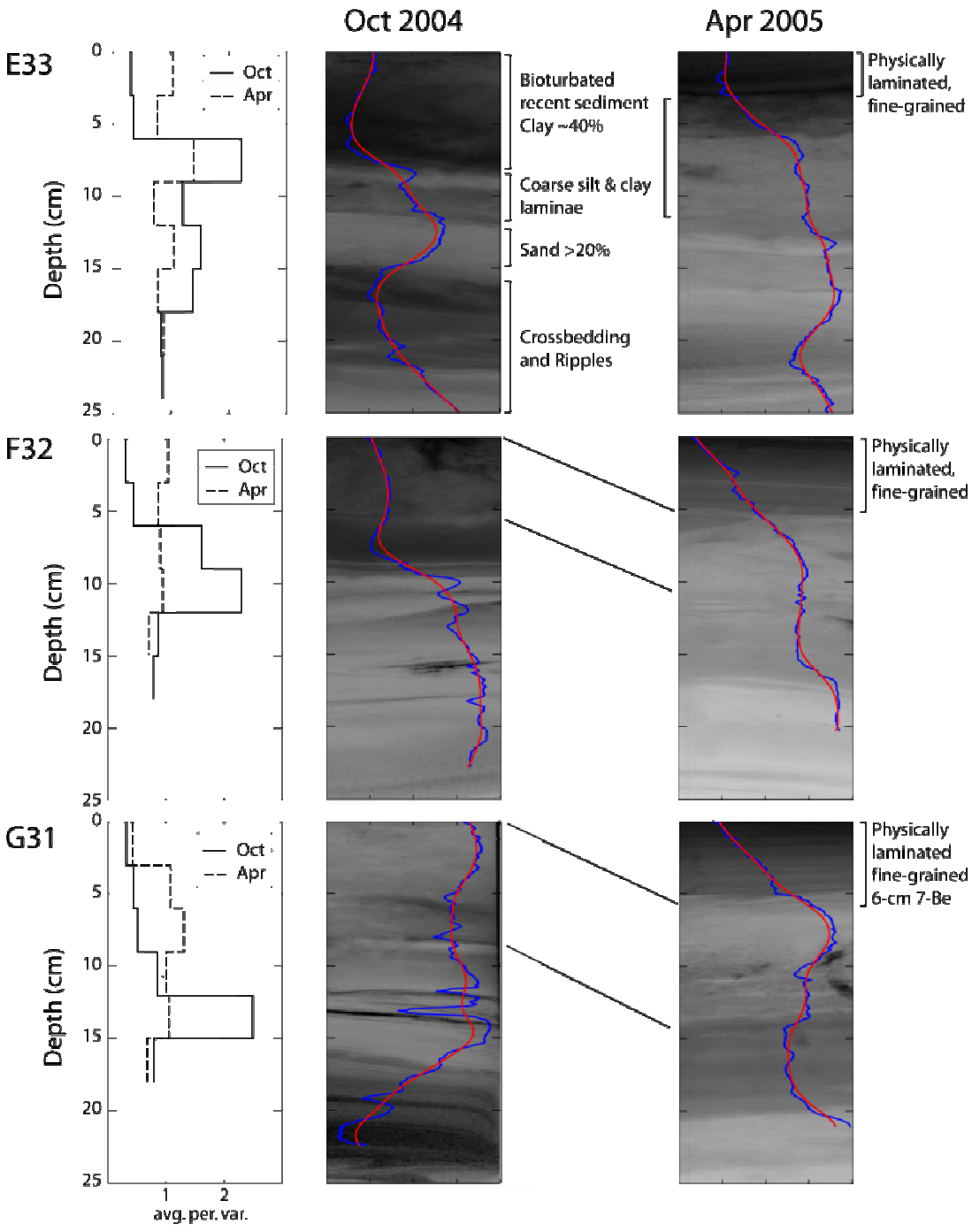

Figure 4.9 – Observed changes in FV for each of the three core repeat locations associated with the Rhône study. Our method is especially effective when examining cores E33 and F32 at the 1, 3, and 5-cm length scales. Core G31 is complicated by a deeply buried layer of high porosity in the October 2004 core, as well as a surface layer thicker than the 1, 3, and 5-cm length scales at which we examined surface variability.

	September 2010				February 2011		
station	**Slope**	**Maximum Porosity**	**r^2**		**Slope**	**Maximum Porosity**	**r^2**
s319	-0.0007	0.47	0.39	**s427**	-0.0014	0.53	0.85
s323	-0.0014	0.53	0.84	**s441**	-0.0013	0.48	0.70
s351	-0.0015	0.49	0.81	**s412**	-0.0012	0.45	0.71
s325	-0.0016	0.56	0.96	**s404**	-0.0013	0.40	0.83
s318	-0.0014	0.51	0.92	**s405**	-0.0006	0.39	0.38
				s436	-0.0010	0.44	0.88
s320	-0.0010	0.52	0.88	**s416**	-0.0008	0.48	0.75
s324	-0.0011	0.47	0.41	**s424**	-0.0010	0.50	0.84
				s428	-0.0010	0.50	0.63
				s444	-0.0009	0.49	0.85
mean	-0.0012	0.51	0.74		-0.0011	0.47	0.74
STD	0.0003	0.03			0.0003	0.05	

Table 4.1 – Slope of the relationship between x-ray intensity and porosity for cores collected on the Waipaoa margin in September 2010 and February 2011. Bold lines are used to group cores collected at the same location on different cruises. Note the similarity in the slopes, both between individual cores, and between cruises. Note also the relative strength of the relationship ($r^2 = 0.74$).

Core	DV	mean DV range
405i	8.4	0.6
405ii	9.0	
436i	8.7	0.9
436ii	7.8	
445i	7.8	3.8
445ii	4.0	
421I	3.4	0.2
421ii	3.2	
425i	6.1	3.8
425ii	11.8	
425iii	7.3	
426i	8.0	1.2
426ii	6.8	
444i	2.9	1.2
444ii	4.1	
451i	6.2	2.3
451ii	6.6	
451iii	9.6	
416	4.1	1.6
428	5.7	

Table 4. 2 – DV values for cores collected at the same location, either on the same multicorer cast (e.g., i, ii, iii), or during repeat occupations on the same cruise (outlined in bold). DV range is greatest in cores with typically high DV, and with one exception, physically laminated cores always exhibit greater DV than their bioturbated counterparts.

Chapter 5:
Summary and Conclusions

Sediment transport and deposition are intrinsically linked, and examining one without the other will result in an incomplete understanding of a sedimentary system. This study builds on previous research by constraining deposition and accumulation by monitoring ocean forcings with *in situ* instrumentation focused on the near-bed, and combining these observations with repeat seabed core collection. The research conducted on the WSS extends our understanding of SMRs by demonstrating examples of both previously observed and novel behavior. As with other SMRs, sediment flux is stochastic, controlled largely by the interplay between river discharge and ocean forcing. That said, local geography (Poverty Bay) inserts a time lag in the river-ocean coherence expected for a SMR system, which has not been documented previously. During storm events of extreme duration, deposition can occur concurrently with discharge, however the more-common case involves a series of resuspension and advection episodes that lead to cross-shelf sediment dispersal. Tectonic controls have resulted in a relatively low-gradient shelf, however the capacity remains for significant offshore transport due to gravity-driven flow. A wave-supported fluid mud occurred during the longest-duration event of the 2010-2011 study year. It was responsible for 40% of the net-annual cross-shelf transport, and generated a seabed deposit that could be observed in x-radiographs of sediment cores. Examining the down-core variability of bulk density preserved in these cores provides insight to the frequency of event occurrence and preservation on longer time scales.

Chapter 2 investigates the relative importance of all events that occurred during the 2010-2011 study year. The nine events during which deposition is observed on the mid-shelf exhibit waves of greater height, and longer period, and relatively slow current velocities. Waves of this nature suggest that forcing conditions were generated locally, and did not represent the arrival of

waves from distant Southern Ocean storms. In contrast, the ten instances of seabed erosion at the mid-shelf occur with waves of shorter height and longer period, and relatively fast current velocities, suggesting the arrival of wave energy associated with storms located away from the study area. During this year of study, only one instance of deposition coincident with river discharge occurs at the tripod sites. This highlights the role of Poverty Bay in mitigating river-ocean coherence, as well the magnitude of the event in question.

Chapter 3 examines this long-duration, river-ocean coherent event closely, providing strong evidence for the presence of WSFM. The exhaustive process of calibrating acoustic instrumentation for use in high-concentration environments is relatively rare, but provides the information necessary to solve the force balance derived from simple buoyancy theory. Even at the conservative gravity-velocities computed using this analytical solution (<3 cm s^{-1}), sediment associated with this WSFM is capable of reaching the shelf edge in a matter of days. Extrapolating along a transect from the mid-shelf to the shelf edge suggests that due to increases in the seabed slope, the actual travel time is likely half that suggested by the original estimate. Furthermore, the relative amount of sediment in suspension within the WSFM is so great that the total sediment flux associated with this gravity-driven flow is more than 7 x greater than near-bed flux outside the flow. The time series of sediment flux can be further extrapolated to predict when deposition may occur during a WSFM event, as well as where on the shelf these deposits should be located. These deposition predictions are corroborated by observations of bed-elevation change from this study, and seabed geochemistry results presented elsewhere (Walsh et al., 2014).

Chapter 4 employs x-radiographs of sediment cores to examine the spatial distribution of sedimentary facies, as a proxy for the type of deposit associated with the WSFM event. In

addition to long-term down-core variability, changes in the seabed surface due to biological and physical reworking are quantified. Despite the biases intrinsic to x-radiograph acquisition and processing, a strong and consistent relationship between pixel intensity and porosity emerges. This relationship is not only found among cores collected on a single cruise, but in fact is repeated within cores collected on a subsequent cruise, when using the same instrumentation. The method developed for quantitatively extracting estimates of down-core variation in sediment bulk density from x-radiographs produces interpolated spatial surfaces for the degree of lamination, which mimic the results of previous studies relying on time-exhaustive laboratory analyses and visual examination. This new method to assess down-core variability (DV) is capable of identifying depositional patterns observed on the scale of decades to centuries. After normalizing for total variability, temporal changes can be identified in the seabed surface due to the implementation of new strata or the destruction of old strata based on a shift in the fractional variability (FV) occurring in the surface sediment. Estimates of FV are normalized to both the length of the core, and the total variation in that core, further enhancing their ability for direct comparison of seasonal seabed evolution. The environments in which this method was tested exhibit different depositional styles, with scales ranging from the entire continental shelf seaward of the Waipaoa River, to a localized region near the mouth of the Rhône River.

In summation, these results present a meaningful step forward in understanding the links between sediment source and sink, as well as between near-bed process and seabed product. Observations made on hourly time scales are used to explain seasonal change in sedimentary facies, which in turn, helps provide an understanding of century-scale accumulation patterns. This research highlights the importance of individual events on the annual sediment-transport

budget, and demonstrates the need to consider multiple time scales of observation when evaluating system dynamics.

References

Allen, G.P., Salomon, J.C., Bassoullet, P., Du Penhoat, Y., De Grandpré, C., 1980. Effects of tides on mixing and suspended sediment transport in macrotidal estuaries. Sedimentary Geology 26, 69-90.

Aylmore, L.A.G., 1993. Use of computer-assisted tomography in studying water movement around plant roots. Advances in Agronomy 49, 1-54.

Alexander, C.R., Walsh, J.P., Orpin, A.R., 2010. Modern sediment dispersal and accumulation on the outer Poverty continental margin. Marine Geology 270, 213-226.

Algeo T.J., Phillips, M., Jaminski, J., Fenwick., 1994. High-resolution x-radiography of laminated sediment cores. Journal of Sedimentary Research A64, 665-703.

Bever, A.J., McNinch, J.E., Harris, C.K., 2011. Hydrodynamics and sediment-transport in the nearshore of Poverty Bay, New Zealand: Observations of nearshore sediment segregation and oceanic storms. Continental Shelf Research 31, 507-526.

Bentley, S.J., and Nittrouer, C.A., 2003. Emplacement, modification, and preservation of event strata on a flood-dominated continental shelf: Eel shelf, Northern California.

Brackley, H.L., Blair, N.E., Trustrum, N.A., Cater, L., Leithold, E.L., Canuel, E.A., Johnsont, J.H., Tate, K.R., 2010. Dispersal and transformation of organic carbon across an episodic, high sediment discharge continental margin, Waipaoa Sedimentary System, New Zealand. Marine Geology 270, 202-212.

Cacchione, D.A., Sternber, R.W., Ogston, A.S., 2006. Bottom instrumented tripods: History, applications, and impacts. Continental Shelf Research 26, 2319-2334.

Cacchione, D.A., Drake, D.E., Kayen, R.W., Sternberg, R.W., Kineke, G.C., Tate, G. B., 1995. Measurements in the bottom boundary layer on the Amazon subaqueous delta. Marine Geology 125, 235-257.

Cartwright, G.M., Friedrichs, C.T., Smith, S.J., 2013. A test of the ADV-Based Reynolds flux method for in situ estimation of sediment settling velocity in a muddy estuary. Geo-Marine Letters 33, 477-484.

DeGeest, A.L., Mullenbach, B.L., Puig, P., Nittrouer, C.A., Drexler, T.M., Durrieu de Madron, X., Orange, D.L., 2008. Sediment accumulation on the western Gulf of Lions, France: The role of Cap de Creus Canyon in linking shelf and slope sediment dispersal systems . Continental Shelf Research 28, 2031-2047.

Drexler, T.M., Nittrouer, C.A., 2008. Stratigraphic signatures due to flood deposition near the Rhône River: Gulf of Lions, northwest Mediterranean Sea. Continental Shelf Research 28, 1877-1894.

Durrieu de Madron, X., Wiberg, P.L., Puig, P., 2008. Sediment dynamics in the Gulf of Lions: The impact of extreme events. Continental Shelf Research 28, 1867-1876.

Fain, A. M. V., Ogston, A. S., Sternberg, R.W., 2007. Sediment transport event analysis on the western Adriatic continental shelf. Continental Shelf Research 27, 431-451.

Farnsworth, K.L., Warrick, J.A., 2007, Sources, dispersal, and fate of fine sediment supplied to coastal California: U.S. Geological Survey Scientific Investigations Report 2007– 5254, 77 p.

Ferre, B., Durrieu de Madron, X., Estournel, C., Ulses, C., Le Corre, G., 2008. Impact of natural (waves and currents) and anthropogenic (trawl) resuspension on the export of particulate matter to the open ocean Application to the Gulf of Lion (NW Mediterranean). Continental Shelf Research 28, 2071-2091.

Foster, G., Carter, L., 1997. Mud sedimentation on the continental shelf at an accretionary margin - Poverty Bay, New Zealand. New Zealand Journal of Geology and Geophysics 40, 157-173.

Friedrichs, C.T., Wright, L.D., 2004. Gravity-driven sediment transport on the continental shelf: implications for equilibrium profiles near river mouths. Coastal Engineering 51, 795-811.

Fugate, D.C., Friedrichs, C.T., 2002. Determining concentration and fall velocity of estuarine particle populations using ADV, OBS and LISST. Continental Shelf Research 22, 1867–1886.

Ryan, W.B.F., Carbotte, S.M., Coplan, J.O., S. O'Hara, A. Melkonian, R. Arko, R.A. Weissel, V. Ferrini, A. Goodwillie, F. Nitsche, J. Bonczkowski, R. Zemsky, 2009. Global Multi-Resolution Topography synthesis, Geochem. Geophys. Geosyst., 10, Q03014

Gerber, T.P., Pratson, L.F., Kuehl, S., Walsh, J.P., Alexander, C., Palmer, A., 2010. The influence of sea level and tectonics on Late Pleistocene through Holocene sediment storage along the high-sediment supply Waipaoa continental shelf. Marine Geology 270, 139-159.

Gomez B., Carter, L., Turstrum, N.A., 2007. A 2400 yr record of natural events and anthropogenic impacts in intercorrelated terrestrial and marine sediment cores: Waipaoa sedimentary system, New Zealand. GSA Bulletin 119, 1415-1432/

Guillén, J., Bourrin, F., Palanques, A., Durrieu de Madron, X., Puig, P., and Buscail, R., 2006. Sediment dynamics during ‘wet’ and ‘dry’ storm events on the Têt inner shelf (SW Gulf of Lions), Marine Geology 234, 129–142.

Hale, R.P., Ogston, A.S., Walsh, J.P., Orpin, A.R., 2014. Sediment transport and event deposition on the Waipaoa River shelf, New Zealand. Continental Shelf Research.

Hamblin, W.K., 1962. X-radiography in the study of structures in homogeneous sediments. Journal of Sedimentary Petrology 2, 201-210.

Healy, T., Stephens, S., Black, K., Gorman, R., Cole, R., Beamsley, B., 2002. Port redesign and planned beach renourishment in a high wave energy sandy-muddy coastal environment , Port Gisborne , New Zealand. Geomorphology 48, 163-177.

Hicks, D. M., Gomez, B., 2000. Erosion thresholds and suspended sediment yields, Waipaoa River Basin, New Zealand. Water Resources Research 36, 1129-1142.

Hicks, D.M., Gomez, B., Trustrum, N.A., 2004. Event suspended sediment characteristics and the generation of hyperpycnal plumes at river mouths: East Coast continental margin, North Island, New Zealand. Journal of Geology 112, 471–485.

Hill P.S., Milligan, T.G., Geyer, W.R., 2000. Controls on effective settling velocity of suspended sediment in the Eel River flood plume. Continental Shelf Research 20, 2095-2111.

Howard, J.D., 1968. X-ray radiography for examination of burrowing in sediments by marine invertebrate organisms. Sedimentology 11, 249-258.

Jaeger, J.M., Nittrouer, C.A., 1995. Tidal controls on the formation of fine-scale sedimentary strata near the Amazon River mouth. Marine Geology 125, 259-281.

Jaramillo, S., Sheremet, A., Allison, M., Reed, A.H., Holland, K.T., 2009. Wave-mud interactions over the muddy Atchafalaya subaqueous clinoform, Louisiana, United States: Wave-supported sediment transport. Journal of Geophysical Research 114, 1-18.

Keil, R. G., Mayer, L. M., Quay, P. D., Richey, J. E., & Hedges, J. I. (1997). Loss of organic matter from riverine particles in deltas. Geochimica et Cosmochimica Acta 61, 1507-1511.

Kineke, G.C., Sternberg, R.W.,Trowbridge, J.H., 1996. Fluid-mud processes on the Amazon continental shelf. Continental Shelf Research 516, 667-696.

Kineke, G.C., Higgins, E.E., Hart, K., Velasco, D., 2006. Fine-sediment transport associated with cold-front passages on the shallow shelf, Gulf of Mexico. Continental Shelf Research 26, 2073-2091.

Kniskern, T.A., Harris, C.K., Mitra, S., Orpin, A.R., 2014. Rapid response sampling of a flood deposit on the waipaoa Shelf, New Zealand. Continental Shelf Research, this issue.

Kniskern, T.A., Warrick, J.A., Farnsworth, K.L., Wheatcroft, R.A., Goñi, M.A., 2011. Coherence of river and ocean conditions along the US West Coast during storms. Continental Shelf Research 31, 789-805.

Kowalczk, A., 2005. The application of digital x-radiograph imaging for the determination of bulk density. Report from NSF Summer Intern Program at Virginia Institute of Marine Sciences, Gloucester Point, VA.

Kuehl, S.A., DeMaster, D.J., Nittroer, C.A., 1985. Nature of sediment accumulation on the Amazon continental shelf. Continental Shelf Research 6, 209-225.

Kuehl, S., Alexander, C., Carter, L., Gerald, L., Gerber, T., Harris, C., McNinch, J., Orpin, A., Pratson, L., Syvitski, J., Walsh, J.P., 2006. Understanding sediment transfer from land to ocean. Eos 87, 281-286.

Lamb, M.P., Parson, J.D., 2005. High-density suspensions formed under waves. Journal of Sedimentary Research 75(3), 386-397.

Lamb, M.P., D'Asaro, E., Parsons, J.D., 2004. Turbulent structure of high-density suspensions formed under waves. Journal of Geophysical Research: Oceans 109, C12026.

Lofi, J., Weber, O., 2001. SCOPIX - digital processing of X-ray images for the enhancement of sedimentary structures in disturbed core slabs. Geo-Marine Letters 20, 182-186.

Ma, Y., Wright, L.D., Friedrichs, C.T., 2008. Observations of sediment transport on the continental shelf off the mouth of the Waiapu River, New Zealand: Evidence for current-supported gravity flows. Continental Shelf Research 28, 516-532.

Macquaker, J.H.S., Bentley, S.J., Bohacs, K.M., 2010. Wave-enhanced sediment-gravity flows and mud dispersal across continental shelves: Reappraising sediment transport processes operating in ancient mudstone successions. Geology 38, 947-950.

Madsen, O. S., 1994: Spectral wave-current bottom boundary layer flows. Proc. ASCE 24th Int. Conf. on Coastal Engineering (ICCE), Kobe, Japan, ASCE, 384–398.

Marion, C., Dufois, F., Arnaud, M., Vella, C., 2010. In situ record of sedimentary processes near the Rhône River mouth during winter events (Gulf of Lions, Mediterranean Sea). Continental Shelf Research 30, 1095-1107.

Martin, D.P., Nittrouer, C.A., Ogston, A.S., Crockett, J.S., 2008. Tidal and seasonal dynamics of a muddy inner shelf environment, Gulf of Papua. Journal of Geophysical Research 113, 1-18.

Miller, A. J., Kuehl, S. A., 2010. Shelf sedimentation on a tectonically active margin: A modern sediment budget for Poverty continental shelf, New Zealand. Marine Geology 270, 175-187.

Milliman, J.D., Meade, R.H., 1983. World-wide delivery of river sediment to oceans. The Journal of Geology 91, 1-21.

Milliman, J.D., Syvitski, J.P.M., 1992. Geomorphic/tectonic control of sediment discharge to the ocean: The importance of small mountainous rivers. The Journal of Geology 100, 525-544.

Milliman , J.D., Farnsworth, K.L., 2011. River discharge to the coastal ocean: a global synthesis. Cambridge University Press, New York, NY.

Moriarty, J.M., Harris, C.K., Hadfield, M.G., 2014. A hydrodynamic and sediment transport model for the Waipaoa shelf, New Zealand: sensitivity of fluxes to spatially-varying erodibility and model nesting. Journal of Marine Science and Engineering 2, 336-369.

Mullenbach, B.L., Nittrouer, C.A., 2000. Rapid deposition of fluvial sediment in the Eel Canyon, northern California. Continental Shelf Research 20, 2191-2212.

Mullenbach, B.L., Nittrouer, C.A., 2006. Decadal record of sediment export to the deep sea via Eel Canyon. Continental Shelf Research 26, 2157-2177.

Nichols , M.M., Biggs, R.B., 1985. Estuaries. In: R.A. Davis, (Ed.), Coastal Sedimentary Environments. Springer, New York, p. 77-186.

Nittrouer, C.A., 1979. The process of detrital sediment accumulation in a continental shelf environment: an examination of the Washington shelf. Ph.D. Thesis, University of Washington, 242 pp.

Ogston, A.S., Cacchione, D.A., Sternberg, R.W., Kineke, G.C., 2000. Observations of storm and river flood-driven sediment transport on the northern California continental shelf. Continental Shelf Research 20, 2141-2162.

Ogston, A.S., Sternberg, R.W., 1999. Sediment-transport events on the northern California continental shelf. Marine Geology 154, 69-82.

Ogston, A.S., Drexler, T.M., Puig, P., 2008. Sediment delivery, resuspension, and transport in two contrasting canyon environments in the southwest Gulf of Lions. Continentla Shelf Research 28, 2000-2016.

Orpin, A.R., Alexander, C.R., Carter, L., Kuehl, S.A., Walsh, J.P., 2006. Temporal and spatial complexity in post-glacial sedimentation on the tectonically active, Poverty Bay continental margin of New Zealand. Continental Shelf Research 26, 2205-2224.

Orsi, T.H., Anderson, A.l., 1999. Bulk density calibration for X-ray tomographic analyses of marine sediments. Geo-Marine Letters 19, 270-274.

Ozdemir, C.E., Hsu, t.J., Balachandar, S., 2010. A numerical investigation of fine particle laden flow in an oscillatory channel: the role of particle-induced density stratification. Journal of Fluid Mechanics 665, 1-45.

Ozdemir, C.E., Hsu, T.J., Balachandar, S., 2011. A numerical investigation of lutocline dynamics and saturation of fine sediment tin the oscillatory boundary layer. Journal of Geophysical Research: Oceans 116, C09012.

Page, M., Trustrum, N., Brackely, H., Gomez, B., Kasai, M.,Marutani, T., 2001. Waipaoa River North Island, New Zealand. In: Marutani, T., Brierley, G., Trustrum, N., Page, M. (Eds.), Source-to-Sink Sedimentary Cascades in Pacific Rim Geo-Systems, pp. 86–100.

Palinkas, C.M., Nittrouer, C.A., Wheatcroft, R.A., Langone, L., 2005. The use of ^{7}Be to identify event and seasonal sedimentation near the Po River delta, Adriatic Sea. Marine Geology 222-223, 95-112.

Palinkas, C.M., Ogston, A.S., Nittrouer, C.A., 2010. Observations of event-scale sedimentary dynamics with an instrumented bottom-boundary-layer tripod. Marine Geology 274, 151-164.

Puig, P., Palanques, A., Guille, J., 2001. Near-bottom suspended sediment variability caused by storms and near-inertial internal waves on the Ebro mid continental shelf (NW Mediterranean). Marine Geology 178, 81-93.

Puig, P., Ogston, A.S., Mullenbach, B.L., Nittrouer, C.A., Sternberg, R.W., 2000b. Sediment transport processes at the head of the Eel submarine canyon. EOS Trans. AGU 81, AGU Fall Meeting 2000, OS61A-14, 632.

Puig , P., Ogston, A.S., Mullenbach, B.L., Nittrouer, C.N., Parsons, J.D., Sternberg, R.W., 2004. Storm-induced sediment gravity flows at the head of the Eel submarine canyon, northern California margin. Journal of Geophysical Research 109, C03019.

Pullen, J.D., Allen, J.S., 2000. Modeling studies of the coastal circulation off Northern California: shelf response to a major Eel river flood event. Continental Shelf Research 20, 2213-2238.

Reid, C., 1999. Waipaoa River at Kanakanaia: a review of flood data. Unpublished report to the Gisborne District Council, New Zealand, 52 pp.

Rose, L.E., Kuehl, S.A., 2010. Recent sedimentation patterns and facies distribution on the Poverty Shelf, New Zealand. Marine Geology 270, 160-174.

Rose, L.E., 2012. Poverty shelf, New Zealand from the Holocene to present: Stratigraphic development and event layer preservation in response to sediment supply, tectonics, and climate. Ph.D. Thesis. The College of William and Mary, 288 pp.

Ross, M.A., Mehta, A.J., 1989. On the mechanics of lutoclines and fluid mud. Journal of Coastal Research 5, 51-61.

Saarinen, T., Petterson, G., 2001. Image analysis techniques. In: Last, W.M., Smol, J.P., (Eds.) Tracking environmental change using lake sediments volume 2: Physical and geochemical methods. Kluwer Academic Publishers, Dordecht, pp. 23-40.

Scully, M.E., Friedrichs, C.T., Wright, L.D., 2002. Application of an analytical model of critically stratified gravity-driven sediment transport and deposition to observations from the Eel River continental shelf, Northern California. Continental Shelf Research 22, 1951-1974.

Scully, M.E., Friedrichs, C.T., Wright, L.D., 2003. Numerical modeling of gravity-driven sediment transport and deposition on an energetic continental shelf: Eel River, northern California. Journal of Geophysical Research 108, 3120.

Shahidul Islam, Md., Tanaka, M., 2004. Impacts of pollution on coastal and marine ecosystems including coastal and marine fisheries and approach for management: a review and synthesis. Marine Pollution Bulletin 48, 624-649.

Sommerfield, C.K., Nittrouer, C.A., 1999. Modern accumulation rates and a sediment budget for the Eel shelf: a flood-dominated depositional environment. Marine Geology 154, 227-241.

Sommerfield, C.K., Nittrouer, C.A., Alexander, C.R., 1999. ^{7}Be as a tracer of flood sedimentation on the northern California continental margin. Continental Shelf Research 19, 335-361.

Slingerland, R., Driscoll, N.W., Milliman, J.D., Miller, S.R., Johnstone, E.A., 2008. Anatomy and growth of a Holocene clinotherm in the Gulf of Papua. Journal of Geophysical Research 113, F01S13.

Sternberg, R.W., Larsen, L.H., 1976. Frequency of sediment movement on the Washington contintnatl shelf: a note. Marine Geology 21, M37-M47.

Traykovski, P, Wiberg, P., Geyer, W.R. 2007. Observations and modeling of wave-supported sediment gravity flows on the Po prodelta and comparison to prior observations from the Eel shelf. Continental Shelf Research 27, 375-399.

Traykovski, P., Geyer, W.R., Sommerfield, C., 2004. Rapid sediment deposition and fine-scale strata-formation in the Hudson estuary. Journal of Geophysical Research 109(F02004), 1-28.

Traykovski, P., Geyer, W.R., Irish, J.D., Lynch, J.F., 2000. The role of wave-induced density driven fluid mud flows for cross-shelf transport on the Eel River continental shelf. Continental Shelf Research 20, 2113-2140.

Trowbridge, J.H., Kineke, G.C., 1994. Structure and dynamics of fluid muds on the Amazon continental shelf. Journal of Geophysical Research 99, 965-874.

Ulses, C., Estournel, C., Durrieu de Madron, X., Palanques, A., 2008. Suspended sediment transport in the Gulf of Lions (NW Mediterranean): Impact of extreme storms and floods. Continental Shelf Research 28, 2048-2070.

Walling, D.E., Webb, B.W., 1996. Erosion and sediment yield: a global overview. IAHS Publications 236, 3–19.

Walsh, J.P., Alexander, C.R., Gerber, T., Orpin, A.R., Sumners, B.W., 2007. Demise of a submarine canyon? Evidence for highstand infilling on the Waipaoa River continental margin, New Zealand. Geophysical Research Letters 34, L20606.

Walsh J.P., Corbett, D.R., Kiker, J., 2014. Short-term evolution of event deposits on the Waipaoa River margin, New Zealand. Continental shelf Research, this issue.

Warrick, J.A., Milliman, J.D., 2003. Hyperpycnal sediment discharge from semiarid southern California rivers: Implications for coastal sediment budgets. Geology 31, 781-784.

Warrick, JA., Xu, J., Noble, M.A., Lee, H.J., 2008. Rapid formation of hyperpycnal sediment gravity currents offshore of a semi-arid California river. Continental Shelf Research 28, 991-1009.

Wells, J.T., Coleman, J.M., 1981. Physical Processes and fine-grained sediment dynamics, coast of Surinam, South America. Journal of Sedimentary Petrology 51, 1053-1068.

Wheatcroft, R.A., Stevens, A.W., Hunt, L.M., Milligan, T.G., 2006. The large-scale distribution of internal geometry of the fall 2000 Po River flood deposit: Evidence from digital X-radiography. Continental Shelf Research 26, 499-516.

Wheatcroft, R.A., Goni, M.A., Hatten, J.A., Pasternack, G.B., Warrick, J.A., 2010. The role of effective discharge in the ocean delivery of particulate organic carbon by small , mountainous river systems, Limnology and Oceanography 55, 161-171.

Wheatcroft, R.A., Wiberg, P.L., Alexander, C.R., Bentley, S.J., Drake, D.E., Harris, C.K., Ogston, A.S., 2007. Post-depositional alteration and preservation of sedimentary strata. In: Nittrouer, C.A., Austin, J.A., Field, M.E., Kravitz, J.H., Syvitski, J.P.M., Wiberg, P.L. (Eds.), Continental Margin Sedimentation: From Sediment Transport to Sequence Stratigraphy. Blackwell Publishing Ltd., Oxford, UK, pp. 101–155.

Wheatcroft, R.A., Borgeld, J.C., 2000. Oceanic flood deposits on the northern California shelf: large-scale distribution and small scale physical properties. Continental Shelf Research 20, 2163-2190.

Wheatcroft, R.A., Sommerfield, C.K., Drake, D.E., Borgeld, J.C., Nittrouer, C.A., 1997. Rapid and widespread dispersal of flood sediment on the northern California margin. Geology 25, 163-166.

Woeffel, F., Elgar, S., 2003. Wave-induced sediment transport and sandbar migration. Science 299, 1885-1887.

Wiberg, P., 2000. A perfect storm: Formation and potential for preservation of storm beds on the continental shelf. *Oceanography* 13(3): 93–99.

Wiberg, P.L., Sherwood, C.R., 2008. Calculating wave-generated bottom orbital velocities from surface-wave parameters. Computers and Geosciences 34, 1243-1262.

Winterwerp, F.C., van Kessel, T., 2003. Siltation by sediment-induced density currents. Ocean Dynamics 53, 186-196.

Wright, L.D., Wiseman Jr., W.J., Yang, Z.S., Bornhold, B.D., Keller, K,H., Prior, D.B., Suhayda, J.N., 1990. Processes of marine dispersal and dposition of suspended silts off the modern mouth of the Huanghe (Yellow River). Continental Shelf Research 10, 1-40.

Wright, L.D., Boon, J.D., Xu, J.P., Kim, S.C., 1992. The bottom boundary layer of the bay stem plains environment of lower Chesapeake Bay. Estuarine Coastal Shelf Science 35, 17–36.

Wright, L.D., Friedrichs, C.T., Kim, S.C., Scully, M.E., 2001. Effects of ambient currents and waves on gravity-driven sediment transport on continental shelves. Marine Geology 175, 25-45.

VITA

2014 Ph.D., Geological Oceanography, University of Washington
Dissertation Title: “Investigating sediment transport on the Waipaoa margin: linking *in situ* observations with preserved deposits”

2011 M.S., Geological Oceanography, University of Washington
Master’s Title: “Sediment input to a submarine canyon: Effects of Typhoon Morakot in Fangliao canyon, SW Taiwan”

2006 Sc.B., Brown University
Thesis: “The geologic evolution of coastal ponds”